**Aus dem Institut für Anatomie und Zellbiologie, Abteilung Neuroanatomie der Albert-Ludwigs-Universität Freiburg im Breisgau**

# Ultrastructural analysis of spine apparatus in CA3 pyramidal neurons following single cell electroporation in Synaptopodin Knockout - mice

vorgelegt von

Dipl. - Biologin Mercedes Küffner

geboren in Bayreuth

21.12.2012

Dekan: Prof. Dr. Ad Aertsen
Promotionsvorsitzender: Prof. Dr. Stefan Rotter

Betreuer der Arbeit: Prof. Dr. Dr. h.c. Michael Frotscher
Ko-Referent: Prof. Dr. Dierk Reiff
Drittprüfer: Prof. Dr. Marco Prinz

Tag der mündlichen Prüfung: 11.04.2013

# Table of Contents

# Summary

The spine apparatus, a membranous extension of the dendrititc smooth endoplasmic reticulum, is located in mature dendritic spines of cortical and hippocampal neurons. This neuronal organelle exists only in a subpopulation of neurons, in large mushroom-shaped spines. The telencephalic protein Synaptopodin obtains a critical role in the formation of spine apparatuses, as this organelle is absent in Synaptopodin-knockout mice. Synaptopodin has been shown to bind actin and actin polymerization in turn contributes to the maintainance of the spine morphology. The overall aim of this thesis was to reveal molecular mechanisms for morphological alterations of CA3 pyramidal neurons at the cellular and subcellular level. To achieve this, single-cell electroporation of CA3 pyramidal neurons in organotypic hippocampal slice cultures was chosen to manipulate the expression of the axonal cell adhesion molecule L1CAM and the postsynaptic protein synaptopodin.

Morphology of CA3 pyramidal neurons was successfully modulated after electroporation of L1CAM and two L1CAM missense mutations. These mutations were shown to interfered with axonal targeting of L1CAM and L1CAM-dependent stimulation of axonal branching.

Genetic complemetation of synaptopodin-deficient neurons lead to the *de novo* formation of spine apparatuses in a cell autonomous manner. The restoration process of spine apparatsues is exclusively mediated by synaptopodin, as transfection studies with KIBRA did not lead to formation of spine apparatuses in spines or dendrites. After genetic complementation the general morphology of these organelles was enlarged in mushroom-shaped spines and dendrites and the total number of spine apparatuses increased in parent dendrites. Pharmacological inhibition of small Rho-GTPases led to increased spine apparatuses in the wild-type, which can be traced back to depleted interdigitating F-actin filaments in between single tubules of the spine apparatus. Changes in spine apparatus morphology correlate with morphological changes in mushroom-shaped spines, as all analyzed conditions with a persistent increase in median surface area of spine apparatuses showed additionally a significant increase for appropriate spines.

# Zusammenfassung

In der vorliegenden Studie wurde mittels Einzelzell-elektroporation morphologische Änderungen auf zellulärer und sub-zellulärer Ebene gezeigt. Nach der Transfektion von L1CAM und zweier Missens-mutationen in Pyramidenzellen konnte gezeigt werden, daß L1CAM für die axonale Verzweigung während der Entwicklung wichtig ist, da die beiden Mutanten ein verändertes Verzweigungsmuster ihrer Axone aufwiesen. Der spine apparatus, ein Organelle postsynatpischer Dornenfortsätze, konnte in Synaptopodin-defizienten Tieren nach genetischer Komplementierung erfolgreich in CA3 Pyramienzellen des Hippocampus wieder hergestellt werden. Dies war nur in Anwesenheit von Synaptopodin möglich, nicht jedoch nach Transfektion mit KIBRA, einem direkten Interaktionspartner. Des weiteren konnte ein Zusammenhang von morphologischen Veränderungen am spine apparatus, hervorgerufen durch genetische Komplementierung, mit den pilzförmigen Dornenfortsätzen, in denen er vorkommt, gezeigt werden. Durch pharmakologische Inhibitoren konnten filamentöse Strukturen, die zum Aufbau des spine apparates gehören als F-aktin filamente identifiziert werden.

# 1. Introduction

## 1.1. The Hippocampus

The hippocampus belongs to the limbic system. The hippocampal architecture is organized in layers and subfields and is one of the most extensively studied structures in the brain. The subfield organization refers to different regions, consisting of the dentate gyrus, hippocampal cornu ammonis (CA) 1- 4, the subicular complex and the entorhinal cortex. Unlike the more recently evolved neocortex, layering in the hippocampus is composed of only three distinct layers: the polymorph layer, the pyramidal cell layer and the molecular layer. In CA-regions, which are themselves organized in layers or strata, the classification refers to the stratum oriens, stratum pyramidale and stratum radiatum. In the dentate gyrus, the polymorph layer is called hilus, the pyramidal cell layer stratum granulosum and the molecular layer refers to the stratum moleculare. Its C-shaped structure in cross-sections is a result of cell density variations, ranging from three to ten cell layers. The hippocampus consists mainly of pyramidal neurons with an apical and basal dendritic tree and the densely packed granule cells of the dentate gyrus, whose branching dendrites all point to the outer molecular layer. Other cell types of the hippocampus are interneurons and Cajal-Retzius cells [Förster *et al.* , 2006].

The hippocampus receives its major afferent nerve fibers via the tractus alveolaris and tractus perforans from the cortex entorhinalis, and via the fornix from the nucleus diagonalis. Efferent fibers leave the hippocampus via the fornix to the corpus mamillare, thalamus, gyrus cinguli, gyrus parahippocampalis and back to the hippocampus. This pathway is called the Papez circuit of the limbic system [Papez, 1937].
The open circuitry of the trisynaptic pathway (Figure 1.1) receives its main input from afferent fibers of layer II in the cortex entorhinalis, projecting to the outer molecular layer of the dentate gyrus through the tractus perforans. Mossy fiber axons from the dentate gyrus (first synapse) innervate proximal dendrites of hippocampal pyramidal CA3 neurons (second synapse). Axons from CA3 pyramidal cells form Schaffer collaterals and project

onto dendrites of CA1 pyramidal cells (third synapse). CA1 cells relay information back to layer V of the cortex entorhinalis.
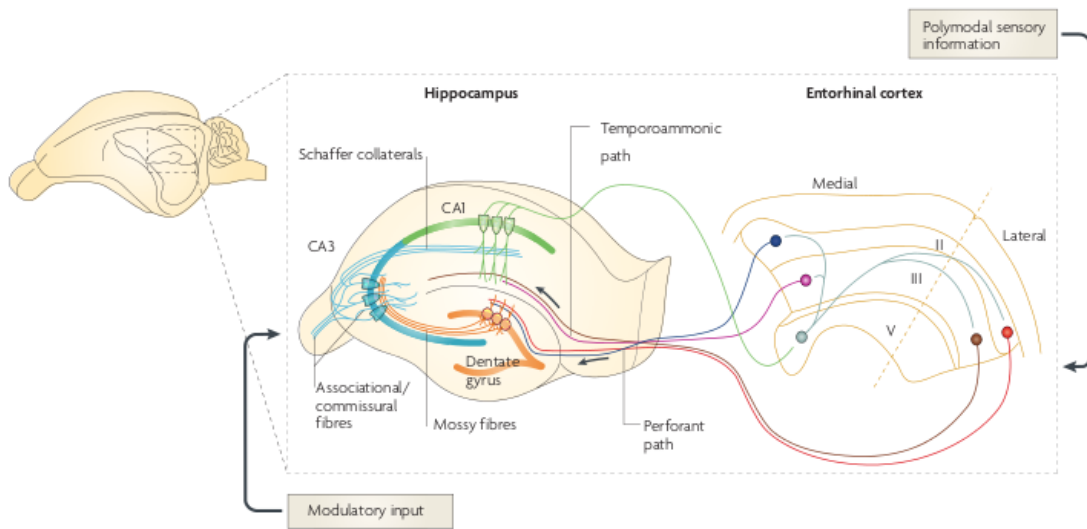


**Figure 1.1.:** The schematic diagram shows the traditional trisynaptic loop of hippocampus wiring. Neurons project from layer II of the entorhinal cortex to granule cells of the dentate gyrus. These in turn project via mossy fibers to CA3 pyramidal cells. Schaffer collaterals projecting from CA3 to CA1 transmit signals to CA1 subregion. These neurons project back to layer V entorhinal cortex. As CA1 neurons can receive direct input from layer II cells of the entorhinal cortex and project back to layer V, a second, directly interconnected pathway is established. From [Neves *et al.* , 2008].

The hippocampal formation interconnects regions in the cortex, which are involved in sensory input processing from the environment and the hypothalamus. Various biological needs, like sleep or hunger [Nicolaidis, 2006], are controlled and regulated in the hypothalamus, whereas the hippocampus deals with processing of emotion, motivation, and may contribute to self-reflection and consciousness [Bartsch *et al.* , 2011]. A second, more commonly known function associated with the hippocampus is learning, episodic memory formation and spatial navigation [Smith & Mizumori, 2006]. It has long been established that the hippocampus is involved in processing complex spatio-temporal patterns and is home to place cells [Eichenbaum, 1999]. Learning and memory formation in the hippocampus, exemplified by electrophysiological and behavioral means, has been studied extensively in various animal models. The clinical importance of hippocampal function in humans is evidenced by the fact that early symptoms at the onset of Alzheimer's disease have been linked to degenerative processes in the hippocampus [Mu & Gage, 2011].

# 1.2. Characteristics of pyramidal neurons: organization and function of dendritic spine compartments in the hippocampus

Pyramidal neurons in the mammalian forebrain, including the cerebral cortex, hippocampal CA-regions and the amygdala, share some structural and functional features including their triangular cell body, a large apical dendrite, basal dendritic trees and their capacity for compartmentalization, allowing them to integrate locally excitatory input. It has been shown that an individual pyramidal neuron receives about 30.000 excitatory and 1.700 inhibitory inputs; the latter are received primarily in perisomatic regions and proximal dendrites. Dendritic spines are the main recipients of excitatory input and provide biochemical compartments that control local synaptic signaling. Distal dendrites in the stratum radiatum and stratum oriens have a high number of spines and a high degree of dendritic arborization. Branching dendrites in the stratum lacunosum-moleculare of the apical dendrite exhibit moderate to small amounts of spines compared to other layers, but show a high percentage of perforated spines ($\sim$ 40%) and inhibitory input ($\sim$ 14% – 17%) [Megías *et al.* , 2001].

## 1.2.1. Spine Morphology

Dendritic spines can be classified according to their shape into filiform, thin, stubby or mushroom-shaped. There is a strong correlation between the size of individual spine heads, ranging from 0.01 $\mu m^3$ to 0.8 $\mu m^3$ [Hering & Sheng, 2001], and their synaptic strength [Schikorski & Stevens, 1997], [Matsuzaki *et al.* , 2001].
During the first few weeks of postnatal life, hippocampal dendrites have numerous filopodia [Papa & Segal, 1996], [Ziv & Smith, 1996]. Some filopodia become spines with synapses, while others withdraw into the dendrite to form synapses on the dendritic shaft [Fiala *et al.* , 1998].

Changes in spine head morphology are controlled by constant (de-) polymerization of actin filaments [Matus *et al.* , 2000], [Star *et al.* , 2002]. Polymerization is regulated by various molecules, including small Rho-GTPases, myosins and cytoskeletal motor proteins [Osterweil *et al.* , 2005], [Ryu *et al.* , 2006]. The source of F-actin, which is enriched in dendritic spines, can be subdivided into a dynamic pool near the postsynaptic density
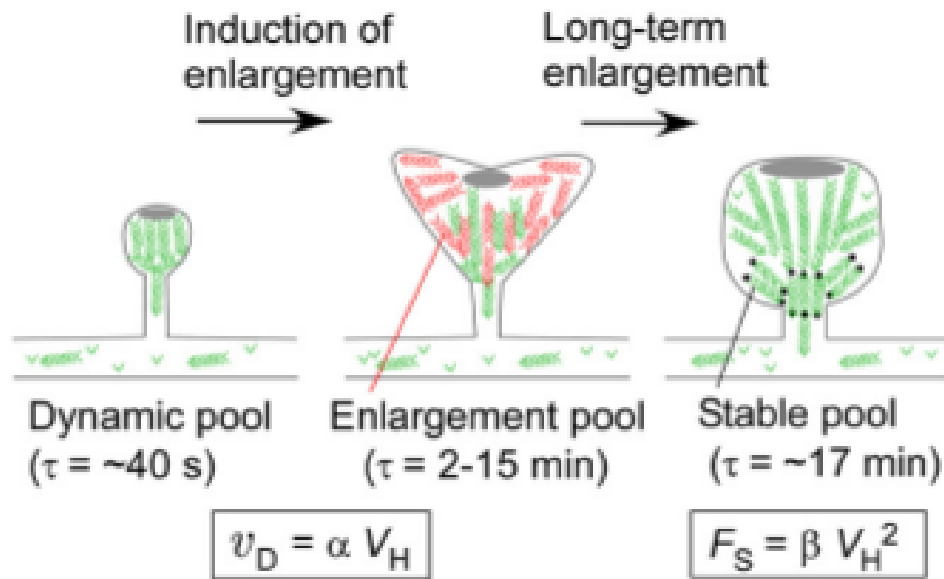
**Figure 1.2.:** Three F-actin pools, which differ in their turnover time constants (t) are present inside the spine compartment. The time constant of the dynamic pool refers to the retrograde actin flow from the plasma membrane to the cytosol. Spine head volume (V H) and velocity of flow (vD) are proportional. During spine enlargement, a second F-actin pool, the enlargement pool appears with a far slower time constant of 2-15 minutes. For spine stability after enlargement a confinement of the second pool is needed, which results in a third, well positioned pool inside the neck or base of the spine head. This third pool is much more rigid and exhibits a turnover rate of approximately 17 minutes. "The absolute amount of the stable pool (FS) is proportional to the square of the spine-head volume", as long-term enlargement requires an increase in size of the stable pool. From [Honkura *et al.* , 2008].

(PSD) with extremely short turnover rates, an "enlargement pool" and a stable pool at the base of the spine head with a slow turnover rate (Figure 1.2).

Mushroom-shaped spines are considered to be quite stable compartments [Fischer *et al.* , 2000] and changes in morphology do not occur as often as in small spines. Motility remains intact to a certain extent, but clearly diminishes over time [Oray *et al.* , 2006]. Nevertheless, the spine compartment has a great variability in shape and size. Depending on the physiological demands, spines are capable of continuously changing morphology in mature neurons. This adaption is controlled at the molecular level by the actin cytoskeleton and scaffolding of associated molecules [Hotulainen *et al.* , 2009], [Dent *et al.* , 2011], [Sommer & Budreck, 2009].

## 1.3. The spine apparatus, an organelle derived from the sER in dendritic spine compartments

In mushroom-shaped spines, actin turnover has been associated with structure and a specialized form of smooth endoplasmic reticulum (sER), called the spine apparatus [Ostroff *et al.* , 2010]. This organelle was discovered in cortical neurons over 50 years ago [Gray, 1959]. Its function has been an enigma ever since. Three-dimensional reconstruction revealed a continuation of sER [Spacek & Harris, 1997] composed of lamellar structures with interdigitating filamentous material, extending from a single tube of sER and penetrating into the spine [Holbro *et al.* , 2009].

Studies in mature hippocampal CA1 neurons have shown that the amount of sER varies in proportion with the spine size. Only 24% of small, thin spines contain some sort of sER, whereas larger mushroom-shaped spines are penetrated by laminae of sER in more than 90%, occupying surface areas of $0.12 - 2.19$ µm$^2$ [Spacek & Harris, 1997]. The sER, invading the spine head through its neck, can establish contact sites with the plasma membrane, which are stabilized by scaffolding proteins and microfilaments [Blaustein & Golovina, 2001], [Delmas & Brown, 2002]. As individual tubules of the spine apparatus sometimes stretch through the spine and occasionally connect to the postsynaptic density (PSD), a potential function of spine apparatus was proposed to deliver components of receptor subunits to the PSD [Naisbitt *et al.* , 2000].

The proportion of mature hippocampal spines in CA1 pyramidal neurons housing a fully elaborated spine apparatus comprises only $10 - 15\%$ [Spacek & Harris, 1997]. Nevertheless, spine apparatuses in mushroom-shaped spines of CA1 pyramidal neurons have been shown to associate with synaptic strength and potentiation in the hippocampus, thereby contributing to compartmentalized synaptic plasticity [Holbro *et al.* , 2009].

Synaptic plasticity can be established in excitatory and inhibitory neurons in a calcium dependent manner [Gerrow & Triller, 2010]. Several studies implicated the spine apparatus in the control of calcium transients [Vlachos, 2011], [Segal *et al.* , 2010], [Deller *et al.* , 2007]. Together with the constrictive neck, the spine apparatus may modulate calcium diffusion and clearance from spine heads (Figure 1.3). The constrictive necks allow calcium diffusion and clearance from spine heads at slower rates than in nonconstrictive compartments (thin and stubby spines) leading to longer lasting and higher calcium transients [Sobczyk *et al.* , 2005], [Majewska *et al.* , 2000], [Noguchi *et al.* , 2005], [Svoboda *et al.* , 1996]. This, in turn, may contribute to different local forms of synaptic plasticity [Müller & Connor, 1991], [Yuste & Denk, 1995], [Yuste *et al.* , 1999],

[Miyata *et al.* , 2000].
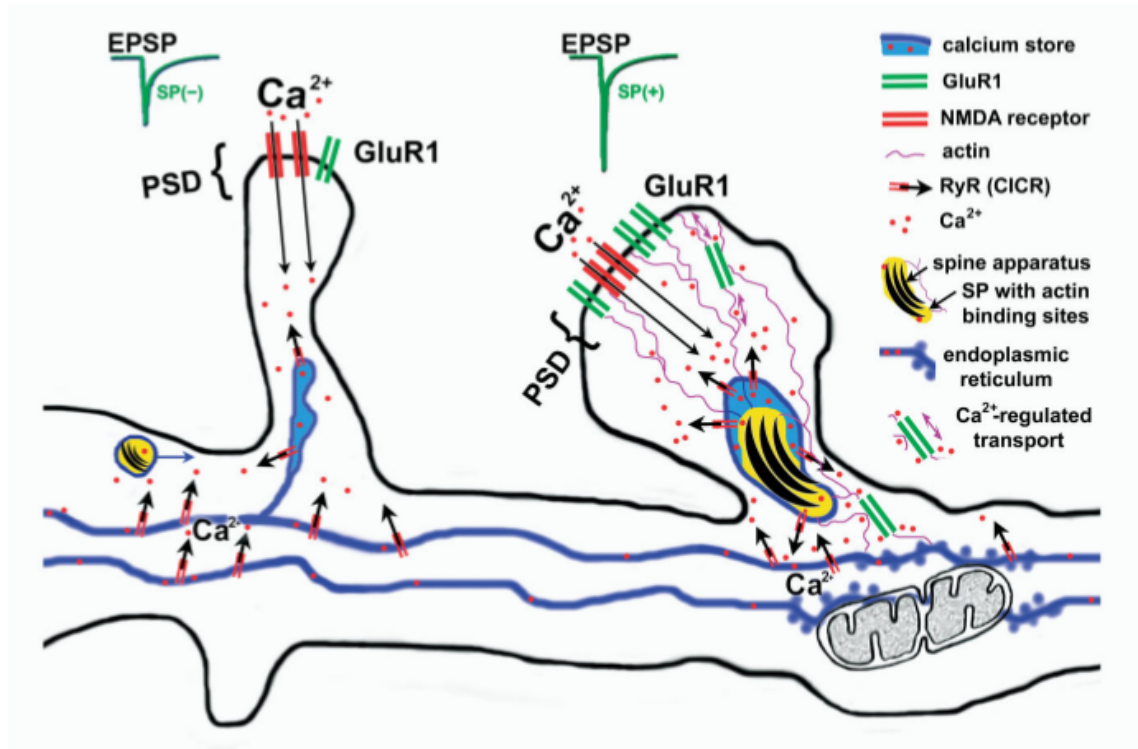


**Figure 1.3.:** Scheme on functional aspects of the spine apparatus and plasticity. Chemical activation (via inducing LTP) of NMDARs leads to a delayed accumulation of synaptopodin positive puncta in dendritic spines. This accumulation is accompanied with an increase of the spine head volume and the the addition of AMPARs and further accumulation of RyR in the spine neck. A crucial step in hippocampal postsynaptic spine plasticity. From [Vlachos *et al.* , 2009] .

The strategic position of an internal calcium store like the spine apparatus within excitatory, large spines and its relation to spine geometry could have direct effects on shaping and segregating calcium transients, perhaps affecting the propagation of calcium sparks from spines into dendritic shafts and/ or vice versa [Spacek & Harris, 1997]. Thus, spine apparatuses may serve as sensors and modulators for spines' activity dependent $[Ca^{2+}]$i kinetics and oscillations.

The lack of markers to detect or label the spine apparatus has led to delayed progress in revealing the function of this unique organelle. Two interesting observations helped to alleviate this problem and enabled scientists in this field to conduct experiments on the functional aspects of the spine apparatus. By the end of the last century, a strong correlation between the spine apparatus and synaptopodin protein was established, as

the regional distribution pattern of spine apparatuses mirrors the expression pattern of synaptopodin [Mundel *et al.* , 1997], [Deller *et al.* , 2000].

A second, more important step towards understanding the function and molecular composition of the spine apparatus, were studies in synaptopodin knockout (KO) mice [Deller *et al.* , 2003].

On the one side, the spine apparatus provides the potential for regulating actin dynamics by its associated protein synaptopodin. Furthermore, the organelle is linked to the regulation of calcium signaling in individual spines during synaptic activity. Both of these two features are refined in this organelle and lead to a high degree of morphological and functional specialization.

## 1.4. The actin associtated protein synaptopodin

Calcium release from stores produces a synaptopodin-dependent transport and accumulation of GluR1 into spines [Vlachos *et al.* , 2009]

Synaptopodins are a poorly understood family of proteins, consisting of the three different family members synaptopodin, synaptopodin 2 and synaptopodin 2-like proteins, all of which having different functional sites of activity (Figure 1.4). Synaptopodin is the founder protein of this family and was originally discovered in foot processes of differentiated kidney podocytes. Its name therefore refers to its two sites of action - synapses and podocytes.

An important observation made 15 years ago led to the identification of synaptopodin, amongst the bulk of postsynaptic molecules in dendritic spines of telencephalic neurons, as the one that is tightly associated with the spine apparatus [Mundel *et al.* , 1997].

To date, at least three different isoforms have been identified, owing to alternative splicing at the N- and C-terminal exons. Synaptopodins have little $2°$ and $3°$ structures, which is due to the extremely high content of prolin ($\sim 20$ percentage) equally distributed along the protein, thus virtually excluding the formation of globular domains [Mundel *et al.* , 1997]. This linear conformation of synaptopodin may result in a side-to-side arrangement along actin filaments.

In the brain and kidney, both in vivo and in vitro, Synaptopodin gene expression is developmentally regulated [Mundel *et al.* , 1997]. During postnatal development of dendritic spines, as well as in podocytes during nephrogenesis, synaptopodin is expressed during later and mature stages, when the typical subcellular architecture has already
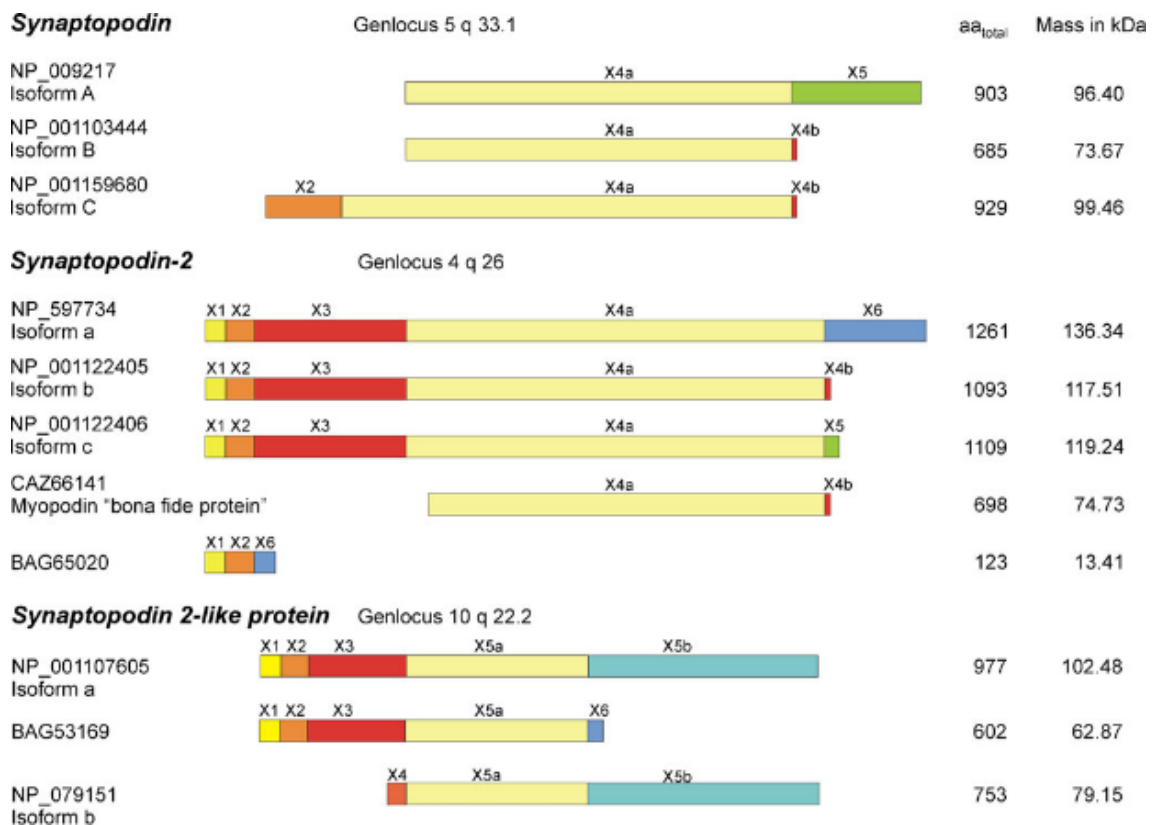
**Figure 1.4.:** Overview on protein structure of the three members of synaptopodin family and their isoforms produced by alternative splicing at C- and N-terminus. From [Chalovich & Schroeter, 2010].

been established. Within the central nervous system, synaptopodin expression pattern by hippocampal principal neurons develops during the first postnatal weeks and increases in parallel with the maturation of spines in the hippocampus. It is restricted exclusively to telencephalic synapses and is associated with the olfactory bulb, cerebral cortex, striatum, and hippocampus. In situ hybridization studies revealed that synaptopodin mRNA is found in the perikaryon only [Roth *et al.* , 2001], [Czarnecki *et al.* , 2005], which suggests that synaptopodin is transported from the cell body into spines. Thus far, actin and few other binding partners of synaptopodin have been identified. The long form that is present in the kidney specifically binds alpha 4-actinin whereas the short isoform present in the brain has two separate binding sites for alpha 2-actinin [Asanuma *et al.* , 2005]. Binding motifs of synaptopodin-2 are similar to synaptopodin but differ in the total number for $\alpha$-actinin and PPxY domains (Figure 1.5).

Furthermore, the MAK-V protein kinase [Kalinichenko *et al.* , 2011], IRSp53 [Yanagida-Asanuma *et al.* , 2007] and KIBRA [Duning *et al.* , 2008] were found to bind to synap-
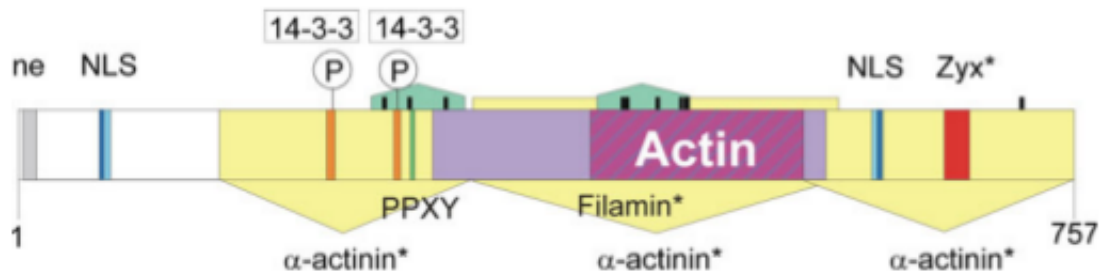
**Figure 1.5.:** Schematical drawing of the core region of mouse synaptopodin-2 encoded by exon 4a. The yellow triangles represent the $\alpha$-actinin binding domains and green domains the proline-rich stretches. The PPxY motif interacts with WW-domains, for example of the KIBRA protein. The binding domains for the 14-3-3 form target protein kinase A and calcium-calmodulin kinase II. From [Chalovich & Schroeter, 2010].

topodin.

Synaptopodin interacts in an isoform specific manner with $\alpha$-actinin, which is important for bundling and elongation process of actin filaments [Asanuma *et al.* , 2005]. Synpo-short converts $\alpha$-actinin- 2–induced short, branched actin filaments into long, unbranched parallel bundles of F-actin. This feature makes Synaptopodin an important key-regulator of actin cytoskeleton rearrangements in mature podocytes and spines (Figure 1.6) and might be important for the spine apparatus' intrinsic stability. In the absence of Synaptopodin, $\alpha$-actinin-2 induces short, branched actin filaments because of its decreased binding affinity for actin [Asanuma *et al.* , 2005].

Additionally, synaptopodin contains two PPxY motifs, which are involved in protein-protein interactions between WW domains and SH3 domains of proline- rich stretches [Chen & Sudol, 1995]. For example, the interaction with the KIBRA protein, also known as kidney and brain expressed protein (KIBRA) or WW domain-containing protein 1 (WWC1), takes place via synaptopodins' PPxY motif, which binds to KIBRAs' WW-domain.

However, the strategic and restricted location of synaptopodin at the base of the spine head indicates that it does not serve merely as a binding protein for the ubiquitous actin cytoskeleton, but may link the restricted intra-compartmental $Ca^{2+}$ sources to the abundantly present actin [Segal *et al.* , 2010], [Vlachos *et al.* , 2008].

The expression of long-term potentiation (LPT) in individual spine heads furthermore seems to be correlated with the presence of synaptopodin. It has been shown that mice
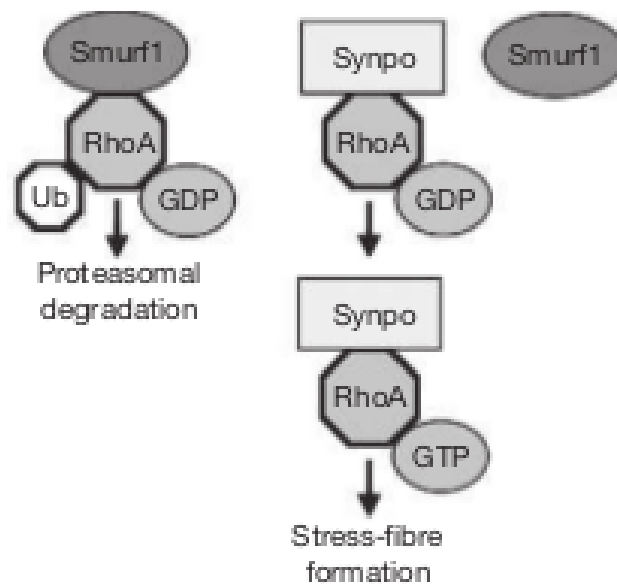
**Figure 1.6.:** A proposed model for the interaction of synaptopodin protein and RhoA signaling. On the left, the situation in the absence of synaptopodin is depicted. In the presence of synaptopodin, Smurf1 binding affinities with RhoA are competitively inhibited and targeting of RhoA for proteasomal degradation processes are blocked. Synaptopodin might be involved in the dynamic reorganization of the actin cytoskeleton by enhancing RhoA activity in specialized compartments in the kidney and the brain. From [Asanuma *et al.* , 2006].

that are deficient in Synaptopodin express reduced LPT *in vitro* and *in vivo* [Deller *et al.* , 2003], [Jedlicka *et al.* , 2008]. After induction of LTP in adult wild-type mice, an increased level of synaptopodin mRNA was observable at 75 minutes and 3.5 hours after the onset of LTP [Yamazaki *et al.* , 2001] and also present after chemical induction of LTP (Figure 1.3) after 90 minutes [Vlachos *et al.* , 2009].

These findings clearly indicate a correlation between synaptopodin and LTP, but correlating the spine apparatus with LTP is not that simple. Juvenile rats at the age of P15 are able to display normal levels of LTP [Dudek & Bear, 1993], [Trommer *et al.* , 1995], just like mature hippocampal neurons at a developmental stage, where no spine apparatuses were detectable.

## 1.5. The cisternal organelle in the axon initial segment (AIS)

The cisternal organelle in the axon initial segment (AIS), exhibits many structural homologies to the dendritic spine apparatus [Peters *et al.* , 1968], [Kosaka, 1980], [Benedeczky *et al.* , 1994]. Both organelles seem to originate from the sER and provide a high degree of local specialization. Additionally, both have striking morphological similarities in the composition of stacks of flat and aligned membranous cisterns, separated by electron dense material [Palay *et al.* , 1968], [Peters *et al.* , 1968] ,[Somogyi *et al.* , 1983] and sometimes found to be in contact with the plasma membrane [Benedeczky *et al.* , 1994], [Tarrant & Routtenberg, 1979]. Furthermore, the dendritic spine apparatus and the cisternal organelle can be tracked by Synaptopodin-immunoreactivity assays, as synaptopodin co-precipitates with the axonal cisternal organelle and the dendritic spine apparatus. The protein synaptopodin specifically labels the interdigitating filamentous material in both organelles, which seems to be responsible for the organelles' coherence or cohesion, as shown by immunogold- labeling of preembedded electron microscopic analysis. Taken together these results reconfirm that synaptopodin is a molecular component of the cisternal organelle [Bas Orth *et al.* , 2007] and the spine apparatus. In synaptopodin-deficient mice, spine apparatuses [Deller *et al.* , 2003] and cisternal organelles are absent, however, in the axon initial segment and in spines, some rudimentary forms of smooth endoplasmic reticulum (single, detached or scattered stacks) are occasionally observable in the absence of synaptopodin (Bas Orth, C. inaugural dissertation, p. 52, (2007) and own observations). Even so, these rudimentary forms of sER did not match the criteria of fully established and functional spine apparatuses or cisternal organelles. Furthermore, both organelles have been implicated in local calcium trafficking, as has been shown for the spine apparatus [Fifková *et al.* , 1983], [Sharp *et al.* , 1993], [Korkotian & Segal, 1998] and the cisternal organelle [Benedeczky *et al.* , 1994]. Furthermore, synaptopodin may be responsible for recruiting calcium sources to the AIS [Bas Orth *et al.* , 2007] and regulates the presence of ryanodine receptors (RyR) in the spine neck [Vlachos *et al.* , 2009]. This implies integrity of neurons' basic intrinsic function: communication between and within a cell by local integration of information. Taken together, both organelles share many structural and functional properties and evolve from the same parent organelle, the sER, with which they share fundamental features. Their specialization in different neuronal parts may result from biological adaption. More practically, compartmentalization of calcium signaling provides diverse

advantages, as diffusion processes are much slower in the bulk cytosol. Additionally, the sER membrane can be used for recharging during refractory time periods or calcium buffering, for example by the highly conserved sarcoplasmatic/ endoplasmatic (SER) $Ca^{2+}$ ATPase (SERCA) type $Ca^{2+}$ pumps, which might be localized in the cisternal organelle, as shown by immunoreactivity [Benedeczky *et al.* , 1994].

Structural differences are manifested in its location and relative frequency of occurrence. As the sER in the axon is less compartmentalized than in dendritic regions, the axonal counterpart of the dendritic spine apparatus is located directly beneath the plasma membrane, often in close proximity to GABAergic terminals [Kosaka, 1980], [Benedeczky *et al.* , 1994]. In mature neurons the cisternal organelle was found to be a regular and common component, being present in almost every AIS of telencephalic principal neurons (Bas Orth, inaugural dissertation, p. 73, (2007)). In the entire AIS with approx. 20 -40 µm length, an average of 3.2 cisternal organelles per 10 µm AIS were present. The spine apparatus in contrast, occurs restrictively in a subset of mushroom-shaped spines (10 - 15 percentage). The cisternal organelle in the AIS has been shown to house SERCA pumps in its membrane [Benedeczky *et al.* , 1994] and functions as an IP$_3$R store [Sánchez-Ponce *et al.* , 2011], whereas the spine apparatus has been associated with RyR governed $Ca^{2+}$ release [Vlachos, 2011].

Nevertheless, the role of the cisternal organelle in the secretory pathway remains an enigma as basic questions concerning its contribution in protein processing have not been an issue of investigation and there are many open questions.

## 1.6. Role of CAMs in synaptic maturation and synaptogenesis

The formation of synapses between neurons in the hippocampus is based on the formation of contacts between the pre- and the postsynaptic components. Little is known about the exact molecular details of synaptogenesis, because the complexity of neuron-neuron interaction is driven by a variety of different neurotransmitters, which are employed in single synapses. The variety of neurotransmitters have to arrange a critical step in development, the inhibitory or excitatory coupling leading either to hyperpolarization or depolarization of the postsynaptic partner. A second factor that makes studies on synaptic connectivity difficult, is the fact that the central nervous system is a non-static system which undergoes changes permanently. Other components, once coupled, can undergo

elimination or reassembly in response to experience. To understand the complexity of the factors leading to recognition and an interplay or coupling of the appropriate synaptic partners to their targets, neuroscience researchers have focused on identifying (families of) molecules and different contributors. Intensively studied candidates are classical cell adhesion molecules (CAM) like integrins, ligand-gated channels and transsynaptic cell-adhesion molecules which are all team players in synaptogenesis. Nevertheless, whether the basic underlying mechanism to guide synaptogenesis is a hierarchical one or is induced by parallel pathways remains unclear [McAllister, 2007].

The first contact between both sides of a synapse is often established by increasing filipodia from axons or dendrites into the external space. It has been shown in vitro and in vivo essays that filipodia dynamics cease and stabilization process is initiated, once filipodia have contacted potential synaptic partners [Jontes & Smith, 2000] and formed into synaptic structures [McAllister, 2007]. Neurotransmitter release is likely to play a role in the stabilization of contact formation processes [Tashiro *et al.* , 2003].

After establishing a first contact via dendritic or axonal filipodia protrusions, pre- and postsynaptic proteins have to be assembled and positioned in the emerging synapse by the dynamic network of actin cytoskeleton [Frost *et al.* , 2010]. Stabilization of filipodia and rapid recruitment of proteins requires transsynaptic interaction, which is provided by "synaptogenic" or "synapse-organizing" molecules [Biederer *et al.* , 2002].

Membrane-spanning molecules, especially the transsynaptic adhesion molecules like Ig-domain proteins, are perfect candidates for establishing pre- and postsynaptic communication during the formation process of synapses. In the 1980s several cell adhesion molecules (CAMs) were identified as factors that promote neuronal adhesion to substrates and may provide a help to understand complex wiring patterns. Membrane-spanning molecules contribute to communication between pre- and postsynaptic sides of the synapse, as neuronal interaction is regulated by activity. Cell adhesion molecules are such contributors with extracellular ligand-binding domains. Theses domains are important for cell-cell recognition during development. CAMs expressed by neurons can be grouped into four different categories: integrins, cadherins, neuroligins and immunglobulin superfamily CAMs [Benson *et al.* , 2000], [Yamagata *et al.* , 2003]. CAMs can bind to the same family members (homophilic) or to other members (heterophilic) via their extracellular domains. Their C-terminus is associated either directly or indirectly to the actin cytoskeleton and can potentially initiate changes in the morphology of spines. On a long-range, CAMs are potential candidates for retrograde transsynaptic signaling and might play a role in long-term actively driven transport by motor proteins in neu-

ronal sER to the nucleus. The Ig superfamily proteins (IgSF) are important guidance cues that have diverse roles in regulating correct neuronal wiring in the nervous system. Besides serving as attractant and repellant, they can also regulate axonal fasciculation. L1CAM protein, a member of the IgSF, contains a large extracellular domain structure that includes modularly arranged six Ig-like and five fibronectin type-III domains. These extracellular domains allow homophilic and heterophilic interactions with numerous extracellular ligands and proteins. Homophilic L1CAM binding leads to the recruitment of ankyrins (Figure 1.7), which in turn plays a role in cell-cell adhesion, axonal growth and fasciculation.
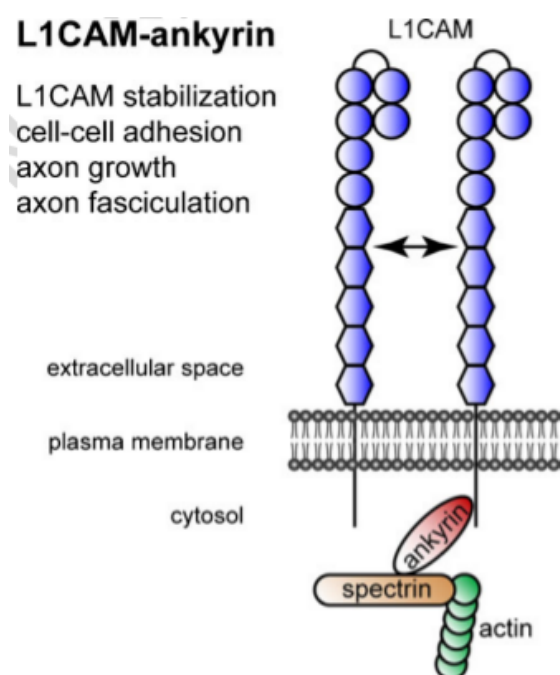


**Figure 1.7.:** Model for the homophilic binding of L1CAM to the actin cytoskeleton via ankyrin. From [Schäfer & Frotscher, 2012].

The L1 protein is found in axons and plays a critical role in neuronal migration, axon growth and synapse formation in the developing nervous system. Missense mutation in the extracellular domains cause severe neurological disorders, inherited in an X-linked recessive pattern and shortly referred to as L1-syndrome.

## 1.7. Aims of the thesis

Endeavor of this study was to shed light on morphological features concerning the presence and composition of the spine apparatus in a mature network of CA3 pyramidal cells. We used confocal imaging and a combination of single cell electroporation (SCEP) and immunoelectron microscopy (IEM) as approaches to manipulate and unravel open questions of this still enigmatic organelle in long-term organotypic slice cultures of synaptopodin KO and C57BL/6 mice. Therefore, this thesis work addressed the following major questions:

1. Does overexpression of the axonal cell adhesion molecule L1CAM promote axonal branching in CA3 pyramidal neurons and is this model system sufficient to evaluate human loss-of-function L1CAM mutations?

2. Is it possible to rescue spine apparatus formation in synaptopodin-deficient mice through restoration of synaptopodin expression at the single-cell level?

3. What are the consequences of elevated and restored synaptopodin levels for spine apparatus morphology?

4. How is spine apparatus morphology affected by pharmacological disruption of neuronal activity and actin (de-) polymerization?

5. Do changes in spine apparatus morphology correlate with morphological changes in mushroom-shaped spines?

# 2. Material and Methods

## 2.1. Animals

The mice used in the experiments were obtained from the breeding stock in the animal facility (ZBMZ Freiburg) of Dr. Alexander Drakew. Animals were genotyped by means of PCR using tail biopsies. Experiments were conducted on wild-type (C57BL/6) and transgenic Synaptopodin knockout (Synpo KO) mice in accordance with German federal laws relating to animal experimentation. Every effort was made to minimize animal suffering.

## 2.2. Organotypic hippocampal slice culture preparation with membrane interface method

Organotypic slice cultures from transgenic Synaptopodin knockout and C57BL/6 mice were prepared from six to seven day-old (P6/P7) neonates. Slices were co-cultivated in vitro in 6-well culture trays containing membranes of Millicell-CM culture plate inserts (Millipore, Schwalbach, Germany) and kept for 21 days in culture (21 DIV). After this period the slices were transfected by Single-cell electroporation (SCEP).

## 2.3. Dissection procedure

Neonatal mice pups were decapitated and the skin was removed. The skulp was opened by cutting from the foramen magnum along its caudal to rostral axis. The brain was removed from the skulp and transferred to a petri dish containing ice-cold Preparation medium which is placed on a pre-cooled metal block. The hippocampi with their entorhinal cortices were dissected by cutting off the tip of the semicircular part of the forebrain.

The cerebellum was removed and cerebral hemispheres were sliced in two parts, excising the diencephala and trimming the hippocampi together with entorhinal cortices in each of the hemispheres. Both hippocampi and entorhinal cortices were aligned on a membrane of a McIllwain automatic tissue chopper and cut perpendicular to its length axis in 300 μm slices. Slices were collected with a humified spatula and transfered into a small petri dish containing ice-cold Preparation Medium and visually inspected under a stereo microscope. Virtually intact slices were selected and individually placed onto sterile, humified semi-porous Millicell-CM culture plate inserts containing 1.0 ml of Incubation medium. To increase their longevity, slices were aligned for co-culturing by positioning CA3-subregions and dentate gyri opposite of each other under a stereo microscope. Slices were subsequently transferred and maintained at 37°C in 5% $CO_2$ humified incubator with complete medium change three times a week for 21 days *in vitro*. Slices were inspected any time before changing the Incubation medium using a stereo microscope and those displaying necrotic features were discarded. For a more detailed protocol of slice preparation see [Förster *et al.* , 2005].

## 2.4. Immunhistochemistry for overexpressed human L1CAM in organotypic hippocampal slice cultures

Slice cultures were washed in phosphate buffered saline (PBS) and fixed in 4% Paraformaldehyde (PFA) one hour at room temperature. The underlying membrane surrounding the slice culture was carefully excised with a scalpel under a stereo microscope and slice cultures were blocked and permeabilized for two hours in freshly prepared blocking solution. Normal Goat Serum Blocking Solution was prepared as following:

| | |
|---|---|
| Normal Goat Serum (blocking) | 5% |
| Bovine serum albumin (stabilizer) | 0.5% |
| Triton X-100 (penetration enhancer) | 0.1% |
| Tween 20 (detergent and surface tension reducer) | 0.05% |
| PBS, pH 7.2 | 0.01 M |

Mix and store at 4°C.

Primary antibodies were diluted in blocking solution, applied and slices were incubated over night at 4°C on a shaker. The following primary antibodies specific to human L1CAM and eGFP were used:

Rabbit Anti-Human L1 (4034) with a dilution factor of 1:1000.
Mab Anti-eGFP (map 3580; Millipore) with a dilution factor of 1:500.

Slice cultures were washed after incubation period in PBS with 0.02% Triton X-100 four times 15 minutes each in the dark at 4°C. Fluorophore labeled secondary antibodies were diluted in blocking solution, applied and incubated over night at 4°C. The following secondary antibodies were used for human L1CAM/eGFP double-immunhistochemistry: Goat Anti-Rabbit cy3 with a dilution factor of 1:1000. Goat Anti-Mouse Alexa 488 with a dilution factor of 1:500. Slice cultures were washed after incubation period in PBS with 0.02% Triton X-100 four times 15 minutes at 4°C. Then, slice cultures were incubated ten minutes in 4',6-diamidino-2-phenylindole (DAPI) to stain DNA or the nucleus and washed in PBS. For mounting, coverslips were dipped into ddH$_2$O 18 MΩ using fine forceps. Subsequently, the excised membrane was transferred into a Petri dish containing a 1:1 mixture of PBS and ddH$_2$O 18 MΩ. A few drops of detergent Triton X-100 were applied to lower surface tension of the liquid. With a brush the slice culture and the underlying membrane inside the Petri dish were positioned onto the glass slide and covered with 20 − 30 µl of Fluoromount. Excess amounts of Fluoromount were absorbed using Kim wipe tissues, the cover-slip sealed with commercial nail polish and stored at 4°C in a microscope slide storage box.

## 2.5. PEI-mediated transfection of NSC-34 cells

The Mouse Motor Neuron-Like Hybrid Cell line NSC-34 was cultured and transfected essentially as described (Marx, M. et al., Neurogenetics, (2012)).

We used the following antibodies for Synaptopodin staining:

Primary:     Rabbit Anti-Synaptopodin (SE-19, 1:2000, Sigma-Aldrich)
Secondary:   Alexa Fluor 647 Goat Anti-Rabbit (IgG far-red, 1:500, Sigma-Aldrich)

## 2.6. Plasmid prepapration

Competent bacteria (*E. coli* DH5alpha, Invitrogen) were transformed with recombinant plasmids as described by the manufacturer. Transformed bacteria were positively selected on LB agar plates containing Kanamycin (50 µg/ml) or Ampicillin (100 µg/ml) as an antibiotic. Single colonies were inoculated in 50 ml (MidiPrep) or 100 ml (MaxiPrep) LB medium containing antibiotics and incubated on a rotating shaker for 16 hours at 37°C. Plasmids were prepared using Plasmid preparation Kits from Promega or Quiagen according to the instructions of the manufacturer. The DNA concentration was determined using a spectrometer (inoLab WTW) and adjusted to 1 µg/µl.

## 2.7. Preparing Lysogeny broth-Medium (LB-Medium)

**Table 2.1.:** Composition of LB-Medium based on a final volume of 1 liter

| Component and final concentration | Amount to add per 1 l |
| --- | --- |
| Bacto-Tryptone | 10 g |
| Bacto-yeast Extract | 5 g |
| NaCl | 10 g |
| ddH$_2$O 18 MΩ | q.s. 1 l |

Components were dissolved in ddH$_2$O 18 MΩ and final volume was adjusted. LB-Medium was sterilized by autoclaving.

## 2.8. Preparing Luria Bertani Agar Plates (LB-Agar plates)

Suspend 35 g of LB-Agar powder (Sigma-Aldrich) in 800 ml ddH$_2$O and adjust final volume to 1 liter by adding ddH$_2$O 18 MΩ. Heat to boiling while stirring to dissolve all ingredients completely. Sterilize by autoclaving for 15 minutes at 121°C. For selecting single clones with Kanamycin- resistance add Kanamycin at a concentration of 50 µg/ml and pour the medium into sterile petri dishes and allow it to cool off.

## 2.9. Incubation- and Preparation Media

**Table 2.2.:** Composition of Incubation- and Preparation Media based on a final volume of 100 ml

| Component and final concentration | Preparation Medium | Incubation Medium |
| --- | --- | --- |
| MEM (2x concentrated) | 50 ml | 25 ml |
| Aqua ad iniectabilia (sterile) | 49 ml | 21 ml |
| Normal Horse Serum (NHS) | - | 25 ml |
| Basal Medium Eagle (BSE) | - | 25 ml |
| Glucose 20% w/v (sterily filtered) | - | 3.125 ml |
| Glutamax 20 mM | 1.0 ml | 1.0 ml |
| NaOH 1 M | 940 µl | 300 µl |

Solutions were mixed and pH was adjusted at room temperature to 7.25 − 7.30 for Incubation Medium or 7.30 − 7.35 for Preparation Medium just before usage.

## 2.10. Single-cell electroporation (SCEP)

The SCEP technique is an excellent method for manipulating selected cells in an otherwise natural environment. Neighboring cells remain unaffected by any kind of plasmid transfection and can be used easily as a reference system or control. The SCEP set-up is composed of an oscilloscope, a headstage with a headstage holder, an Axoproator, a monitor and a joystick (Figure 2.1). The joystick allows to control horizontal, vertical or axial movements of the headstage in a velocity-based manner. With the Axoporator different parameters which influence the pulse-application like pulse-duration and pulse-width can be modulated.
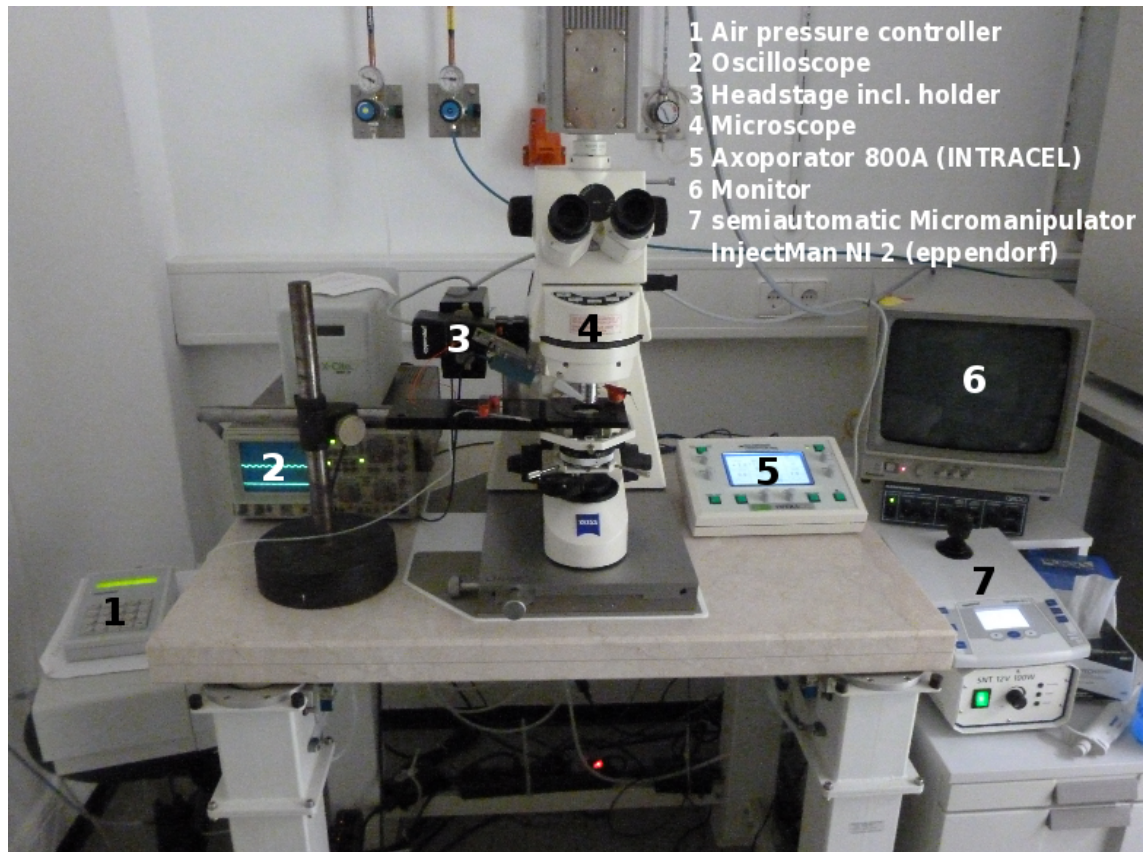
**Figure 2.1.:** The SCEP-set up is composed of an oscilloscope (2), a microscope (4) with objective lenses of 4x and 63x magnification. Application of air pressure from the controller (1) to the headstage holder prevents reflux of the construct due to capillary action. Different parameters like train and width of the applied rectangular pulse can be chosen with the Axoporator (5). The headstage holder (3) can be moved with a joystick of the semiautomatic Micromanipulator (7) at multiple velocities horizontally, vertically and axially, which can be followed on the monitor (6).

## 2.11. Transfection Medium

**Table 2.3.:** Composition of Transfection Medium based on a final volume of 500 ml

| Component and final concentration | Amount to add per 500 ml |
| --- | --- |
| D-PBS, 0.1 M | 487.5 ml |
| Glucose 20% w/v | 12.5 ml |

Transfection Medium was sterilized by filtration using a vacuum pump (Millipore XF 5423050) and pH adjusted to 7.30 - 7.40.

## 2.12. Electroporation Buffer for adjusting plasmid-DNA

As plasmid-DNA concentration is a critical factor for successful transfection using SCEP, a final plasmid concentration was adjusted to 1.0 µg/µl by diluting the DNA with Electroporation Buffer.

**Table 2.4.:** Composition of Electroporation Buffer (4-fold concentration) at a final volume of 50 ml

| Component and final concentration | Amount to add per 50 ml |
| --- | --- |
| NaCl, 138.0 mM | 1.6 g |
| KCl, 5.4 mM | 0.08 g |
| $MgCl_2$, 1.0 mM | 57 µl from 3.5 M stock |
| Hepes, 5.0 mM | 0.24 g |
| $ddH_2O$ 18 M$\Omega$ | q.s. 50 ml |

The buffer was sterilized by filtration and pH adjusted to $7.30 - 7.40$.

## 2.13. Single-cell electroporation (SCEP)

After 21 days in culture, slices were selected for SCEP. As criteria served a virtually intact morphology as judged by the integrity of the CA pyramidal cell layers and the granule cell layer of the dentate gyrus. The Axoporator parameters were set to a frequency of 100 Hz, a voltage of -2.2 V, a train of 2.0 s and a width of 2.0 ms. The time window

for giving the electric pulse has to be selected with regard to the size of transfection construct, as mass transfer of macromolecules depend on size and permeability. The membrane with the slice culture was inserted into the well-holder and filled with 2.5 ml of Electroporation Buffer (bathing solution). The well-holder was inserted under UV-light condition in the microscope dish and conductance was established. Borosilicate glass capillaries (Harvard Apparatus LTD + Filament, 1.2 mm outer diameter x 0.69 mm inner diameter) were pulled with a micropipette puller (parameter settings: heat = 770, velocity = 17, time = 255) and the filament-fused glass-pipette was filled with 2.5 − 3 µl of Synaptopodin-eGFP construct. The fluid-filled capillary was screwed onto the headstage by inserting the silver chlorinated electrode into the diluted plasmid construct and the headstage was screwed onto its holder. With a joystick the capillary was moved into the bathing solution. As soon as the tip of the pipette meets the surface of the bathing solution, the input resistance is a critical parameter to be checked. At input resistances higher than 20 M$\Omega$, the construct will hardly be able to diffuse out of the pipette, according to air pockets or viscosity constrictions. If the input resistance falls below a certain level of approximately 5 M$\Omega$, the tip of the glass capillary may be broken or damaged. Both cases lead to very poor or no success. By navigating the joystick with one hand and lowering the objective of the microscope with the other, the capillary can be positioned in close vicinity to any cell of interest. The tip of the capillary should always be kept in focus during this process to avoid damaging of the capillary and/ or slice culture. Whenever the outer membrane of a cell body is touched, the transmembrane potential increases, as can be directly observed on the display of input resistance control. As soon as the input resistance has reached a well defined threshold, a rectangular pulse of -2.2 V is applied in close vicinity to the outer membrane. Small hydrophilic pores form and allow the negatively loaded construct to pass the membrane and enter the cell of interest. To withdraw the capillary, the Axoporator has to be switched to 'axial' movement. Once an appropriate distance to the cell of interest is achieved, 'axial' position is switched off and a new cell body for electroporation can be chosen. Slice cultures were subsequently washed with incubation medium a few times after the end of slice culture transfection, to flush away residual Electroporation Buffer. It is possible to manipulate up to 50 - 100 cells per slice culture in a time-frame of 20 minutes. After 20 minutes slice culture should be washed and placed back into the incubator.

Success of SCEP strongly depends on the vitality of the selected cell, the integrity of slice culture, the distance of the glass capillary tip to the cell membrane and the subsequent transmembrane potential. eGFP-fluorescence was checked daily starting one

day after transfection using a fluorescence microscope (Olympus MO81). A successfully transfected green fluorescent pyramidal neuron (Figure 2.2, right) tagged to the Synaptopodin-eGFP construct is depicted and a second neuron (Figure 2.2, left), potentially an excitatory spiny stellate interneuron can be seen. Only successfully transfected pyramidal neurons from CA3 region, which exhibit bright green-fluorescence for three consecutive days after transfection were further analyzed. Interneurons were not taken into consideration.
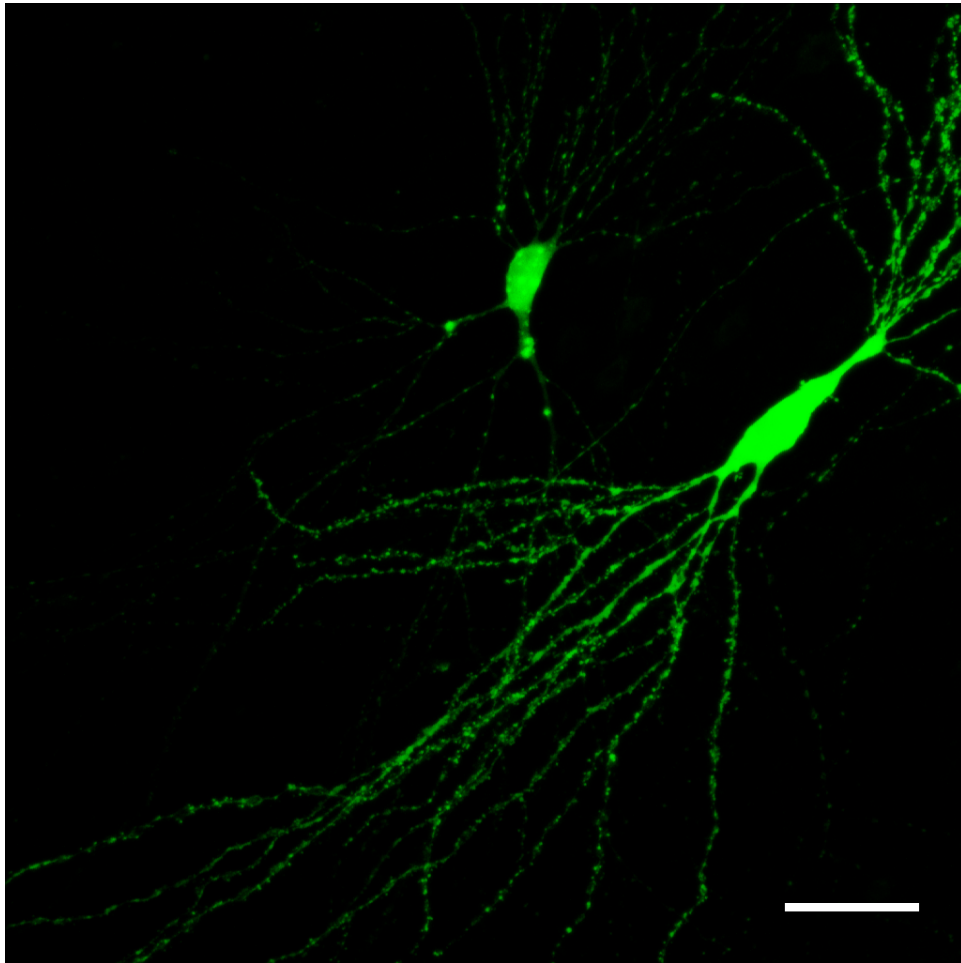


**Figure 2.2.:** Confocal z-stack of a CA3 pyramidal neuron transfected with eGFP-Synaptopodin construct using SCEP. A branching basal dendritic tree extends from the base of the cell soma. In the background a second transfected cell, probably an excitatory spiny stellate interneuron, is depicted. Scale: 50 μm.

## 2.14. Plasmid construct

The construct, which was used in the present study to transfect individual CA3 pyramidal neurons in slices from Synpo KO and C57BL/6 littermates at DIV 21 ($+$/- one day) refers to the short form of Synaptopodin in accordance with previous publications [Mundel et al. , 1997], [Asanuma et al. , 2005], [Bas Orth et al. , 2007] and will be referred to as "synpo short". The 100 kDa isoform of the synpo short splice variant, which is present in the brain, has a cDNA coding sequence of 2070 bp corresponding to 690 amino acids. Synpo-short has, compared to the 110 kDa isoform present in the kidney, a distinct C-terminus lacking amino acids 1 – 244 and differs in the 3' coding region and 3' untranslated region [Asanuma et al. , 2005], [Chalovich & Schroeter, 2010].

## 2.15. Preparation of buffers and solutions for Pre-embedding Protocol using Immuno-Electron Microscopy

All buffers and solutions were freshly prepared, dissolved or diluted in the appropriate volume of $ddH_2O$ 18 M$\Omega$ and pH adjusted to 7.40 before usage.

**Table 2.5.:** Composition of 0.2 M Sørenson's Phosphate Buffer (0.2 M PB) based on a final volume of 600 ml

| Component and final concentration | Amount to add per 600 ml |
| --- | --- |
| $NaH_2PO_4$ ● $H_2O$ (Sodium dihydrogen phosphate Monohydrate) | 4.14 g |
| $Na_2HPO_4$ (Di-Sodium hydrogen-phosphate anhydrous) | 14.2 g |
| $ddH_2O$ 18 M$\Omega$ | q.s. 600 ml |

Sørenson's Phosphate Buffer (0.1 M PB) was obtained by diluting 0.2 M PB and $ddH_2O$ 18 M$\Omega$ in a mixing ratio of 1:1.

**Table 2.6.:** Composition of 50 mM Tris-buffered-saline (50 mM TBS) based on a final volume of 200 ml

| Component and final concentration | Amount to add per 200 ml |
| --- | --- |
| Tris-base, 50 mM | 1.515 g |
| NaCl, 150 mM | 2.19 g |
| ddH$_2$O 18 M$\Omega$ | q.s. 200 ml |

**Table 2.7.:** Composition of 25 mM Phosphate buffered saline (25 mM PBS) based on a final volume of 1 liter

| Component and final concentration | Amount to add per 1 l |
| --- | --- |
| NaCl, 137 mM | 8 g |
| KCl, 2.7 mM | 200 mg |
| Na$_2$HPO$_4$O (dibasic, anhydrous), 10 mM | 1.44 g |
| KH$_2$PO$_4$O (monobasic, anhydrous), 2 mM | 240 mg |
| ddH$_2$O 18 M$\Omega$ | q.s. 1 l |

**Table 2.8.:** Composition of Cryoprotectant based on a final volume of 200 ml

| Component and final concentration | Amount to add per 200 ml |
| --- | --- |
| PB, 0.1 M | 80 ml |
| Glycerol, 1.4 M | 10% |
| Sucrose, 2.3 M | 25% |
| ddH$_2$O 18 M$\Omega$ | 80 ml |

Dilute 0.1 M PB in ddH$_2$O 18 M$\Omega$ in a mixing ratio of 1:1 for a final concentration of 50 mM PB. Mix 50 mM PB with 10% Glycerol and 25% Sucrose and dissolve solution on a stirrer.

## 2.16. Toxin application

The following neurotoxins were freshly prepared before usage, mixed with appropriate amounts of incubation medium (1 ml per well) and chronically bath-applied directly after SCEP transfection for three consecutive days

| Neurotoxin | Stock concentration | Working concentration | Dilution factor for 1 ml Incubation medium |
|---|---|---|---|
| TTX (sodium-channel blocker) | 1 mM | 1 µM | 1 µl |
| ROCK-inhibitor Y-27632 | 10 µM | 10 nM | 1 µl |
| *Clostridium difficile* toxinB | 1.49 µM | 2 pM | 1.34 µl |
| Latrunculin A | 63.211 mM | 2.5 µM | 39.55 nl |

## 2.17. Pre-embedding protocol for Immuno-electron microscopy

Successfully transfected neurons in slice cultures were pre-fixed three days after transfection for 24 hours in 4% PFA with 0.1% Glutaraldehyde (EM grade, 25%). Slices were washed one hour in 0.1 M PB and incubated in a cryoprotective medium (diluted with dH$_2$O 18 MΩ in a mixing ratio of 1:1) for 30 - 60 minutes. Subsequently slices were transferred to undiluted cryoprotective medium for one hour. To separate slices from their membranes, they were transferred to fresh cryoprotective medium and carefully detached with a brush under a stereo microscope. Slices were subsequently transferred each onto a grid with plastic walls. These bins, made to specification, were dipped for five to six seconds inside a plastic box filled with Isopentane or 2-Methylbutane. The plastic box was placed inside a polystyrene box filled with liquid nitrogen under a fume cupboard for cryopreservation of slices. As soon as slices turn whitish, they were transferred back to a 6-well culture tray with cryoprotective medium. Subsequently, slices were washed 10 minutes in 0.1 M PB and 15 - 30 minutes in 50 mM TBS each. Unspecific labeling was blocked for one hour with 20% Normal Goat Serum (NGS) in 50 mM TBS. Slices were incubated 24 hours at 4°C on a rotation shaker with primary antibody (Fab conjugate 1.4 nm Nanogold$^©$ gold-antibody, Nanoprobes) diluted 1:500 in 50 mM TBS with 2% NGS. Next day, slices were washed for one hour in 50 mM TBS. Incubation was conducted in 2° gold-coupled secondary antibody (Clontech Living colors, full length; 1.4 nm, polyclonal, 1:100) in 50 mM TBS with 2% NGS over night at 4°C on a rotary shaker. Slices were washed for 30 minutes in 50 mM TBS. Post-fixation of slices for ten minutes was performed in 1% Glutaraldehyde in 25 mM PBS. Subsequently, slices were washed in 25 mM PBS for at least 15 minutes and in dH$_2$O for one minute. Silver intensification was performed with HQ SILVER™ ENHANCEMENT KIT (Nanoprobes). In a 24-well culture tray two drops of solution A and two drops of solution B were mixed

thoroughly with a round bended glass pasteur pipette per well before adding and mixing two drops of solution C. Slices were transferred into the mix and incubated in a drawer for seven minutes.
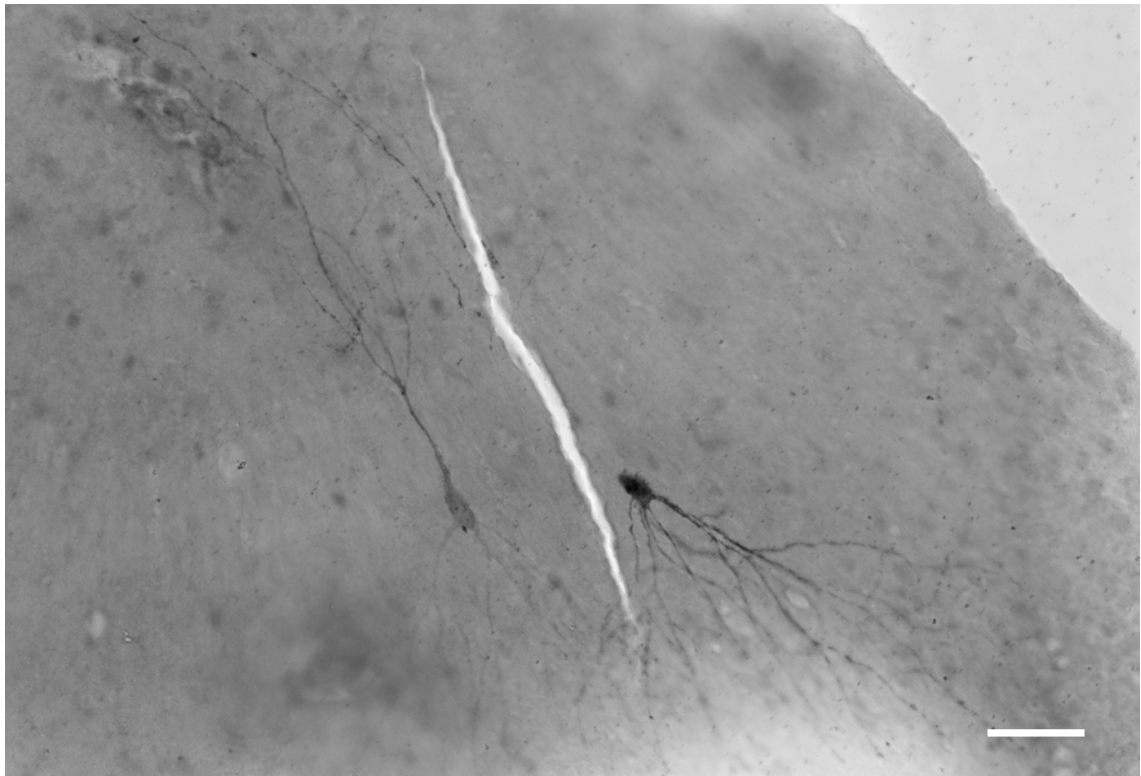


**Figure 2.3.:** light microscopic image of two successfully transfected CA3 pyramidal cells after pre-embedding for Immuno-electron microscopy. Scale: 100 μm.

After silver intensification, slices were washed in $ddH_2O$ and in 0.1 M PB for 10 minutes each and checked for positively stained neurons under a stereo light microscope (Figure 2.3). Osmification/post-fixation took place in 0.5% osmium tetroxide (one part of 4% osmium solution was mixed with seven parts of 6.86% sucrose) for 40 minutes under a fume hood. Slices were washed four to six times in 0.1 M PB five minutes each. Further steps were carried out in labeled glass snap-cap vials under a fume hood. For dehydration steps and incubation with uranyl acetate make sure to cap the vials to prevent slices from falling dry. Dehydrate slices first in 50% and 60% ethanol for 10 minutes each, after dehydrating them in 70% ethanol containing 1% uranyl acetate for 35 minutes. Snap-cap vials should be covered with aluminum foil during incubation time, as uranyl acetate is light sensitive. Further dehydration takes place in an ascending ethanol series of 90, 95 and (2x) 100% ethanol for 10 minutes each. Dealcoholize slices

two times in propylene oxide for 5 minutes each and incubate them in a 1:1 mixture of propylene oxide and Durcupan for 45 to 60 minutes before Durcupan embedding. Change Durcupan resin after 45 to 60 minutes and leave vials covered with parafilm and plastic cap either over night at room temperature or for two days at 4°C. Open vials were put for 20 minutes on a heating block to slightly warm up the resin for increasing the viscosity and to avoid irreversible resin polymerization. Transfer warmed slices with a toothpick to mold release agent coated glass slides for flat embedding. Small metal weights were put on top to hold cover slips in place. Slides were transferred into a 56°C heating furnace for two days to let the resin polymerize.

For re-embedding into gelatin capsules, stained neurons were cut out of the resin block with a razor blade. Capsules filled with Durcupan for polymerization were transferred in a 56°C heating furnace for another two days. The resin block was re-sliced in trapezoid slices with a glass blade, cut with a diamond blade in ultrathin slices of about 55 nm (Ultracut Leica EM UC6) and transferred to Formvar coated grids. If the contrast is lower than desired, slices can be transferred to uranylacetate for 35 minutes and to lead citrate for two minutes to further enhance contrast. After desiccation grids were channeled into the high-vacuum chamber of a transmission electron microscope (Philips EM 100, camera and software Gatan Inc.) where images of random sections have been taken. The ultrathin sectioning and most imaging have been generously conducted by EM-technical assistants Barbara Joch and Sigrun Nestel. Further image processing was carried out with cell^P_Olympus, ImageJ 1.45 software. Statistical computing and graphs were plotted in Ⓡ.

| star code | Meaning |
|---|---|
| n.s. (not significant) | $P > 0.05$ |
| * | $P \leq 0.05$ |
| ** | $P \leq 0.01$ |
| *** | $P \leq 0.001$ |

## 2.18.  Criteria for mushroom-shaped spines

For identification of mushroom-shaped synapses in random electron microscopy images, the following criteria were used. A structure was considered as a mushroom-shaped synapse when (I) the pre- and postsynaptic cell show outstanding synaptic densities, (II) the presynaptic axon terminal contains numerous vesicles and (III) a synaptic cleft is

visible between these two associated elements.

If the plane of section does not pass the synaptic cleft at the right angle, the cleft may not be visible or may appear blurred in electron microscopy images of frontal or oblique sections. Therefore, only synapses were included which matched at least the first two of the three mentioned criteria. Nevertheless, it is worth mentioning that Immunoelectron microscopy classification of fixed structures depict a 'snapshot' of a defined time-point, and spines are capable to modulate their morphology quite rapidly, i.e. due to elevated F-actin levels [Hering & Sheng, 2001].

## 2.19. Criteria for spine apparatuses

The spine apparatus is a highly specified organelle, present predominantly in a subpopulation of 10- 15 % (data from hippocampal area CA1) in mature mushroom-shaped spines containing a perforated PSD [Spacek & Harris, 1997]. As approximately 48 % of all spines contain some type of smooth endoplasmic reticulum (sER) [Spacek & Harris, 1997], criteria for analyzing fully developed spine apparatuses in ultrathin sections have to be chosen with great care. Therefore, categories for identifying spine apparatuses in postsynaptic spines and dendritic compartments were elected as follows. As these organelles consist of alternating stacked discs of sER and dense material in between, a minimum of three discs interconnected by two clouds of dense material was considered to be a distinct spine apparatus, eliminating potential confusions with singular tubules of sER.

The number of silver-intensified gold granules, which are directed against the eGFP fused part of Synaptopodin were used to identify successfully transfected pyramidal CA3 neurons and subcellular compartments. A spine apparatus was considered to be labeled, when more than two granules were present at the outlines of a distinct organelle. If there were one or two granules present, the labeling was counted as background and those spine apparatuses were not statistically analyzed.

## 2.20. Criteria for quantitative analysis of spine apparatuses

To compare surface areas of spine apparatuses in hippocampal CA3 region of different conditions in greater detail, ultrastructural tissue was serially cut and manually traced during Immunoelectron Microscopy procedure. As manually tracing is is a highly laborious work, images from spine apparatuses and spines were taken randomly as screenshots. Perimeters of single spine apparatuses which do not discriminate the upper mentioned qualitative criteria were retraced (in µm) with the 'open polygon tool' and appropriate surface areas (in µm$^2$) were calculated with Olympus professional imaging software 'Cell P'. As a graphical output of this exploratory data analysis, which aims to summarize the main characteristics of data sets, violin plots were chosen. Violin plots typically show the 'five-number summary' of all boxplot parameters, consisting of the median (Q2, 50th percentile) together with the first quartile (Q1, 25th percentile) and the third quartile (Q3, 75th percentile). These parameters describe the 'box' part of the plot. The Interquartile Range (IQR) represents the length of the box (IQR = Q3 – Q1), is a measure of variability in the sample and can be used to compare samples. The whiskers, which extend from both ends of the box to the lower and upper inner fences, are mathematically defined as [Q1 – 1.5(IQR)] and [Q3 + 1.5(IQR)]. Fences therefore illustrate possible outliers of the data. If one whisker is much longer than the other, it indicates that the data is probably skewed in the direction of the longer whisker. In our studies a skewness to the left is quite often the case, as upper mentioned criteria for selecting spine apparatuses include all organelles with increased surface area but eliminates small structures, which either represent a single sER tubulus penetrating a spine or an oblique plane of sectioning. The violin plot combines the 'five-number summary' of the boxplot with an overview of a rotated kernel density estimator, a smoothed histogram to each side of the box reflecting the probability density function of a random variable. Comparisons of groups were carried out in ®, a 'Language and Environment for Statistical Computing' [R Development Core Team, 2009] with the non-parametric 'Wilcoxon Rank Sum and Signed Rank Test', which performs one- and two-sample tests on vectors of data .

For calculating statistical significance and p-values the non-parametric 'Wilcoxon Rank Sum and Signed Rank Test' has been chosen, which performs one- and two-sample Wilcoxon tests on vectors of data. This function allows ties and computes exact p-values, as samples contain less than 50 finite values. As it is always dodgy to handle

small sizes of finite values per condition, the 'Wilcoxon Rank Sum and Signed Rank Test' was combined with an exact computation of p-values for all samples.

For open questions and issues concerning statistical problems the comprehensive guides [Zoefel, 2000] and [Sachs, 2003] were consulted.

# 3. Results

Single cell electroporation was used to as an approach to investigate molecular mechanisms for morphological alterations of CA3 pyramidal neurons at the cellular and subcellular level.

## 3.1. L1CAM promote axonal branching in CA3 pyramidal cells

To demonstrate feasibility of SCEP technique, cDNA of human L1CAM wild-type (L1wt) and two L1CAM missense mutations, L1-R184Q and L1-W1036L were overexpressed in long-term slice cultures [Schäfer *et al.*, 2010] as a proof of concept. Individual CA3 pyramidal cells were electroporated with plasmid cDNA of L1CAM fused to eGFP after 21 DIV (Figure 3.1 A) and immunostained with antibodies against human L1CAM and eGFP five days after transfection (Figure 3.1 B).

Confocal z-stacks were taken to visualize extended axonal and dendritic arbors of transfected cells and analyzed with Sholl analysis (Figure 3.1 C-E). In the wild-type situation, immunostaining of L1CAM was strong in somata and along axons, which were identified by their presynaptic boutons (arrows, Figure 3.1 C). In dendritic arbors L1CAM expression was less pronounced (arrowheads) and often below detection level. Co-expression of eGFP coupled to L1-R184Q was restricted in pyramidal cells to neuronal cell bodies (arrowheads) and proximal processes (Figure 3.1 D), whereas distal dendrites or axons (arrows) did not express L1-R184Q. This indicates that the L1-R184Q mutation prevents axonal targeting of L1CAM. If low concentrations of L1-W1036L plasmid were transfected, analyzes of the subcellular distribution of L1-W1036L revealed a similar expression pattern to L1-R184Q mutation. However, by transfecting higher plasmid concentrations, co-immunostaining for this mutant was detectable additionally in dendrites (Figure 3.1 E). This finding is consistent with previous observations in dissociated
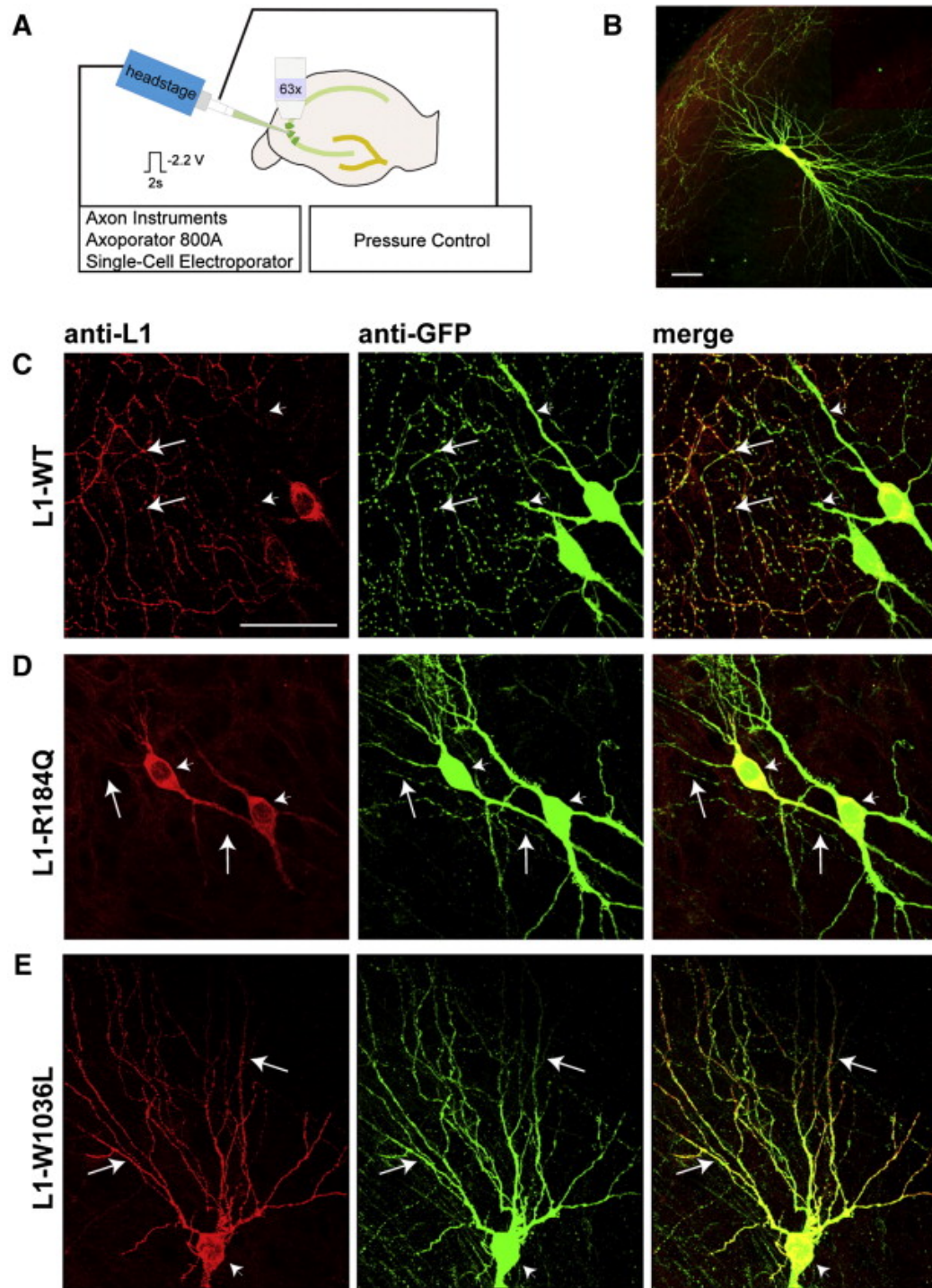
**Figure 3.1.:** Different L1 trafficking defects in CA3 pyramidal neurons are caused by L1 mutations. (A) Schematic drawing of the single-cell electroporation setup with the chosen parameters for electroporation of L1 and/or eGFP constructs. (B) A CA3 pyramidal neuron expressing human wild-type L1 and eGFP in a hippocampal slice transfected at 21 DIV. (*Continued on next page*)

**Figure 3.1.:** (*Continued from previous page*) (C) Axonal localization of human wild-type L1 (L1wt) of eGFP-positive neurons. White arrows show typical presynaptic boutons. Dendritic expression level of L1wt is very low or beyond detection levels (arrowheads). (D) Co-expressing L1-R184Q (red) and eGFP (green) shows the localization of L1-R184Q in the soma (arrowheads) and in proximal dendrites, whereas almost no expression was detected in axons (arrows). (E) Co-expression of L1-W1036L (red) and eGFP (green) reveals a strong localization of this L1 mutation in the soma (arrowheads) and in dendritic trees (arrows). All images represent z-stack projections from at least 58 xy-confocal sections comprising the complete extension of eGFP-fluorescently labeled neuronal processes. In total, 20 neurons from five independent experiments were investigated (L1wt: n=7; R184Q: n=6; W1036L: n=7). Scale bars (B–E): 50 µm.

neuronal cultures and strengthens the hypothesis that there are different mechanisms which cause trafficking defects of L1-R184Q and L1-W1036L mutations.

Axonal and dendritic morphogenesis and their structural remodelings are fundamental neuronal activities which involve L1CAM and related family members [Yamamoto *et al.* , 2006], [Ango *et al.* , 2008], [Schmid & Maness, 2008]. We therefore examined whether the expression of wild-type or mutant L1 affects axonal or dendritic arbor complexity of transfected CA3 pyramidal neurons. Neurons expressing eGFP alone or together with L1 constructs were traced for their eGFP-positive axonal and dendritic arbors (Figure 3.2 A-D) and investigated with Sholl analysis [Sholl, 1953]. Concentric circles with increasing diameter (Figure 3.2 E-L) were chosen to quantify the number of intersections of axonal and dendritic arbors. In the absence of L1wt overexpression, analyzes revealed that neurons expressing L1wt display an increased axonal arbor complexity compared to neurons expressing L1-R184Q, L1-W1036L or eGFP alone (Figure 3.2 E-G). In contrast, such alterations were not observed in these neurons for dendritic arbor complexity (Figure 3.2 I-K). Thus, insufficient axonal targeting of the investigated L1 mutants interferes with L1-mediated axon arborization in organotypic hippocampal slice cultures.
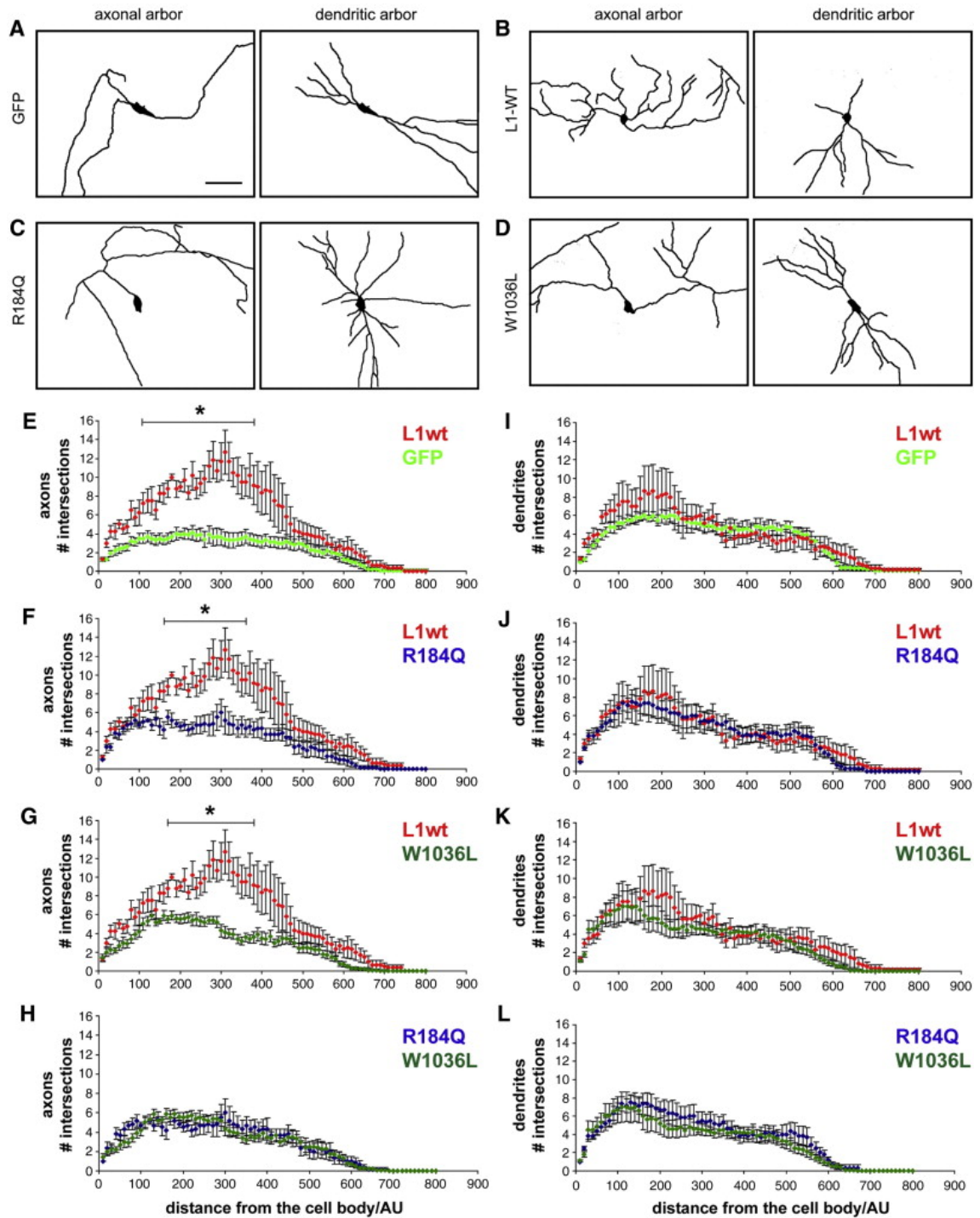
**Figure 3.2.:** The L1 mutations R184Q and W1036L interfere with L1-mediated axonal sorting processes. NeuronJ-based reconstructions of axons and dendritic arbors from CA3 pyramidal neurons expressing eGFP alone (A) or together with human wild-type (B) or mutant L1 (C-D). (E–L) Graphs showing 2D Sholl analysis of indicated conditions for the number of axonal (E–H) and dendritic (I–L) branching points at radial distance from cell bodies. In total, 32 neurons were analyzed (eGFP alone: 10; L1wt: n=7; R184Q: n=6; W1036L: n=9). *= $p < 0.05$, Student's t-test, unpaired, two-tailed). Scale bar: 100 μm.

## 3.2. Spine apparatuses in organotypic hippocampal slices

The formation of the spine apparatus is restricted to a neuronal sub-population [Spacek & Harris, 1997], [Bas Orth *et al.* , 2007] and strongly depends on the expression of synaptopodin [Mundel *et al.* , 1997], [Czarnecki *et al.* , 2005]. The absence of the spine apparatus in synaptopodin-deficient mice even demonstrated an essential role of synaptopodin for the generation of this organelle. In the present work, it was hypothesized that the rescue of synaptopodin expression in synaptopodin-deficient mice may lead to the restoration of spine apparatuses. To test this hypothesis, SCEP was chosen as a method to transfect individual neurons in the CA3 region of organotypic hippocampal slice cultures. This neuronal sub-population in the hippocampus has been already identified housing these enigmatic organelles *in vivo* [Kremerskothen *et al.* , 2005], [Deller *et al.* , 2007]. To overexpress synaptopodin, an eGFP fused mouseSynaptopodin construct (eGFP-mSynpo) was used. Organotypic hippocampal slices from C57BL/6 (wild-type) and synaptopodin-KO mice were cultured for 21 DIV and then electroporated and processed for Immunoelectron microscopy (IEM) after an additional cultivation period of three days. IEM was performed with antibodies specific to eGFP, which enabled to unambiguously identify transfected neurons.

In the wild-type, spine apparatuses in SCEP-transfected CA3 pyramidal cells of long-term slice cultures were observed (Figure 3.3 C, D). They were labeled by silver-enhanced immunogold granules (1.4 nm) confirming the localization of eGFP-mSynpo to the spine apparatus after SCEP. To compare the morphology of spine apparatuses in the wild-type (Figure 3.3 A, B) with those after Synaptopodin-overexpression, surface areas of spine apparatuses were measured, which consist of a minimum of three stacks. In the wild-type, examination of five individual CA3 pyramidal cells revealed 29 spine apparatuses present in spines and 13 in dendritic profiles. After introduction of eGFP-mSynpo cDNA spine apparatuses were predominantly present in dendritic compartments (a total number 23 from 35 out of three neurons from independently analyzed slice cultures were investigated). Morphology of spine apparatuses was preserved and median surface area did not alter after SCEP-transfection compared to un-electroporated organelles in mushroom-shaped spines of the wild-type.

Nevertheless electroporation in the wild-type led to a higher total number of spine apparatuses in dendritic sections (Figure 3.8 A). This altered distribution of organelles after overexpression enables us to evaluate potential effects of Synaptopodin-overexpression
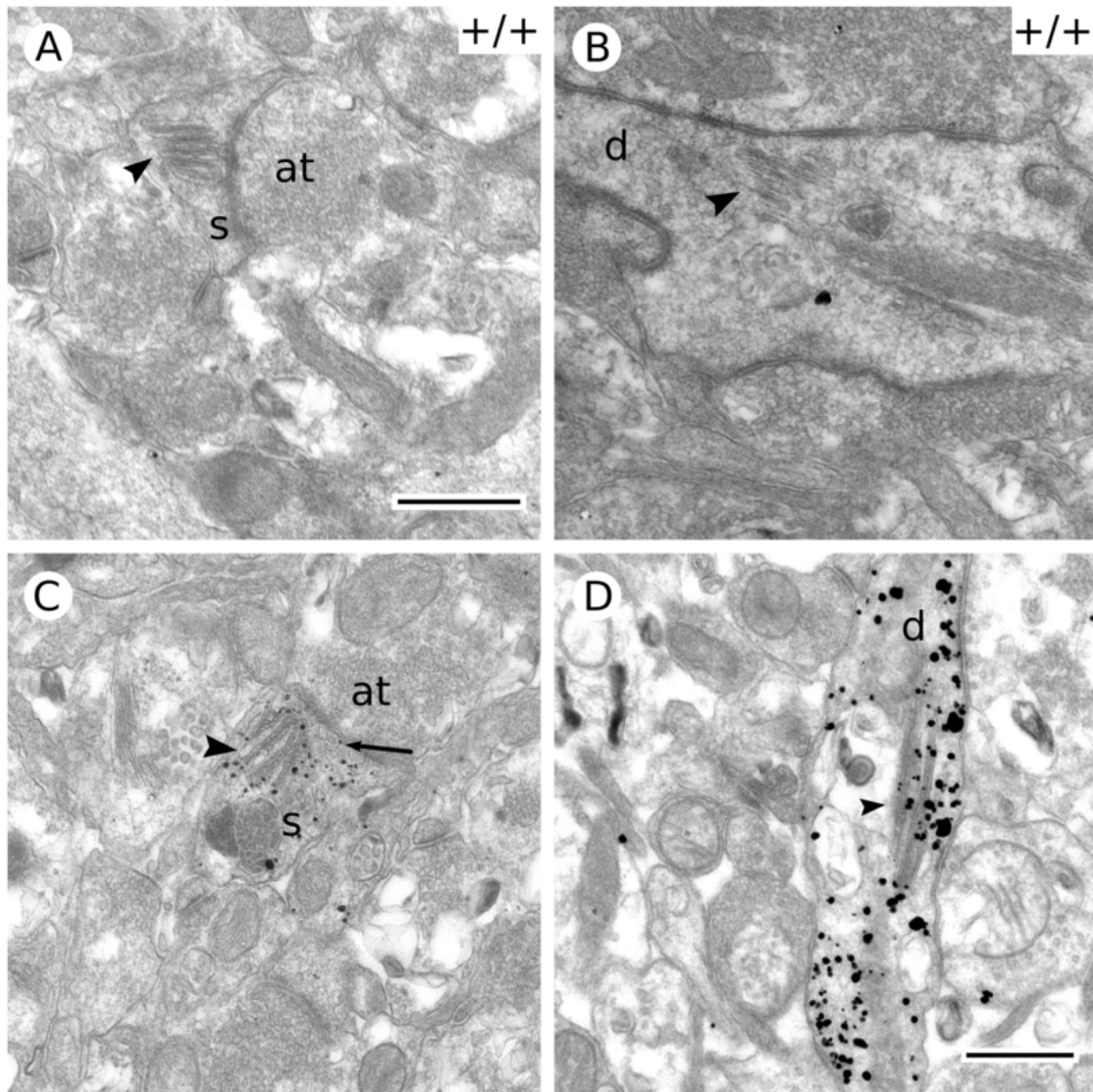
**Figure 3.3.:** Spine apparatuses in CA3 pyramidal cells of the wild-type (A - B) and after SCEP-transfection (C - D). Immunolabeling is against the eGFP part of the fused construct (1.4 nm gold granules, silver intensified). (A) Wild-type spine apparatuses (black arrowheads) are present predominantly in mushroom-shaped spines (s) with perforated synapses. (B) Only few organelles were traced in dendrites (d). (C - D) Ultrastructure of a spine apparatus after electroporation remains unaltered in mushroom-shaped spines, but organelles occur predominantly in dendrites. Herein spine apparatuses are larger compared to the wild-type. Scale bars (A - D): 0.5 µm.

after SCEP-electroporation. The appearance and sorting of these organelles into mushroom-shaped spines might depend on the expression level of synaptopodin. As the eGFP-mSynpo construct enters the cytoplasm of the cell body by application of low voltage

(-2.2 V) and membrane permeation, elevated levels of Synaptopodin cDNA might have led to saturated protein levels and thereby an increased number of spine apparatuses formed in distal dendrites.

Overexpression of eGFP-mSynpo does not interfere with their morphology and surface area remains unaltered for those organelles, which were observed in mushroom-shaped spines. In dendrites, where spine apparatuses often exhibit an elongated shape, SCEP-transfection led to a higher total number and significantly increased surface areas (p-value = 0.00731; Table 3.1) if compared to un-transfected organelles. A summary of parameters including medians, IQRs, confidence intervals and significance levels for each condition is listed in the first table Table A.1 of the attachment.

Even though the spine apparatus was first described in scientific literature more than 50 years ago [Gray, 1959], the awaken interest in this organelle recently derives from scientific publications, which link this organelle with its calcium-sequestering ability to spine plasticity [Segal *et al.*, 2010]. This was possible after the pioneering experiments using behavioral tests in the radial arm maze together with electrophysiological recordings in the CA1 region of synaptopodin KO mice [Deller *et al.*, 2003]. The authors were able to provide a link between the lack of the spine apparatus organelle, a decrease in LTP and deficits in spatial learning. As the spine apparatus is closely associated with mushroom-shaped type of spines, which are quite stable compartments in terms of their actin turnover rate, we were also interested, if morphological alterations in the spine apparatus are related with changes in appropriate mushroom-shaped spines. Therefore surface areas of spines housing a spine apparatus were measured. If both parameters were related to each other, morphological changes in the spine apparatus should affect the spine compartment. Calculations for surface areas of mushroom-shaped spines the wild-type did not reveal severe morphological changes (p-value = 0.372; Table 3.1), if compared to those after SCEP-transfection. This indicates that neither spines nor intrinsic spine apparatuses were morphologically affected by overexpression of Synaptopodin.

## 3.3. Restored spine apparatuses after genetic complementation

The spine apparatus is absent in Synaptopodin-deficient mice [Deller *et al.*, 2003], which underlines the essential role of Synaptopodin for the development of this enigmatic organelle. This can be unambigiously confirmed after sectioning of hippocampi and IEM

analysis of 6 individual animals (data not shown). A major working hypothesis of the present study is that the spine apparatus may be restored in CA3 pyramidal neurons by the delivery of recombinant mSynpo. Therefore, eGFP-mSynpo was reversely introduced via electroporation in individual CA3 pyramidal cells in the adult neuronal network of Synaptopodin-deficient entorhinal-hippocampal slice cultures at 21 DIV.

In fact, spine apparatuses formed in a cell-autonomous manner. This *de novo* formation of whole organelles after genetic complementation provides the first evidence for rescuing spine apparatuses in hippocampal CA3 pyramidal cells of Synaptopodin KO slice cultures. In six neurons a total amount of 76 analyzed spine apparatuses formed after genetic complementation. These organelles were distributed as follows: 24 in spines, 43 in dendrites and 9 spine apparatus-like structures, which formed ectopically, in the perikaryon (Figure 3.8 A). The panoramic view (Figure 3.4 A) shows a total amount of five *de novo* formed spine apparatuses in mushroom-shaped spines and in dendrites of a single Immunoelectron microscopic image. *De novo* formation of spine apparatuses led to a highly significant increase in surface area of spine apparatuses in spines (Figure 3.4 A, pink; C) compared to those, which have been investigated after overexpression in the wild-type (p-value = 9.91E-05; Table 3.1). Visual inspections indicate that (re-)introduction of Synaptopodin either for genetic complementation in Synaptopodin KO slices or after overexpression in the wild-type affects also the site of occurrence of this inimitable organelles. In both cases spine apparatuses emerged predominantly in dendrites (43 out of 76 from 6 transfected Synaptopodin KO mice). Furthermore, surface areas of spine apparatuses in dendrites (Figure 3.4 A, dark blue, B) were highly enlarged (p-value = 3.44E-04; Table 3.1) after genetic complementation, if compared to organelles after overexpression in the wild-type.

Interestingly, a significant gain in surface area was also computed for mushroom-shaped spines after the restoration of spine apparatuses, if compared to mushroom-shaped spines in the KO (p-value = 0.0014). As mushroom-shaped spines in the KO were generally rare to observe, spines were also statistically compared to those after overexpression in the wild-type, which led to a significance in the same range (p-value = 0.00242; Table 3.1). Even though mushroom-shaped spines did not enlarge to the same extent than *de novo* formed spine apparatuses after genetic complementation.
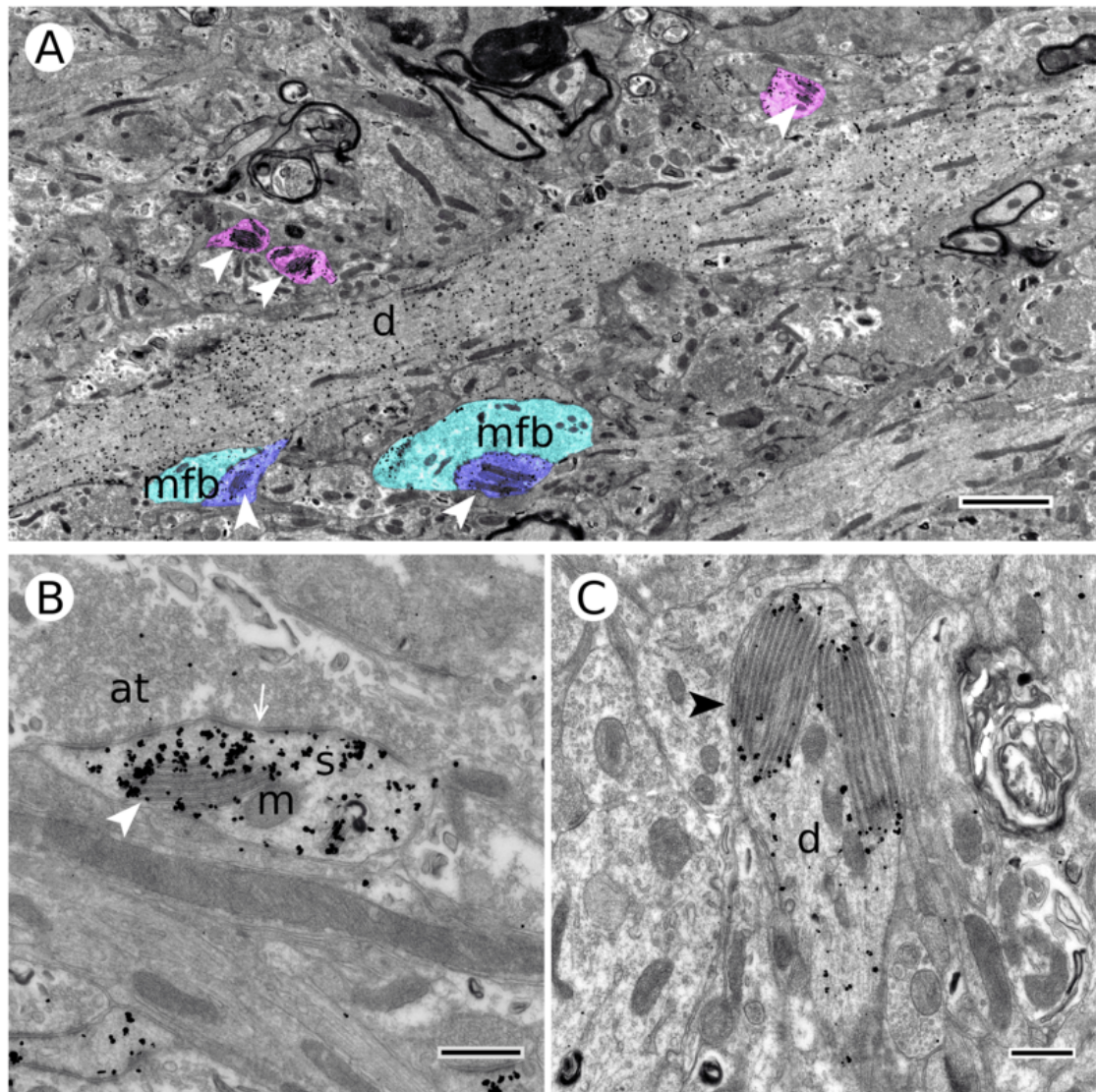
**Figure 3.4.:** (A – C) Ultrastructural overview of *de novo* formed spine apparatuses in CA3 pyramidal cells of Synaptopodin KO mice after genetic complementation. (A) The panoramic view provides an impressive overview on reestablished spine apparatuses in dendrites (d) (white arrowheads, highlighted in pink) and in mushroom-shaped spines (dark blue). Parts of mossy fiber boutons (mfb) are colored in light blue. (B) Higher magnification of an immunolabeled spine apparatus (white arrowhead) in a mushroom-shaped spine (s) with a perforated PSD (arrow). The spine apparatus is located in close vicinity to a mitochondrion (m). (C) Enormously enlarged spine apparatus consisting of numerous single stacks (black arrowhead) in a dendritic cross-section (d). Scale bars A: 2 µm, B, C: 0.5 µm.

## 3.4. Ectopic formation of spine apparatus-like structures in the perikaryon

In the wild-type, synaptopodin protein is localized in dendrites and spines and absent in the perikaryon in late developmental stages [Czarnecki *et al.* , 2005]. Furthermore, the presence of synaptopodin protein is restricted to dendritic areas at P5 [Czarnecki, 2005]. Restoration of spine apparatuses in CA3 pyramidal cells of Synaptopodin deficient slices revealed the formation of *de novo* spine apparatus-like structures in an ectopic cellular compartment, the perikaryon. These newly formed arrangements exhibit a honeycomb appearance with diffuse immunolabeling against eGFP-mSynpo, but without interdigitating filamentous dense material (Figure 3.5 A). Theses structures were not observed after overexpression of synaptopodin in wild-type CA3 neurons (Figure 3.5 B).
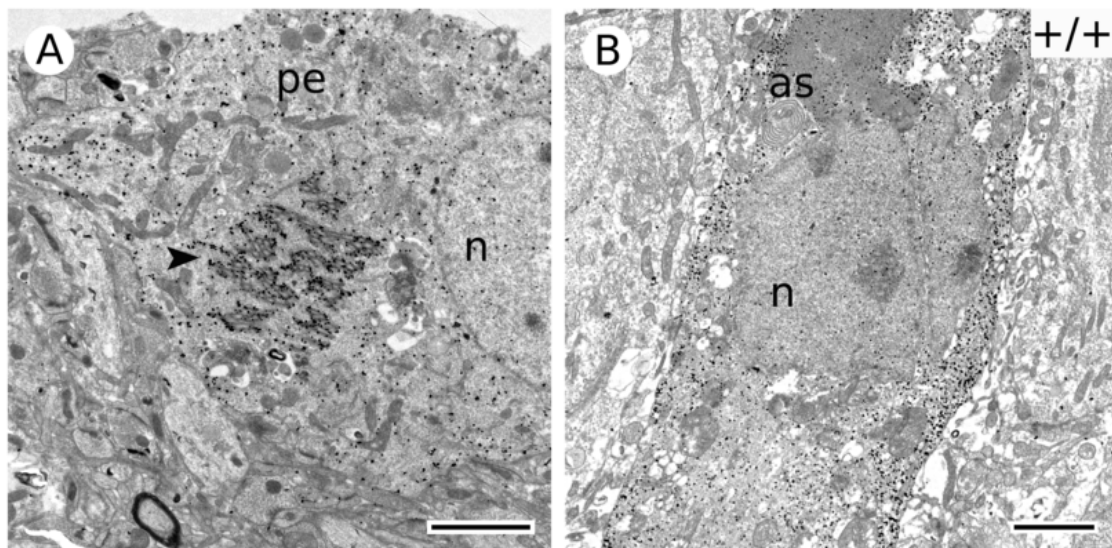


**Figure 3.5.:** (A) Ectopic formation of spine apparatus-like organelles (black arrowhead) in the perikaryon of a CA3 pyramidal cell after re-introduction of synaptopodin cDNA. These structures were arranged in a honeycomb-shape. (B) In perisomatic regions of wild-type slices no spine apparatus-like organelles were detected. Abbreviations: perikaryon (pe), nucleus (n), axon sheath (as). Scale bars A, B: 2 μm.

The uptake of Synaptopodin cDNA with SCEP at P21, takes place in the perikaryon of targeted neurons due to accessibility of the pipette and might influence protein transport and trafficking pathways at late developmental time-points. Re-introduction of undefinable amounts of plasmid might also saturate protein trafficking pathways and cause the formation and retention of spine apparatus-like structures in ectopic compartments.

The absence of interdigitating filamentous material might additional be a hint for further speculations about the actin cytoskeleton and its role in establishment of polarity within neuronal transport mechanisms.

## 3.5. Overexpression studies with KIBRA

The absence of spine apparatuses in synaptopodin KO mice demonstrated that Synaptopodin is essential for the formation of spine apparatuses in vivo. The role of Synaptopodin in actin organization might be a critical factor for spine apparatus formation. Therefore we tested the hypothesis that overexpression of a functionally related interaction partner may compensate for the loss of synaptopodin and spine apparatus formation in synaptopodin KO mice. KIBRA, a protein which binds via intrinsic WW-domains to synaptopodins' two PPxY sites, is such an interaction partner. In the kidney, KIBRA and Synaptopodin protein exhibit a high degree of co-localization in podocytes. Furthermore, KIBRA has been shown to act in actin organization via polarization of the actin cytoskeleton [Duning *et al.* , 2008] and synapse function [Makuch *et al.* , 2011], [Schneider *et al.* , 2010]. Following SCEP of CA3 pyramidal neurons with eGFP-KIBRA slices from fife different animals were processed for IEM using antibodies specific to eGFP. In the absence of synaptopodin not a single spine apparatus was found in transfected CA3 pyramidal neurons under these conditions (Figure 3.6 A, C, F).

However, after overexpression of eGFP-KIBRA in slices from wild-type mice KIBRA displays a somato-dendritic localization in CA3 neurons, being perinuclear enriched. Large clusters of KIBRA protein appeared especially in the perikaryon (Figure 3.6 F) with diameters up to 1.045 µm. Clusters were also observed in dendrites (Figure 3.6 D) with diameters up to 0.712 µm but quite rarely found in spines (Figure 3.6 B).

This observation supports the hypothesis that KIBRA-overexpression can not induce the formation of spine apparatuses, even though it is indirectly coupled to the actin cytoskeleton [Schneider *et al.* , 2010]. This highlights the unique role of Synaptopodin and its ability to drive the formation of the spine apparatus organelle. The formation of larger clusters is completely absent after KIBRA overexpression in Synaptopodin-KO mice (few smaller ones were observed in dendrites as depicted in (Figure 3.6 C)). We can only hypothesize about the appearance of clusters. The interplay between synaptopodin and KIBRA might have led to the formation of heterodimers, which in turn might be responsible for the appearance of clusters in the perikaryon and in dendrites.
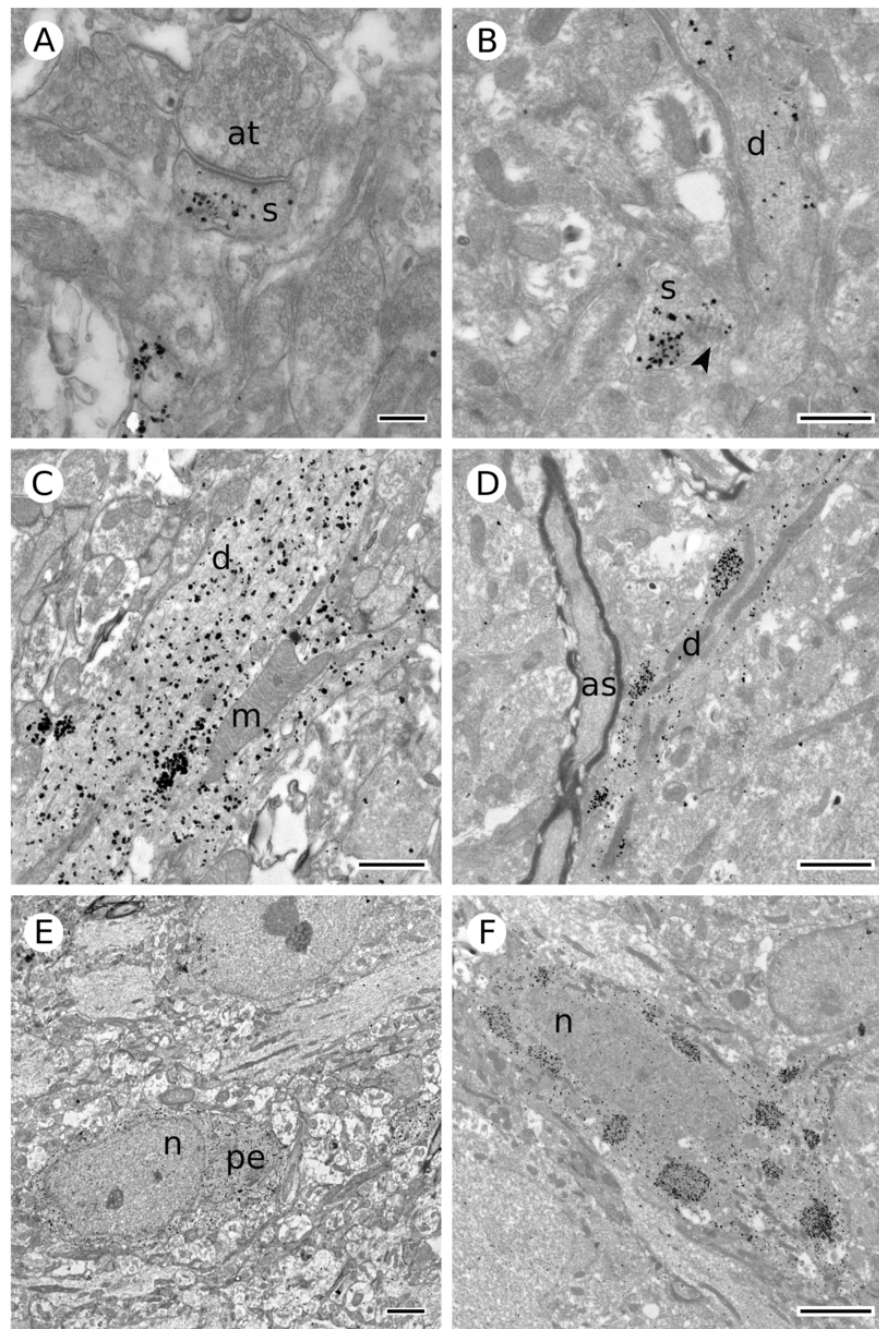
**Figure 3.6.:** (A, C, E) Overexpression of eGFP-KIBRA cDNA does not lead to restoration of spine apparatuses in the absence of Synaptopodin in CA3 pyramidal cells. Immunolabeling against eGFP depicts the presence of the eGFP-KIBRA fusion protein. (B, D, F) In the presence of synaptopodin eGFP-KIBRA accumulates in large clusters after overexpression. (F) In the perikaryon clusters appeared in an ellipsoid shape surrounding the nucleus. (D) Clusters were additionally visible in dendrites. The dark structure in this image next to the dendrite is a myelinated axon sheath (as). (B) In mushroom-shaped spines cluster formation, here next to a spine apparatus, was quite rare. Abbreviations: spine (s), axon terminal (at), dendrite (d), mitochondrion (m), perikaryon (pe) and nucleus (n). Scale bars: A: 0.2 µm, B: 0.5 µm, C, E: 2 µm, D, F: 1 µm.

## 3.6. Heterozygous spine apparatuses: formation is independent of reduced Synaptopodin levels

Previous studies by Deller showed that the spine apparatus is lost in synaptopodin KO mice [Deller *et al.* , 2003] and comparison between median surface areas of *de novo* formed spine apparatuses led to a morphological increase compared to those in wild-type slices after overexpression. However, it remained an open research question whether heterozygous synaptopodin mice display deficits in the formation and morphology of spine apparatuses.

Therefore we interested if the spine apparatus formation and its morphology is regulated in genetic dose dependent manner. Age-matched Synaptopodin heterozygous CA3 pyramidal cells of entorhinal-hippocampal slices were electroporated with eGFP-mSypo and surface areas of spine apparatuses were measured in pre-embedded IEM-sections. Spine apparatuses of two individual neurons were analyzed which showed the following distribution: 17 organelles were found in mushroom-shaped spines and only three in dendrites (Figure 3.7 B), (Figure 3.8 A).

This distribution is in line with the situation in the wild-type. Comparison of surface areas from heterozygous spine apparatuses in spines with those from the wild-type revealed a slight increase, which barely missed significance (p-value = 0.0553; Table 3.1). Spine apparatuses in dendrites were not statistically evaluated due to the limited total numbers herein.

More interestingly, mushroom-shaped spines (Figure 3.7 A) were extremely enlarged if compared to those of the wild-type (p-value = 1.94E-04; Table 3.1) or to those spines from synaptopodin KO mice (p-value = 0.00326; Table 3.1). Aged-matched mushroom-shaped spines of synaptopodin heterozygote animals were indeed more similar to those after genetic complementaton, even though heterozygous slices were left un-electroporated.

Spine apparatus formation is therefore not regulated in genetic dose dependent manner and its morphology in a heterozygous background is similar to the wild-type. Furthermore, no spine apparatuses were detected in the perikaryon, which is also consistent with the situation in the wild-type. Nevertheless, mushroom-shaped spines display enlarged surface areas. In heterozygous animals the relation between surface areas of spines and spine apparatuses, which were unaltered after synaptopodin re-(introduction) is somehow disrupted and no explanations can be provided thus far for this observed phenomenon.
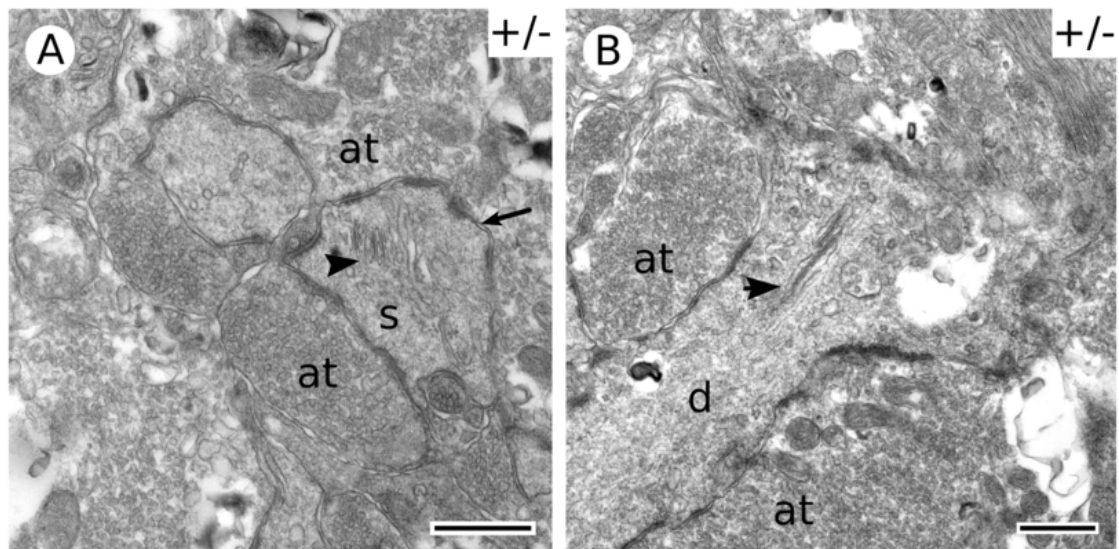
**Figure 3.7.:** CA3 pyramidal cells from heterozygous Synaptopodin mice show spine apparatuses with a wild-type like appearance. (A) Spine apparatus (black arrowhead) in a perforated mushroom-shaped spine (arrow). (B) Spine apparatus in dendrites (d) were quite rare. The depicted organelle is opposing a large axon terminal (at). Scale bars A, B: 0.5 µm.

## 3.7. Quantitative analysis of spine apparatuses in relation to mouse Synaptopodin expression levels

Quantitative analysis provide a detailed view on median surface areas from spine apparatuses (in µm$^2$) in relation to mSynpo expression levels together with their distribution. The clustered-stacked Column Chart (Figure 3.8 A) shows total numbers of spine apparatuses according to their compartmental appearance in a color-coded manner. Spine apparatuses in spines are highlighted in 'purple', spine apparatuses in dendrites in 'lightgreen' and spine apparatus-like structures in somata in 'sandbrown'. The color-code for spine apparatuses in violin plots is consistent with the one in the clustered-stacked Column Chart. Surface areas of mushroom-shaped spines appear selectively in violin plots and are color-coded in 'lightblue'. Total numbers of spine apparatuses and appropriate mushroom-shaped spines are equal for all conditions.

Violin plots show two dashed grey lines indicating the upper and lower borders of the Interquartile Range (IQR) of the situation after genetic complementation and a dashed red line, highlighting the median of the same condition. The total number of individually analyzed neurons (No neurons) are provided below the labeling of the x-axis and numbers

**Table 3.1.:** Statistical significance with the 'Wilcoxon rank sum and signed rank test' on surface areas of spine apparatuses and related spines in relation to mSynpo expression levels

**Surface area of spine apparatuses in mushroom-shaped spines in relation to Synaptopodin expression levels**

| Conditions | WT+mSynpo ($n = 12$) | | | KO+mSynpo ($n = 24$) | | | Heterozygous ($n = 17$) | | |
|---|---|---|---|---|---|---|---|---|---|
| | W | p-value | star code | W | p-value | star code | W | p-value | star code |
| WT ($n = 29$) | 154 | 0.581 | - | - | - | - | 162 | 0.0553 | - |
| WT+mSynpo ($n = 12$) | - | - | - | 35 | 9.91E-05 | *** | - | - | - |

**Surface area of appropriate mushroom-shaped spines in relation to Synaptopodin expression levels**

| Conditions | WT+mSynpo ($n = 12$) | | | KO ($n = 07$) | | | KO+mSynpo ($n = 24$) | | | Heterozygous ($n = 17$) | | |
|---|---|---|---|---|---|---|---|---|---|---|---|---|
| | W | p-value | star code | W | p-value | star code | W | p-value | star code | W | p-value | star code |
| WT ($n = 29$) | 142 | 0.372 | - | 128 | 0.306 | - | - | - | - | 89 | 1.94E-04 | *** |
| WT+mSynpo ($n = 12$) | - | - | - | - | - | - | 56 | 0.00242 | ** | - | - | - |
| KO ($n = 7$) | - | - | - | - | - | - | 20 | 0.0014 | ** | 15 | 0.00326 | ** |

**Surface area of spine apparatuses in dendrites in relation to Synaptopodin expression levels**

| Conditions | WT+mSynpo ($n = 23$) | | | KO+mSynpo ($n = 43$) | | | Heterozygous ($n = 3$) | | |
|---|---|---|---|---|---|---|---|---|---|
| | W | p-value | star code | W | p-value | star code | W | p-value | star code |
| WT ($n = 13$) | 69 | 0.00713 | ** | - | - | - | 7 | 0.111 | - |
| WT+mSynpo ($n = 23$) | - | - | - | 235 | 3.44E-04 | *** | - | - | - |

of spine apparatuses and appropriate spines (n) are given above the x-axis. Absolute numbers, medians, Interquartile ranges and confidence levels for each analyzed condition are summed up in the first table of the appendix (Table A.1).

In general, most medians are located in the lower range of data and show a resulting skewness to the right (indicated by right tails). This distribution mirrors the previously chosen criterion to investigate spine apparatuses with at least three distinct tubules (to avoid the likelihood of confusion with single sER tubules inside spines or misinterpretations from oblique sections).

For spine apparatuses in spines the Interquartile Range is quite narrow and medians lie in the same range for the wild-type (median: 0.0238 µm$^2$; IQR: 0.0184), the heterozygous (median: 0.0346 µm$^2$; IQR: 0.0134) and the wild-type transfected with mSynpo (median: 0.0276 µm$^2$; IQR: 0.0221). Dispersion, median and the length of the right tail increases tremendously after genetic complementation (median: 0.0721 µm$^2$; IQR: 0.157; Figure 3.8 B), which is also reflected in the highly significant increase compared to mSynpo overexpression in the wild-type (p = 9.91 E-005, Table 3.1 upper table).

Spine apparatuses in dendrites (Figure 3.8 D) are more sensitive to elevated levels of
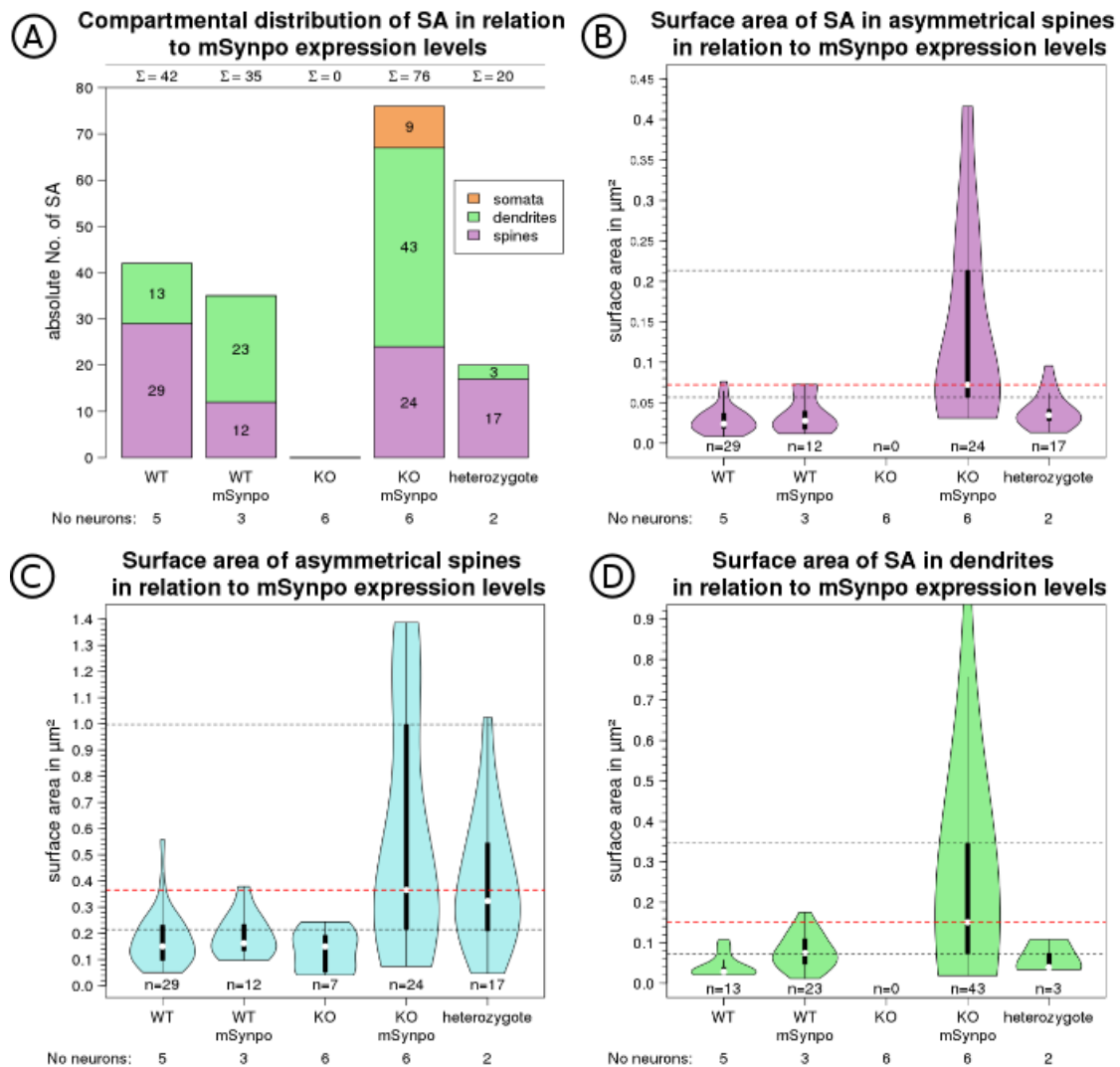
**Figure 3.8.:** (A) Total numbers of spine apparatuses in relation to Synaptopodin expression levels and compartments. Elevated mSynpo levels after re-(introduction) led to a predominant appearance of spine apparatuses in dendritic sections. After genetic complementation some spine apparatus-like structures formed ectopically on-site of transfection in the perikaryon. (B) The median surface area of spine apparatuses in spines is highly increased after genetic complementation. (C) This tendency is perfectly mirrored by appropriate spines. An exception of this co-enlargement of spines and spine apparatuses can be seen in heterozygous mice, where selectively mushroom-shaped spines enlarged. (D) Spine apparatuses in dendrites were more affected by altered mSynpo levels than those in spines.

synaptopodin, as indicated by their increased surface areas after re-(introduction) of mSynpo. Overexpression of synaptopodin in the wild-type leads to increased surface areas of spine apparatuses (median: 0.0742 $\mu m^2$; IQR: 0.0621) herein, if compared to wild-type spine apparatuses in dendrites (median: 0.0282 $\mu m^2$; IQR: 0.0123). *De novo* formed spine apparatuses in dendrites (median: 0.15 $\mu m^2$; IQR: 0.274) after genetic complementation (Figure 3.8 D) show similar out-ranging surface areas and an increased positive skewness of data than the ones in spines. Application of non-parametric Wilcoxon rank sum test revealed statistical significance after overexpression of synaptopodin (p = 0.00713, Table 3.1 lower table) compared to the wild-type and after genetic complementation (p = 3.44 E-04, Table 3.1 lower table) compared to overexpression in the wild-type.

Surface areas for heterozygous spines (Figure 3.8 B) were enlarged (median: 0.323 $\mu m^2$; IQR: 0.335), if compared to wild-type ones (median: 0.15 $\mu m^2$; IQR: 0.134) or to those in the synaptopodin KO (median: 0.15 $\mu m^2$; IQR: 0.141). Mushroom-shaped spines housing *de novo* formed spine apparatuses show the same tendencies than intrinsic spine apparatuses. They exhibit highly enlarged surface areas (median: 0.366 $\mu m^2$; IQR: 0.783), if compared to spines of the synaptopodin KO as well as to those after synaptopodin overexpression in the wild-type (median: 0.162 $\mu m^2$; IQR: 0.1).

## 3.8. Is the correlation between spine apparatuses and spines still ensured with elevated Synaptopodin levels?

Is the correlation between spine apparatuses and spines still ensured or guaranteed by elevated Synaptopodin levels? If changes in surface area of spine apparatuses directly influence the appropriate spines, the relation between them should not be altered. Generally, a shift of medians to more centered positions can be observed by dividing surface areas of spine apparatuses by their appropriate spines.

In the wild-type the quotient surface areas of spine apparatuses by surface areas of mushroom-shaped spines is directly proportional (Figure 3.9. The median of the transfected wild-type (median: 0.169 $\mu m^2$; IQR: 0.0755) is almost equal to that one of the wild-type (median: 0.165 $\mu m^2$; IQR: 0.068). In the heterozygous condition the quotient (median: 0.0989 $\mu m^2$; IQR: 0.0951) is smaller compared to the one in the wild-type (p

**Ratios of SA's surface area vs spine's surface area in relation to mSynpo expression levels**
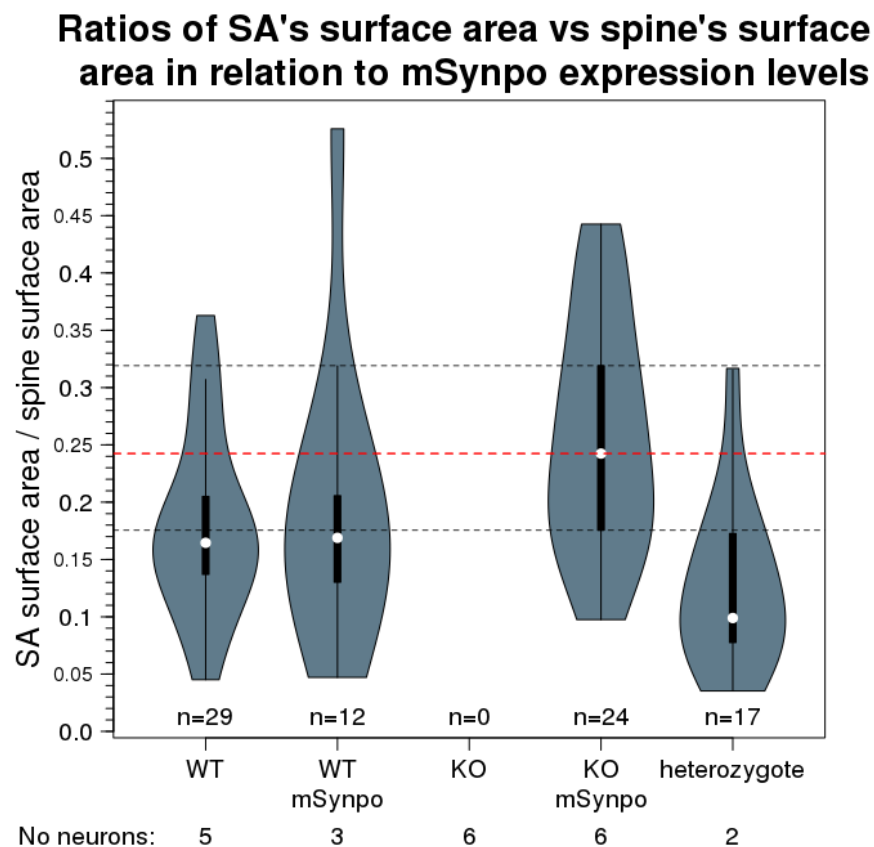
**Figure 3.9.:** The quotient for spine apparatuses divided by appropriate spines remains direct proportional after overexpression in the wild-type as indicated by their equal medians. The gain of surface areas for spines and intrinsic spine apparatuses is not always direct proportional to each other, as can be seen in the heterozygous situation and after re-introduction of synaptopodin.

$= 0.0147$; Table 3.2). In the rescue situation the quotient (median: 0.242 $\mu m^2$; IQR: 0.144) is smaller compared the one in the wild-type (p $= 0.0411$; Table 3.2). The median of the heterozygote condition is much smaller, because the gain of surface area for spines was larger than the gain for spine apparatuses. For the transfected KO condition the quotient reflects the opposite. Spine apparatuses gained surface area, which was not reflected in the same range for appropriate spines.

The quotient perfectly mirrors our previous findings by comparing individual conditions separately. A detailed list of all medians, Interquartile Ranges and confidence levels is given in the second table of the appendix (Table A.2).

**Table 3.2.:** Ratios of spine apparatuses over appropriate mushroom-shaped spines in relation to mSynpo levels

| | Ratios of SA's vs spines' surface area in relation to mSynpo expression levels | | | | | | | | |
|---|---|---|---|---|---|---|---|---|---|
| Conditions | WT+mSynpo ($n = 12$) | | | KO+mSynpo ($n = 24$) | | | Heterozygous ($n = 17$) | | |
| | W | p-value | star code | W | p-value | star code | W | p-value | star code |
| WT ($n = 29$) | 174 | 1 | - | - | - | - | 353 | 0.0147 | * |
| WT+mSynpo ($n = 12$) | - | - | - | 83 | 0.0411 | * | - | - | - |

## 3.9. Transfected NSC-34 cells suggest a role of small Rho GTPases for spine apparatus formation

Mouse Motor Neuron-Like Hybrid Cell lines (NSC-34) are fusion products derived from embryonic mouse spinal cord cells enriched with motor neurons and mouse neuroblastoma. They display a multipolar neuron-like phenotype [Cashman *et al.* , 1992]. NSC-34 cells are known to be sensitive to treatments that affect cytoskeletal organization and can be used for investigation of neurotoxic effects *in vitro*. NSC-34 cells were transfected with either eGFP alone or eGFP-mSynpo used in slice cultures, and treated with mushroom toxin Phalloidin, known to have a high affinity in binding to F-actin, but not to monomeric globular G-actin. Phalloidin therefore works far better than antibody-mediated antigen detection, which can not distinguish between F-actin and G-actin isoforms.

We aimed to visualize Synaptopodin expression using PEI-mediated transfection in relation to Phalloidin-stained F-actin in an undifferentiated cell line *in vitro* [Marx *et al.* , 2012]. Cultured NSC-34 cells were transfected either with eGFP alone or eGFP-mSynpo. Rhodamin-phalloidin was used to label selectively the F-actin pool and intracellular distribution in this cell line.

Transfection of eGFP alone reveals a uniformly distributed appearance of eGFP in NSC-34 cells, as indicated in the upper panel (Figure 3.10 A). Transfection of the eGFP-mSynpo construct, which has been applied with the same concentration (1 µg/µl) than for electroration with the SCEP setup, leads to a more constricted co-localization of F-actin fibers inside cells (Figure 3.10 B). In the lower panel (Figure 3.10 C), a clear reduction of F-actin fluorescence and eGFP-mSynpo signal can be seen after treatment with the Rho-signaling inhibitor *Clostridium difficile* toxin B, confirming previous studies in neuronal cultures [Vlachos *et al.* , 2009] and affirming the influence of small Rho-GTPases on the presence and availability of Synaptopodin.
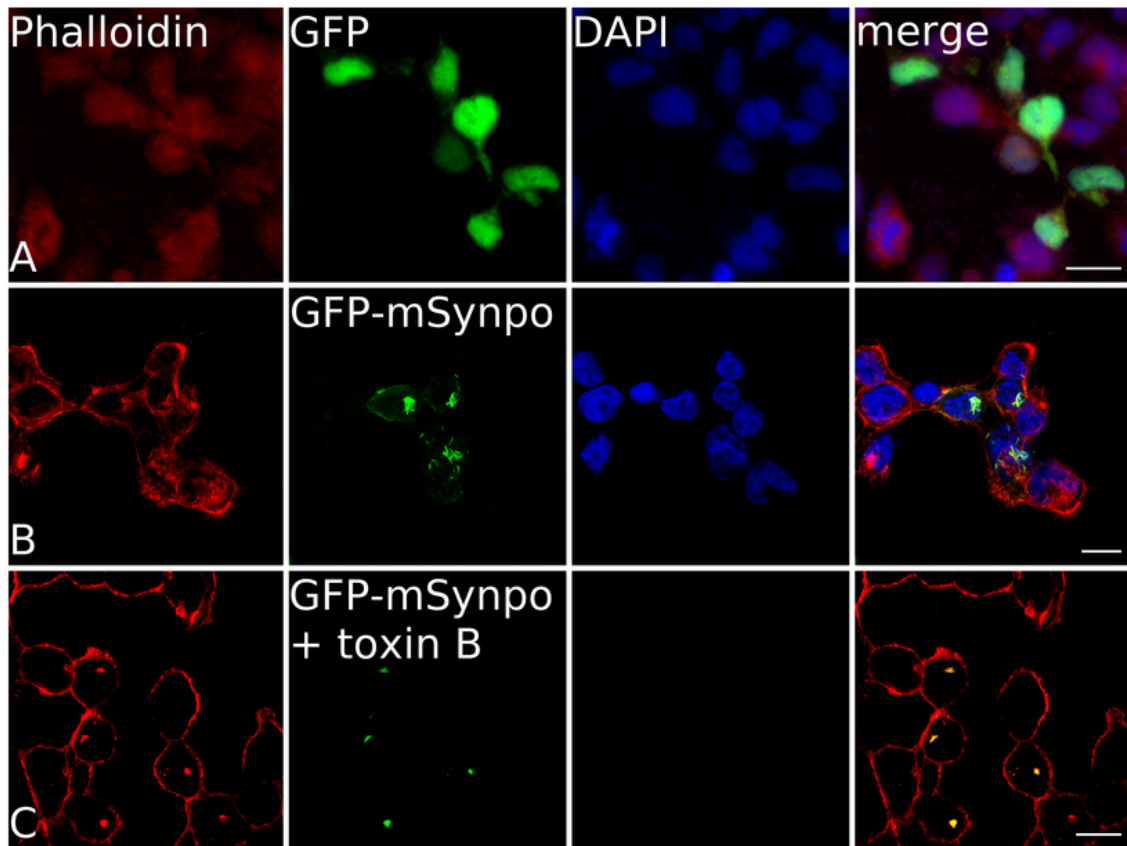
**Figure 3.10.:** (A) Phalloidin-stained F-actin (red) in NSC-34 cells suggest a role for small Rho-GTPases in alterations of Synaptopodin expression. Transfection with eGFP alone (green) shows a uniform distribution in NSC-34 cells, whereas transfection of eGFP-mSynpo (B) remains constricted to a smaller area inside individual cells. (C) After treatment with *Clostridium difficile* toxin B a strong decrease of intrinsic F-actin levels is accompanied with a reduced fluorescence of eGFP-mSynpo. Scale bars A: 1 µm, B, C: 10 µm.

## 3.10. Spine apparatus morphology after treatment with inhibitors

In vivo-like experiments revealed the molecular requirements on how to rescue spine apparatus organelles in CA3 pyramidal neurons. In vitro experiments showed a potential influence of F-actin inhibition with *Clostridium difficile* toxin B on reduced Synaptopodin expression levels *in vitro*. Therefore we were interested, if spine apparatus morphology is affected by pharmacological disruption of neuronal activity and actin (de-) polymerization. Inhibitors were bath-applied for a total period of three days directly after electro-

poration of mSynpo in the KO and on wild-type slices, which were left un-transfected. Inhibitors were applied as is customary in scientific literature.

### 3.10.1. Restoration process of spine apparatus is independent on neuronal activity

There is no data from scientific literature about a direct influence of sodium-channel blocker TTX on spine apparatuses or spines housing such an organelle. Morphological changes on spines induced by treatment of TTX in organotypic hippocampal slices may occur, although, there is still little information and conflicting data in scientific literature. An increase in spine density was proposed [Drakew *et al.* , 1999], whereas other laboratories did not measure any changes in spine density due to TTX treatments [McKinney *et al.* , 1999], [Tyler & Pozzo-Miller, 2003]. Chronic treatments of sodium-channel blocker TTX leads to individual spine head protrusions [Richards *et al.* , 2005] and an increased proportion of thin spines accompanied by a reduced proportion of mushroom-shaped spines [Tyler & Pozzo-Miller, 2003]. Remaining spines were significantly longer with significantly larger spine head diameters. The authors suggest that spine elongation is promoted by a reduced level of neuronal activity.

We were interested, if pharmacological blockade of synaptic activity has an impact on morphing processes of spine apparatuses and if morphology of appropriate mushroom-shaped spines might be modulated as well. For this endeavor, the sodium-channel blocker Tetrodotoxin (TTX) was applied to slices with a working concentration of 1 µM after genetic complementation in the KO and in wild-type slices. After disruption of neuronal activity, spine apparatus morphology seems to be enlarged for *de novo* formed organelles in spines and dendrites compared to untreated rescued ones (Figure 3.11 A, C; Figure 3.4 B, C). Mushroom-shaped spines did not further enlarge surface areas due to treatment with TTX, compared to those after genetic complementation without pharmacological inhibition of neuronal activity. Mushroom-shaped spines which were already enlarged after genetic complementation, were used as reference. No additional morphological increase was measured after pharmacological inhibition of neuronal activity. This was also the case for intrinsic spine apparatuses and might be not surprising, as expansion and growth should reach a limit.

In the wild-type treated with TTX morphology of spine apparatuses and mushroom-shaped spines seem to be enlarged due to the blockade of neuronal activity (Figure 3.11 B, Figure 3.3 A).
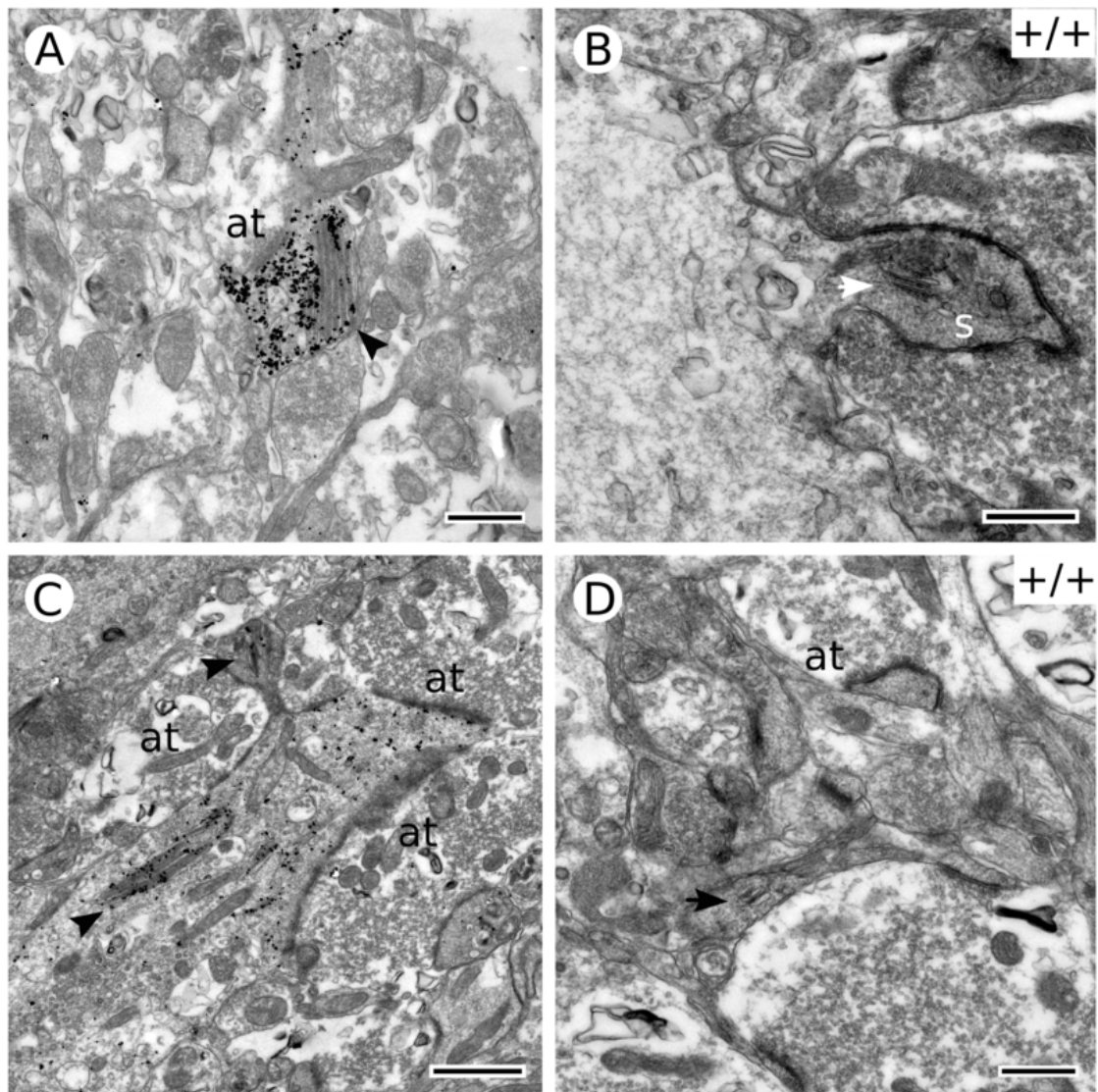
**Figure 3.11.:** Spine apparatus formation after treatment with TTX in wild-type and Synaptopodin transfected KO slice cultures (A, C). (B, D) Treatments with 1 µM TTX for three consecutive days seems to enlarge spine apparatus morphology in mushroom-shaped spines (s) and in dendrites (d) compared to pharmacological untreated wild-type slices. This enlargement seems to apply also for spine apparatuses after genetic complementation treated with TTX. Scale bars A, B, D: 0.5 µm, C: 1 µm.

Only recently, there is growing evidence that spines containing Synaptopodin may have mechanisms to counteract toxic effects. Spines housing a fully elaborated spine apparatus may be more resistant to toxic treatments than other spines not equipped with this organelle. For example, Vlachos and co-workers proposed a protective role against toxic treatment with Latrunculin for spines containing Synaptopodin. Spines without

this protein were more severely affected [Vlachos *et al.* , 2009]. Okubo-Suzuki proposed a protective role for Synaptopodin in the stabilization of F-actin fibers, leading to a stabilized activity-dependent increases in spine volume, as 'exogenous Synaptopodin suppressed staurosporine-dependent disruption of F-actin stress fibers' [Okubo-Suzuki *et al.* , 2008]. Our results suggest that this proposed protective mechanism against different neurotoxic inhibitors may apply not only for dissociated neuronal cultures but also for a mature network of hippocampal organotypic slices after blocking neuronal activity with TTX. Whether this protective mechanism is regulated by the protein Synaptopodin, by the spine apparatus itself or by the properties of highly specialized mushroom-shaped spines remains an issue for further investigations. We propose that the increase in spine motility, which drives the formation of filiform protrusions and leads to a general decreased spine density due to application of TTX in the bath does not affect all types of hippocmpal spines to the same extent. Mushroom-shaped ones containing a spine apparatus might be able to compensate due to an yet unknown mechanism.

## 3.11. Perturbing the actin monomer-polymer equilibrium by application of small Rho GTPase inhibitors

Dendritic spine formation and stability are highly dependent on the presence of microtubules and F-actin filaments, the latter being enriched in dendritic spines. The actin monomer-polymer equilibrium can be easily disturbed by application of toxins interfering with the crucial role of the Rho family of small GTPases in remodeling and reorganization of F-actin bundles. Of the 22 Rho GTPases identified to date, there are three members, RhoA, Rac1 and Cdc42, which are best characterized regarding their role in actin dynamics. They act as molecular switches to trigger various aspects concerning intracellular actin dynamics, alternating reversibly between an inactive GDP-bound and an active GTP-bound isoform. Rho GTPases were studied extensively and are well known to regulate different aspects of dendritic development [Negishi & Katoh, 2005].

### 3.11.1. *Clostridium difficile* toxin B

Treatment with *Clostridium difficile* toxin B catalyzes glucosylation of all Rho proteins and thereby inactivates the Rho-cascade as a whole, causing the loss of F-actin fibers. As Synaptopodin associates with bundling and stabilization of F-actin, we were interested, if pharmacological disruption of actin-depolymerizing *Clostridium difficile* toxin B affects morphing processes of spine apparatuses.

Treatments with toxin B (working concentration: 2 pM) had no deleterious effects on *de novo* formed spine apparatuses after genetic complementation in spines (Figure 3.12 A, Figure 3.4 B), but severely affected morphology of spine apparatuses in spines of the wild-type (Figure 3.12 B, Figure 3.3 A). The base to keep spine apparatuses grounded or in shape has been lost in a subset of spine apparatuses in spines (Figure 3.12 B, red arrowhead) leading to a complete loss of interdigitating filamentous material in some of these unique organelles. This gives us some insights into the intrinsic composition of spine apparatuses. Chronic treatment with *Clostridium difficile* toxin B led at least partially to the loss of the filamentous material in between individual sER tubules indicating that this filamentous material consists of condensed or constricted F-actin fibers [Capani *et al.* , 2001].

The loss of filamentous material and strong cohesive internal pool in between individual tubules of a subset of spine apparatuses led to a widely-dispersed morphology and/or to the onset of degradation and disassemble. This interpretation perfectly fits to the function of Synaptopodin protein in linking the spine apparatus assembly to growing F-actin fibers, which was severely disturbed after long-term treatments (for three consecutive days) with *Clostridium difficile* toxin B in wild-type slices.

Spine apparatuses in dendrites of wild-type slices were unaffected, if treated with toxin B (data not shown), whereas *de novo* formed dendritic spine apparatuses were strongly affected by the effects of actin-depolymerizing *Clostridium difficile* toxin B (Figure 3.12 C) compared to those after genetic complementation, as indicated by their disorganized and wide-ranging morphology herein.

Mushroom-shaped spines in the wild-type were also directly affected by perturbation of the actin monomer-polymer equilibrium and increased their surface areas (Figure 3.12 B). As re-introduction of Synaptopodin cDNA led already to a profound enlargement of spines housing a *de novo* formed spine apparatus, which were used as a reference, no further enlargement was observed after treatments with toxin B (Figure 3.12 A).

Inhibition of the entire Rho GTPases pathway blocks both, the F-actin polymerizing
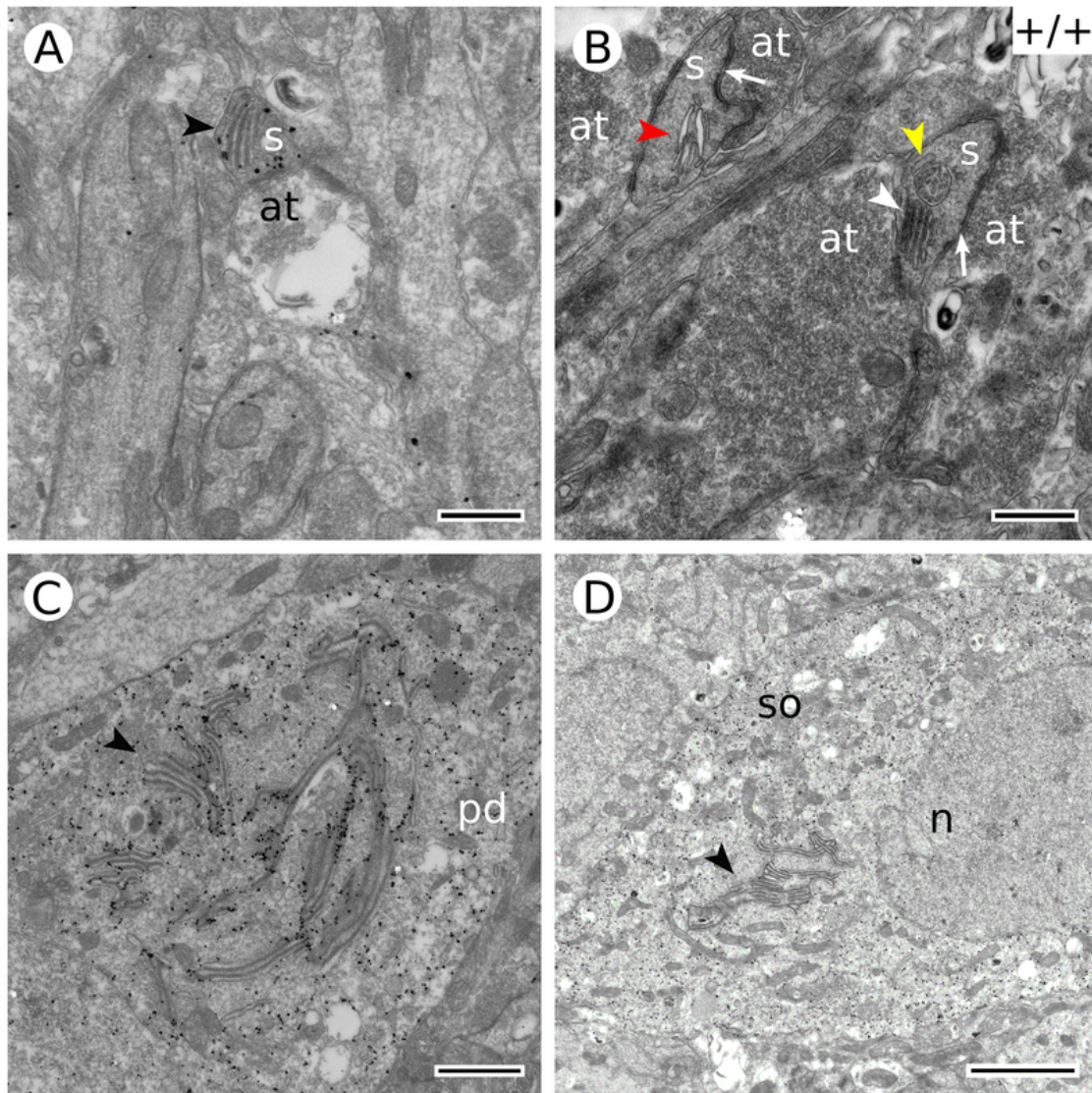
**Figure 3.12.:** Perturbing the actin monomer-polymer equilibrium by treatment with *Clostridium difficile* toxin B leads to severe morphological defects of spine apparatuses and mushroom-shaped spines in the wild-type. (A) After genetic complementation spine apparatuses (black arrowheads) (s) did neither show any deleterious effects in mushroom-shaped spines, nor in distal or proximal dendritic (pd) parts (C). (D) The appearance of spine apparatus-like organelles in the soma (so) near the nucleus, was also seen after re-introduction of synaptopodin in former KO slices, which is in charge for this ectopic formation. (B) In spines of the wild-type a spine apparatus (red arrowhead) is depicted, which is more severely affected by treatment with actin-depolymerizing toxin B, than its close-by counterpart to the right (white arrowhead). The interconnecting filaments are completely lost and the remaining discs have probably lost cohesiveness. The multivesicular body next to a spine apparatus (B, yellow arrowhead) might be also an indicator for deleterious effects on the spine or intrinsic spine apparatus. Scale bars: A, B: 0.5 μm, C: 1 μm, D: 2 μm.

factors Rac1 and Cdc42, leading to a stable actin network and the G-actin stabilizing factor RhoA, leading to a loose actin network. This strong effect interfered with spine apparatus intrinsic stability and general morphology in the wild-type condition. Functionality might probably be also affected, due to the break-down of constricted F-actin bundles, which connect single sER tubules.

Inhibition of Rho-GTPase cascade as a whole also interfered with the compartmental distribution of spine apparatuses. Both, in the wild-type and after genetic complementation in the KO, the previously observed distribution pattern for spine apparatuses shifted toward a uniform one, where *de novo* formed organelles appeared in relatively high numbers in somatic regions (Figure 3.12 D).

## 3.11.2. ROCK-Inhibitor Y-27632

Cellular functions of the most prominent Rho GTPase RhoA include myosin phosphorylation, formation of stress fibers and focal adhesion. ROCK I and ROCK II are RhoA's downstream effectors and are selectively associated with the GTP-bound active form of RhoA. ROCK II is strongly enriched in pyramidal cells of the hippocampus. It has been shown by several scientific groups that ROCK inhibition leads to a loss of stress fibers and focal adhesion [Fujisawa *et al.* , 1996], [Uehata *et al.* , 1997], [Liao *et al.* , 2007]. Considering the results obtained by chronic application of *Clostridium difficile* toxin B and its influence on morphological destabilization of spine apparatuses based on the loss of internal F-actin fibers in wild-type slices, it remained uncertain, whether inhibition of one Rho GTPase in particular regulates the dynamics and increase of the spine apparatus, or if all of them collaboratively were involved in this effect. In the following, the question of whether the inhibition of a single GTPase, RhoA, in particular is sufficient to regulate the dynamics and increase of spine apparatuses was investigated.

The ROCK-Inhibitor Y-27632 (working concentration: 0.1 µM) was used for treatment of slice cultures, as Y-27632 addresses both ROCK isoforms by binding to their ATP-dependent kinase domains.

Compartmental distribution of spine apparatuses in the KO after genetic complementation and in wild-type CA3 pyramidal cells remained unaltered after treatment with Y-27632. *De novo* formed spine apparatuses and their related mushroom-shaped spines were similarly affected after treatments with Y-27632 (Figure 3.13 B), if compared to *Clostridium difficile* toxin B. Late endosomal multivesicular bodies (MVBs) were present in high absolute numbers in close vicinity to spine apparatuses in spines (Figure 3.13 A,

yellow arrowhead) and some appeared in parental dendrites. The appearance of MVBs selectively occurred after treatments with small Rho-GTPases inhibitors. In adult wild-type hippocampal CA1 pyramidal neurons ($> P21$) a total overlap of 8.3 % between sER and endosomal compartments - including MVBs - was calculated by serial sectioning of Immunoelectron microscopy [Cooney *et al.* , 2002].
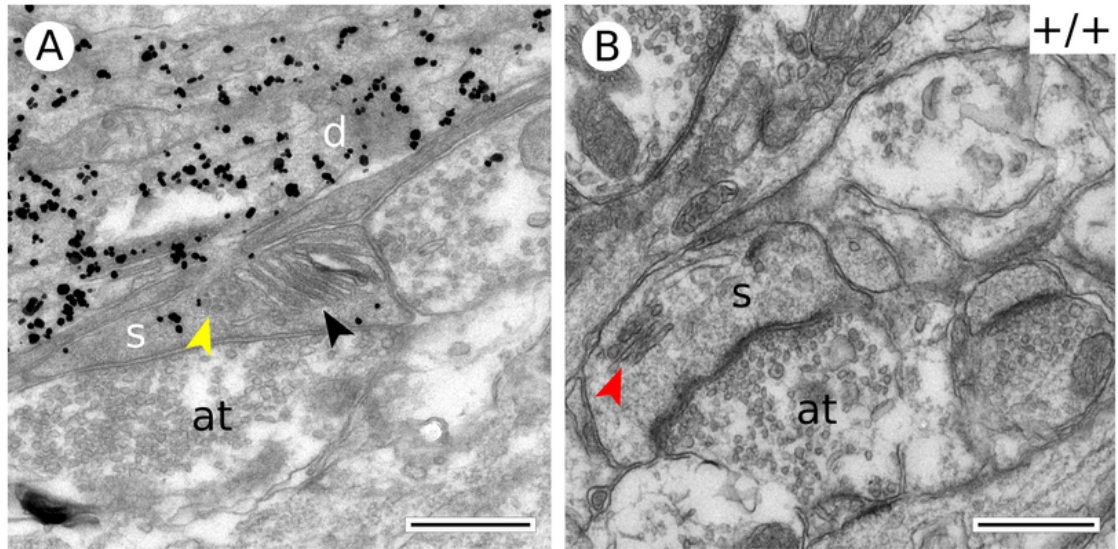


**Figure 3.13.:** Morphological deleterious effects after treatments with ROCK-Inhibitor Y-27632 on rescued and wild-type derived spine apparatuses. (A) A newly emerged spine apparatus after genetic complementation (black arrowhead) in a mushroom-shaped spine (s) adjacent to a multivesicular body (yellow arrowhead) seems to be under deconstruction after treatment with ROCK inhibitor Y-27632 for three consecutive days, as individual tubules detach from the organelles' closely packed shape. (B) The spine apparatus in the spine of the wild-type condition has completely lost its interdigitating filaments (red arrowhead) and individual tubules are decomposing. Scale bars A: 0.5 µm, B: 1 µm.

MVBs may be involved in the local recycling and degradation processes of single, detached sER tubules of spine apparatuses in spines, quite similar to endoplasmic reticulum-associated degradation process (ERAD). *De novo* formed spine apparatuses in dendritic compartments, which were tremendously affected by *Clostridium difficile* toxin B treatments were less severely affected and increase of surface areas was smaller after treatment with Y-27632. In the wild-type condition the general deleterious effects were again more tremendous than in the transfected KO (Figure 3.13 B). In some cases, spine apparatuses were completely depleted due to the loss of intrinsic F-actin fibers. Individual tubules lost cohesion and appeared in a wide-ranging morphology or seemed to be under degra-

dation. Due to the lack of absolute numbers of spine apparatuses in dendrites of the wild-type ($n = 1$; (Figure 3.15 A), no predictions or conclusions can be provided for this compartment. Taken together, observations obtained by application of ROCK-Inhibitor Y-27632 in the wild-type, underlines the importance of a balanced Rho-ROCK pathway for intact spine stability [Lin & Koleske, 2010] and intact morphological appearance of spine apparatuses.

### 3.11.3. Latrunculin A

Latrunculin A, a marine toxin with a high degree of stability in context of long term treatments [Spector *et al.* , 1989] causes the shortening and thickening of stress fibers by modulating actin filaments. It binds to G-actin and inhibits the rate of nucleotide exchange [Yarmola *et al.* , 2000] causing structural alterations and making it impossible for G-actin to polymerize [Morton *et al.* , 2000]. As as a general stability of spines containing synaptopodin against treatments with Latrunculin was already proposed [Vlachos *et al.* , 2009], we were interested in morphological effects of Latrunculin A (working concentration: 2.5 µM) on spine apparatus morphology. Spine apparatuses and related spines in the transfected KO condition were much less affected (Figure 3.14 A) than in the wild-type. Prolonged treatment of slice cultures with Latrunculin A partially resulted in fragmentation of spine apparatuses to ER mini-stacks (Figure 3.14 B). It remains unclear, if it was due to the strong deleterious effects, which led to limitation in absolute numbers and survival of transfected cells and a rare appearance of organelles. This constraint only allows, to draw preliminary conclusions on a basis of qualitative observations and exploratory data analysis.
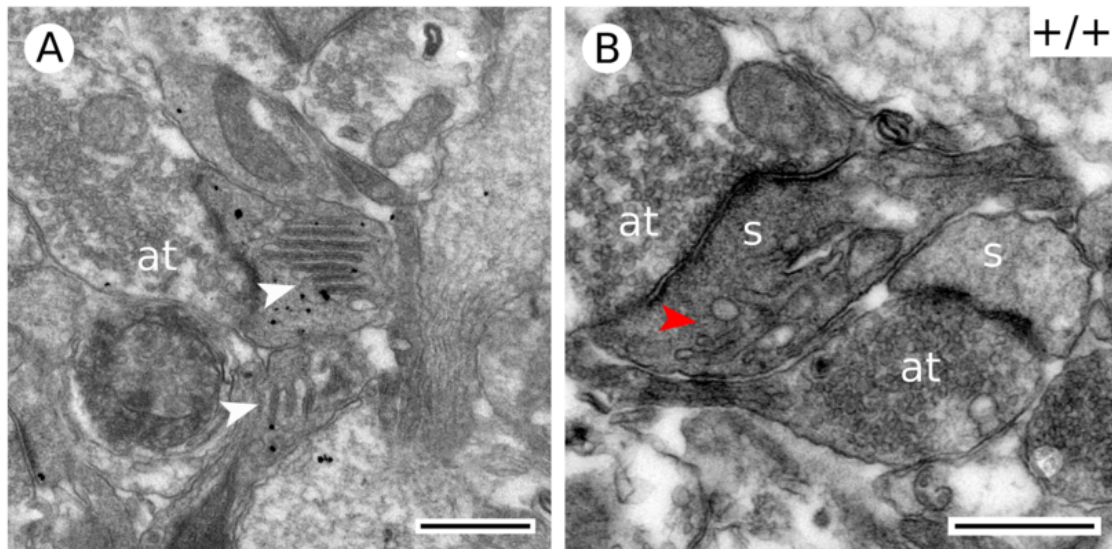
**Figure 3.14.:** Spine apparatuses exhibit great morphological defects after treatment with Latrunculin A. (A) Reestablished spine apparatuses (white arrowheads) in mushroom-shaped spines (s) did not show severe morphological defects after treatment with Latrunculin A. (B) The spine apparatus on the left (red arrowhead) seems to be under deconstruction after treatment with Latrunculin A for three consecutive days. The interconnecting F-actin based filaments have completely vanished and the stacked discs of endoplasmic tubes are under defragmentation. Scale bars A, B: 0.5 μm.

## 3.12. Spine apparatuses in relation to treatments with different inhibitors

As morphological observations showed tremendous differences for the Synaptopodin-transfected KO condition and for the untransfected wild-type condition, both will be analyzed separately concerning the impact of pharmacological inhibitors. Spine apparatuses treated with Latrunculin A were included in all violin plots and clustered-stacked Column Charts for visualizing general tendencies, even though quantitative statistical analysis can not be conducted, as the confidence level of 95% is reached only for spine apparatuses and related spines.

## 3.12.1. Quantitative analysis of rescued spine apparatus treated with inhibitors

The clustered-stacked Column Chart (Figure 3.15 A) gives an overview on spine apparatuses according to their compartmental distribution. Spine apparatus-like structures were present in the perikaryon, which can in all probability traced back to the introduction of Synaptopodin at late developmental time points (P 27-29), as this phenomenon occurred also in the KO transfected with synaptopodin cDNA. *De novo* formed spine apparatuses after treatments with pharmacological inhibitors, were present predominantly in dendrites, with one exception for toxin B, which was appeared almost uniformly in dendrites, spines and the perikaryon. The number of intact spine apparatuses was severely reduced after treatments with pharmacological inhibitors of Rho GTPases and accompanied by the appearance of late endosomal compartments (MVBs), which were often observed in close vicinity to spine apparatuses. The presence of MVBs is a clear indicator for processes of decomposition or degradation.

The total spread of data for spine apparatuses and spines is constricted to a small range around the median (Figure 3.15 B, C) if compared to the untreated Synaptopodin transfected control. As spine apparatuses have already increased surface area after genetic complementation, increase in surface area for spine apparatuses due to treatments with pharmacological inhibitors is generally small. This applies for spines, dendrites and somatic regions. Spine apparatuses in spines treated with toxins show medians slightly higher than untreated control (0.072 $\mu m^2$; IQR: 0.157). This was computed for TTX (0.094 $\mu m^2$; IQR: 0.042), *Clostridium difficile* toxin B (0.103 $\mu m^2$; IQR: 0.062), ROCK-inhibitor Y-27632 (0.082 $\mu m^2$; IQR: 0.086) and for Latrunculin A (0.10 $\mu m^2$; IQR: 0.069). Off note, a confidence level of 95% was reached for Latrunculin-treated slices and *de novo* formed spine apparatuses. Nevertheless, the obtained increase was not significant, if compared to the untreated control. After treatment with inhibitors, narrow IQRs fall completely within the broad range of the untreated control. Related mushroom-shaped spines (Figure 3.15 C) remained almost unaffected by any kind of pharmacological inhibition, if compared to their control, those after synaptopodin reintroduction. This becomes obvious by comparing medians of spines treated with TTX (0.362 $\mu m^2$; IQR: 0.21), *Clostridium difficile* toxin B (0.363 $\mu m^2$; IQR: 0.249), ROCK-inhibitor Y-27632 (0.341 $\mu m^2$; IQR: 0.231) and with Latrunculin A (0.404 $\mu m^2$; IQR: 0.088) to the median of the control condition (0.366 $\mu m^2$; IQR: 0.783). The small variations did not lead to any statistical significance (Table 3.3).

In dendrites (Figure 3.15 D), some extraordinary large outliers are visible on the upper whiskers of *Clostridium difficile* toxin B, TTX and control condition. The median for spine apparatuses in the untreated control (0.15 µm$^2$; IQR: 0.274) is higher and range of data is completely covered by spine apparatuses treated with TTX (0.21 µm$^2$; IQR: 0.274) and ROCK-inhibitor Y-27632 (0.186 µm$^2$; IQR: 0.206). Only dendritic spine apparatuses treated with *Clostridium difficile* toxin B clearly fall out of range with a median of 0.674 µm$^2$ (IQR: 0.892) and exhibit high statistical significance ($p = 1.23$ E-06). For perisomatic regions a confidence level of 95% was reached only for control and toxin B treated condition where no statistical significance was computed, as *Clostridium difficile* toxin B treated condition falls within the broad range of data covered by control condition (data not shown).

*De novo* formed spine apparatuses and related spines are protected against deleterious effects and treatments with pharmacological inhibitors blocking neuronal activity or Rho GTPases. Neither pharmacological disruption of neuronal activity nor inhibition of actin de-polymerization affected morphology of *de novo* formed organelles. The only exception, toxin B, had some impact on newly formed organelles in dendrites.

All calculated medians, IQRs and other variables can be looked up in Table A.1 and the computed statistical significance is summarized in Table 3.3.
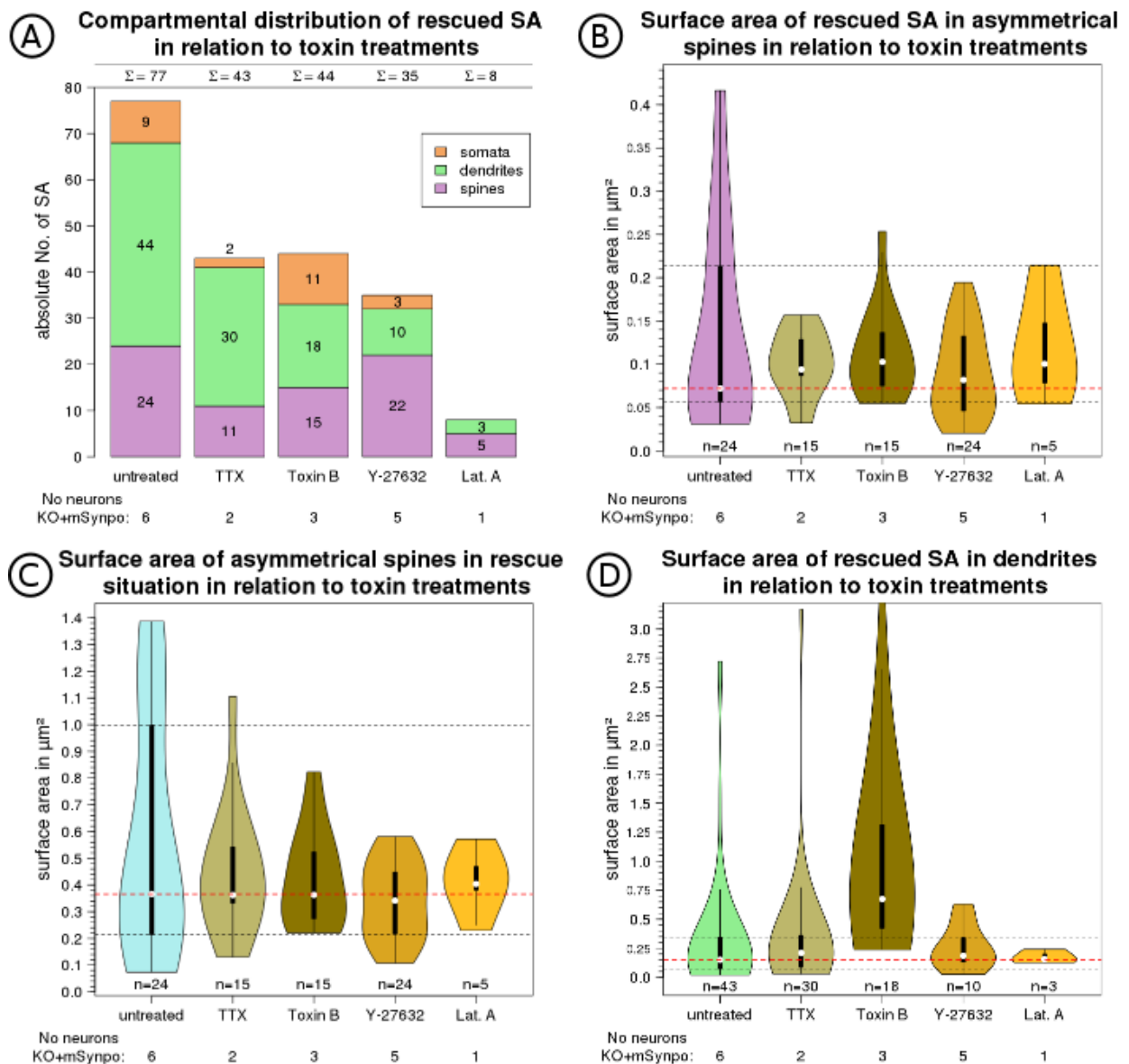
**Figure 3.15.:** (A) The compartmental distribution shows numbers of *de novo* formed spine apparatuses in relation to treatments with different pharmacological inhibitors. (B) Surface areas of spine apparatuses were in line with control. (C) This applies as well for related mushroom-shaped spines after treatment with inhibitors. (D) Newly formed organelles in dendrites increased significanty only after treatment with *Clostridium difficile* toxin B ($p = 1.23E - 06$).

**Table 3.3.:** Exact calculation of p-values of *de novo* formed spine apparatuses in relation to different toxin treatments

**Rescued SA in mushroom-shaped spines ($n = 24$) in relation to inhibitors**

| TTX ($n = 15$) | | | toxin B ($n = 15$) | | | Y-27632 ($n = 24$) | | | Latrunculin A ($n = 5$) | | |
|---|---|---|---|---|---|---|---|---|---|---|---|
| W | **p-value** | star code | W | **p-value** | star code | W | **p-value** | star code | W | **p-value** | star code |
| 173 | 0.853 | - | 159 | 0.558 | - | 335 | 0.341 | - | 55 | 0.801 | - |

**Mushroom-shaped spines after genetic complementation ($n = 24$) in relation to inhibitors**

| TTX ($n = 15$) | | | toxin B ($n = 15$) | | | Y-27632 ($n = 24$) | | | Latrunculin A ($n = 5$) | | |
|---|---|---|---|---|---|---|---|---|---|---|---|
| W | **p-value** | star code | W | **p-value** | star code | W | **p-value** | star code | W | **p-value** | star code |
| 183 | 0.943 | - | 187 | 0.853 | - | 345 | 0.257 | - | 60 | 1 | - |

**Rescued spine apparatuses in dendrites ($n = 44$) in relation to inhibitors**

| TTX ($n = 30$) | | | toxin B ($n = 18$) | | | Y-27632 ($n = 10$) | | | Latrunculin A ($n = 3$) | | |
|---|---|---|---|---|---|---|---|---|---|---|---|
| W | **p-value** | star code | W | **p-value** | star code | W | **p-value** | star code | W | **p-value** | star code |
| 577 | 0.452 | - | 101 | 1.23E-06 | *** | 190 | 0.583 | - | 61 | 0.9 | - |

**Rescued spine apparatus-like structures in the perikaryon ($n = 9$) in relation to toxin treatments**

| TTX ($n = 2$) | | | toxin B ($n = 11$) | | | Y-27632 ($n = 3$) | | |
|---|---|---|---|---|---|---|---|---|
| W | **p-value** | star code | W | **p-value** | star code | W | **p-value** | star code |
| 7 | 0.727 | - | 41 | 0.552 | - | 17 | 0.6 | - |

## 3.12.2. Wild-type spine apparatuses in relation to treatments with different inhibitors

The clustered-stacked Column Chart gives an overview on the compartmental appearance of spine apparatuses (Table 3.4, A). Spine apparatuses in the wild-type treated with different pharmacological inhibitors were more affected than those, which formed newly after genetic complementation. This allows us some insight into spine apparatuses and related mushroom-shaped spines studied without overexpression of synaptopodin. The statistical dispersion for spine apparatuses and spines, indicated by the IQRs is generally much higher after treatments with inhibitors, if compared to untreated wild-type. The median for surface areas of wild-type spine apparatuses in spines (0.024 $\mu m^2$; IQR: 0.018) is smaller compared to those treated with inhibitors like TTX (0.037 $\mu m^2$; IQR: 0.027), *Clostridium difficile* toxin B (0.046 $\mu m^2$; IQR: 0.059) and ROCK-inhibitor Y-27632 (0.041 $\mu m^2$; IQR: 0.039) (Table 3.4, B).

Spine apparatuses seem to be severely affected if treated with Rho-GTPases inhibitors as internal coherence might be lost due to missing interdigitating filaments. This observation is perfectly mirrored by the obtained increase for their surface areas. This increase is statistical significant for treatments with *Clostridium difficile* toxin B (p = 0.033) and for treatments with ROCK-Inhibitor Y-27632 (p = 0.037). Nevertheless, it is worth mentioning that significance for spine apparatuses treated with sodium-channel blocker TTX was close to achieve (p = 0.059). Spines housing spine apparatuses were similarly affected. The median surface area of wild-type mushroom-shaped spines (0.162 $\mu m^2$; IQR: 0.1; Figure 3.16) is smaller than the median surface areas of those after application of TTX (0.262 $\mu m^2$; IQR: 0.207), *Clostridium difficile* toxin B (0.338 $\mu m^2$; IQR: 0.259) and ROCK-inhibitor Y-27632 (0.266 $\mu m^2$; IQR: 0.299) and a broader range of data was covered by IQRs (Table 3.4, C). As confidence level of 95% was not reached for Latrunculin A due to the small sample size, it is not statistically analyzed. The obtained increase for spines treated with different pharmacological inhibitors is statistical significant for all other conditions with p-values covering the same range (TTX: p = 0.018, *Clostridium difficile* toxin B: p = 0.044; ROCK-inhibitor Y-2762: p = 0.018). The total amount of spine apparatuses present in dendritic areas were quite few after treatments with pharmacological inhibitors, affirming the compartmental distribution in the wild-type. Only after treatments with TTX and *Clostridium difficile* toxin B, the number of spine apparatuses are sufficient to reach a confidence level of 95% and to draw some conclusions. Median surface areas after treatment with TTX (0.056 $\mu m^2$; IQR:

**Table 3.4.:** Exact calculation of p-values for wild-type spine apparatuses and spines in relation to treatments with different inhibitors

**Surface area of wild-type SA in spines ($n = 29$) in relation to treatments with inhibitors**

| TTX ($n = 16$) | | | toxin B ($n = 5$) | | | Y-27632 ($n = 10$) | | | Latrunculin A ($n = 3$) | | |
|---|---|---|---|---|---|---|---|---|---|---|---|
| W | **p-value** | star code | W | **p-value** | star code | W | **p-value** | star code | W | **p-value** | star code |
| 152 | 0.0589 | - | 29 | 0.0334 | * | 80 | 0.0365 | * | 26 | 0.286 | - |

**Surface area of wild-type spines ($n = 29$) in relation to treatments with inhibitors**

| TTX ($n = 16$) | | | toxin B ($n = 5$) | | | Y-27632 ($n = 10$) | | | Latrunculin A ($n = 3$) | | |
|---|---|---|---|---|---|---|---|---|---|---|---|
| W | **p-value** | star code | W | **p-value** | star code | W | **p-value** | star code | W | **p-value** | star code |
| 133 | 0.0183 | * | 31 | 0.0436 | * | 72 | 0.0179 | * | 16 | 0.0823 | - |

**Surface area of wild-type SA in dendrites ($n = 13$) in relation to treatments with inhibitors**

| TTX ($n = 7$) | | | toxin B ($n = 6$) | | |
|---|---|---|---|---|---|
| W | **p-value** | star code | W | **p-value** | star code |
| 38 | 0.588 | - | 29 | 0.416 | - |

0.038) and *Clostridium difficile* toxin B (0.046 µm$^2$; IQR: 0.024) both exceed the one in the wild-type (0.028 µm$^2$; IQR: 0.012) (Table 3.4, D). Although spine apparatuses in dendrites show increased surface areas, statistical significance was not achieved and the number of analyzed organelles does not allow to draw further conclusions for dendritic organelles.

Both spine apparatuses and mushroom-shaped spines show a clear increase of surface areas and ample morphology and were affected by pharmacological disruption of neuronal activity and actin de-polymerization.
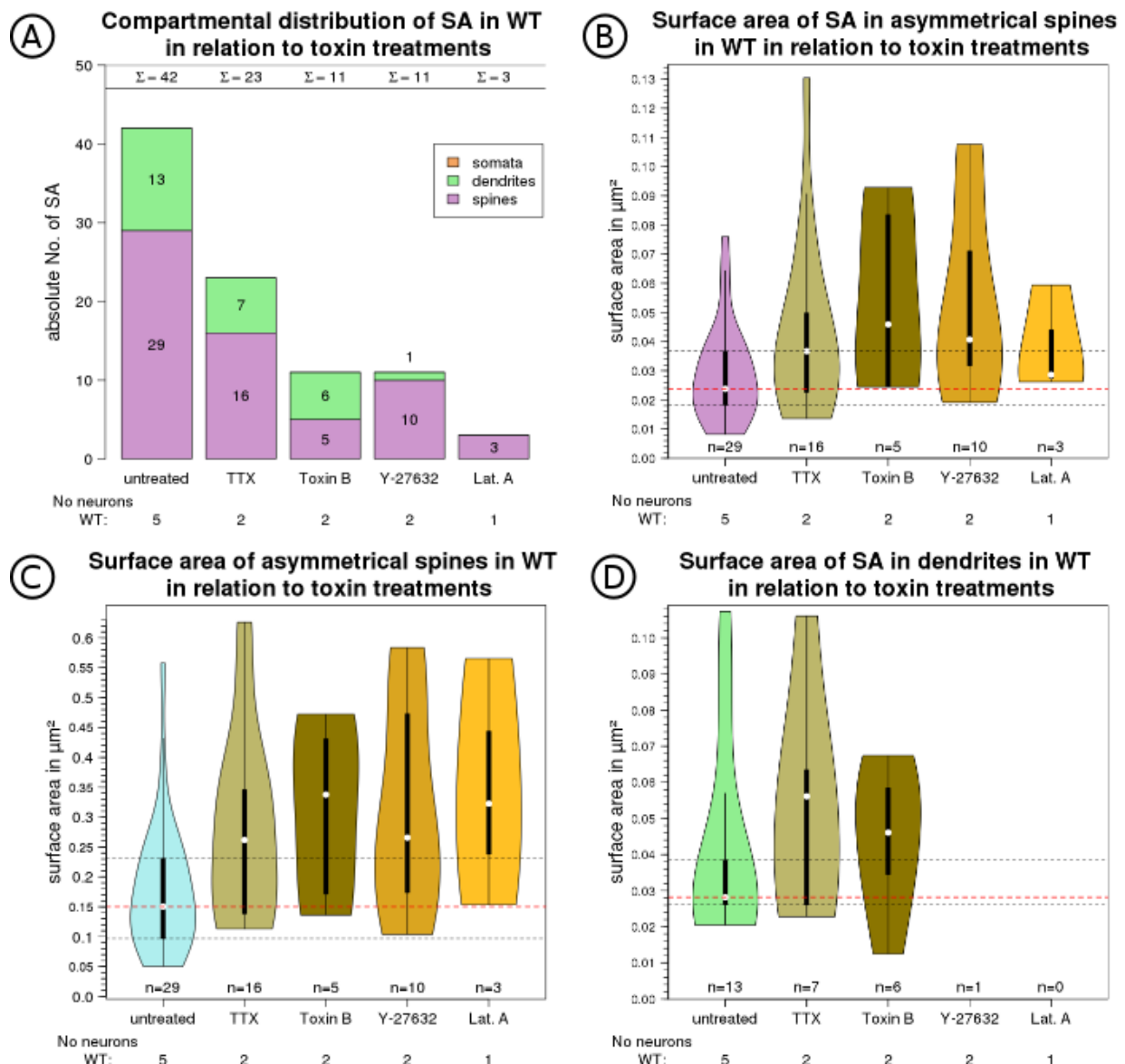
**Figure 3.16.:** (A) Overview on the compartmental distribution of spine apparatuses in the wild-type in relation to different pharmacological inhibitors. Violin plots show increased surface areas of wild-type spine apparatuses (B) and related mushroom-shaped spines (C) in relation to treatments with TTX and different Rho-GTPase inhibitors. Treatments with Rho GTPase inhibitors lead to significantly enlarged surface areas for spine apparatuses and related mushroom-shaped spines. (D) Surface areas of dendritic spine apparatuses did not show any significant enlargement after treatment with inhibitors.

### 3.12.3. Is the correlation between spine apparatuses and spines still ensured after treatments with different inhibitors?

Median surface areas of spine apparatuses were divided by those of related spines. The relation between mushroom-shaped spines and intrinsic spine apparatuses remained unaffected (Figure 3.17 A, B) as variations are small and no statistical significance was calculated (Table 3.5). Medians and IQRs can be found Table A.2.
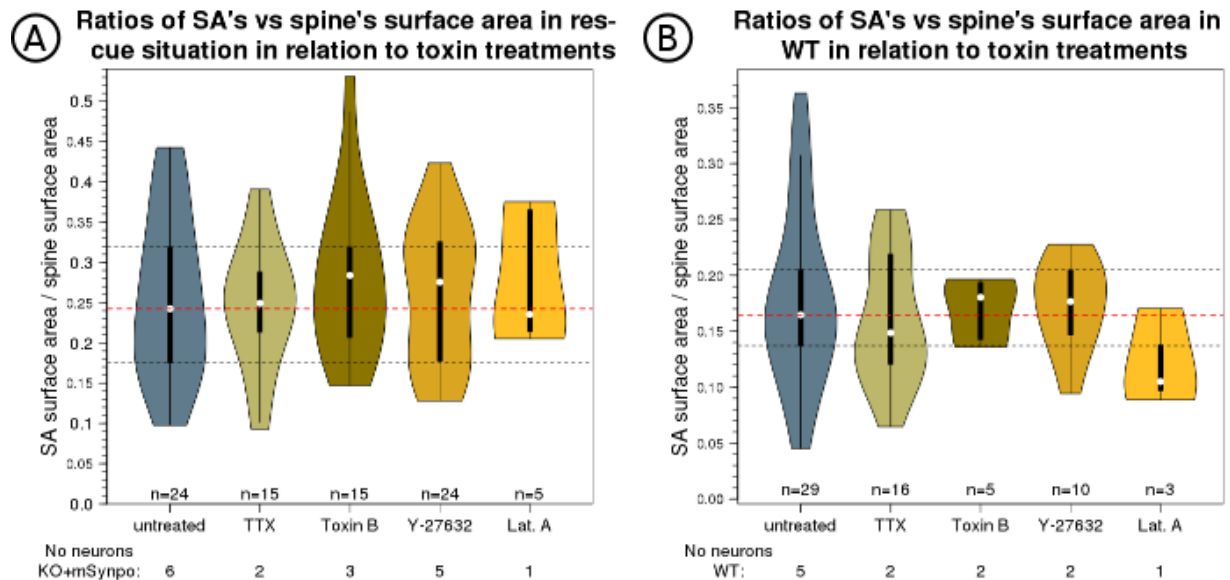


**Figure 3.17.:** The quotient surface areas of spine apparatuses divided by related spines' shows a direct correlation between both

This result suggests that mushroom-shaped spines housing spine apparatuses have the ability to enlarge and adapt to internal changes of actin de-polymerizing inhibitors in the same range than intrinsic spine apparatuses. Enlarged surface areas of spine apparatuses led to an enlargement of related mushroom-shaped spines. This was observed in the wild-type and for *de novo* formed organelles after genetic complementation.

**Table 3.5.:** Exact calculation of p-values for the ration of spine apparatuses over related spines in relation to treatments with inhibitors

**Ratios of SA's vs spines' surface area in the rescue situation ($n = 24$) in relation to inhibitors**

| TTX ($n = 15$) | | | Toxin B ($n = 15$) | | | Y-27632 ($n = 24$) | | | Latrunculin A ($n = 5$) | | |
|---|---|---|---|---|---|---|---|---|---|---|---|
| W | **p-value** | star code | W | **p-value** | star code | W | **p-value** | star code | W | **p-value** | star code |
| 184 | 0.921 | - | 153 | 0.449 | - | 280 | 0.878 | - | 48 | 0.518 | - |

**Ratios of wild-type SA's vs spines' ($n = 29$) in relation to inhibitors**

| TTX ($n = 16$) | | | Toxin B ($n = 5$) | | | Y-27632 ($n = 10$) | | | Latrunculin A ($n = 3$) | | |
|---|---|---|---|---|---|---|---|---|---|---|---|
| W | **p-value** | star code | W | **p-value** | star code | W | **p-value** | star code | W | **p-value** | star code |
| 268 | 0.404 | - | 72 | 1 | - | 136 | 0.788 | - | 64 | 0.207 | - |

## 3.13. Spine apparatuses in spines vs spine apparatuses in dendrites

Are spine apparatuses in spines smaller compared to dendritic ones in the wild-type. Does this apply also for *de novo* formed organelles? If compartmental constrictions and peculiarities are responsible for morphological constraints of spine apparatuses in spines, these organelles would gain surface area, if they are located in parental dendrites. If compartmental constrictions do not have any influence on the surface area of spine apparatuses and if size of these organelles is regulated or influenced more by other terms, the surface area should remain unaltered. This inter-compartmental / intra-conditional comparison revealed the following. *De novo* formed organelles show a morphological increase if present in dendrites, compared to those in spines after treatments with different inhibitors. Of note, spine apparatuses after genetic complementation barely missed significance. Wild-type spine apparatuses contrariwise gained surface areas selectively after overexpression and not after treatments with pharmacological inhibitors. All p-values can be found Table 3.6.

**Table 3.6.:** Exact Wilcoxon rank sum test on Surface area of SA in spines vs. Surface area of spine apparatuses in dendrites

| Conditions | total numbers | W | p-value | star code |
|---|---|---|---|---|
| WT | 29 / 13 | 123 | 0.07681 | |
| WT + mSynpo | 12 / 23 | 50 | 0.001598 | ** |
| WT + TTX | 16 / 07 | 41 | 0.3411 | |
| WT + toxin B | 05 / 06 | 17 | 0.7922 | |
| WT + Y-27632 | 10 / 01 | 8 | 0.5455 | |
| | | | | |
| Heterozygote | 17 / 03 | 16 | 0.3579 | |
| | | | | |
| KO + mSynpo | 24 / 43 | 371 | 0.05844 | |
| KO + mSynpo + TTX | 11 / 30 | 125 | 0.01536 | * |
| KO + mSynpo + toxinB | 15 / 18 | 1 | 3.857E-009 | *** |
| KO + mSynpo + Y-27632 | 22 / 10 | 43 | 0.0027 | ** |

# 4. Discussion

The hippocampus is essential for the consolidation of information from short-term memory to long-term memory and for spatial navigation. Its clinical importance is demonstrated by the observation that first pathological signs of Alzheimer's Disease manifest in the hippocampus [Ballmaier *et al.* , 2008], [Allen *et al.* , 2011], [Mu & Gage, 2011]. Hippocampal CA3 pyramidal neurons play a key role for the processing, storage and recall of spatial information in the hippocampal network [Lisman, 1999]. They receive major excitatory input by mossy fibers from granule cells of the dentate gyrus and give rise to Schaffer collaterals, the excitatory efferents innervating CA1 pyramidal neurons. A single granule cell axon gives rise to about 15 large mossy fiber boutons in the CA3 region, and a single CA3 pyramidal neuron receives input from approximately 50 mossy fiber axons [Amaral *et al.* , 1990]. The total length of the axonal plexus from single CA3 neurons can be as long as 150 - 300 mm, and a single CA3 cell may contact as many as 30.000 to 60.000 neurons in the ipsilateral hippocampus [Johnston & Amaral, 2003]. On the other hand, it has been estimated that a single CA1 neuron may be innervated by more than 5.000 ipsilateral CA3 pyramidal cells [Johnston & Amaral, 2003].

Therefore, the identification of molecular mechanisms involved in morphogenesis and structural plasticity of CA3 pyramidal neurons at the cellular, subcellular and ultrastructural level are essential to understand both synaptic transmission and hippocampal network formation.

The overall aim of this thesis project was to reveal molecular mechanisms for morphological alterations of CA3 pyramidal neurons at the cellular and subcellular level. To achieve this, single-cell electroporation of CA3 pyramidal neurons in organotypic hippocampal slice cultures was used to manipulate the expression of the axonal neural cell adhesion molecule L1CAM and of the postsynaptic protein synaptopodin which is essential for the formation of the spine apparatus. This approach was applied in slice cultures from wild-type mice to evaluate the axon branching capability of human L1CAM compared to disease-associated loss-of-function L1CAM mutations at the cellular level. Moreover, slice cultures from wild-type as well as synaptopodin-knockout mice were used to

study morphological changes and *de novo* formation of the spine apparatus after forced synaptopodin expression in single CA3 pyramidal neurons at the ultrastructural level. Finally, spine apparatus restoration and morphology following long-term application of pharmacological agents suspected to interfere with spine apparatus (re-) formation were investigated.

Therefore, this thesis work addressed the following major questions:

1. Does overexpression of the axonal cell adhesion molecule L1CAM promote axonal branching in CA3 pyramidal neurons and is this model system sufficient to evaluate human loss-of-function L1CAM mutations?

2. Is it possible to rescue spine apparatus formation in synaptopodin-deficient mice through restoration of synaptopodin expression at the single-cell level?

3. What are the consequences of elevated and restored synaptopodin levels for spine apparatus morphology?

4. How is spine apparatus morphology affected by pharmacological disruption of neuronal activity and actin (de-) polymerization?

5. Do changes in spine apparatus morphology correlate with morphological changes in mushroom-shaped spines?

## 4.1. Expression of the axonal cell adhesion molecule L1CAM promotes axonal branching in CA3 pyramidal cells

The role of L1CAM as an essential factor for axonal growth and guidance in the developing nervous system is well established [Maness & Schachner, 2007]. In addition, L1CAM is a potent inducer of axon branching *in vitro* [Hoffman *et al.* , 2008], [Moon & Gomez, 2010], [Cheng & Lemmon, 2004], [Schäfer & Frotscher, 2012].

The importance of L1CAM is further demonstrated by numerous human pathological mutations in the L1CAM gene, which cause a spectrum of neurological disorders referred to as L1 syndrome [Vos & Hofstra, 2010], [Schäfer & Altevogt, 2010]. The present results obtained from organotypic slice cultures showed that expression of human wild-type L1CAM by single-cell electroporation increases axonal arbor complexity

of CA3 pyramidal neurons. In general, the observed effects confirm that genetic manipulation of single CA3 pyramidal neurons in organotypic slice cultures is sufficient to induce morphological changes and did not interfere with their viable maintenance within neuronal networks, because L1CAM-dependent axon growth is primarily mediated by cell-cell interactions [Barry *et al.* , 2010]. In contrast, the two different human pathological L1CAM missense mutations p.R184Q and p.W1036L interfered with axonal targeting of L1CAM and L1CAM-dependent stimulation of axonal branching. Immunostaining using antibodies specific for overexpressed human L1CAM revealed that both mutations cause trafficking defects which disrupted axonal targeting and thereby the function of L1CAM [Schäfer *et al.* , 2010]. These findings are in agreement with previous studies in transgenic L1-CAM mice carrying a knockin of the human pathological mutation p.C264Y. This genetic mouse model exhibits axonal targeting defects [Rünker *et al.* , 2003] similar to those observed in human patients carrying L1CAM mutations [Kenwrick *et al.* , 2000]. However, the generation of transgenic mouse models is still a highly laborious technique and there is a need for alternative model systems to study pathomechanistic aspects of L1 syndrome. In this regard, the results not only provide a proof of principle for the successful modulation of CA3 pyramidal neuron morphology using the single-cell electroporation, but also demonstrate its utility to assess consequences of human gene mutations suspected to affect neuronal morphology.

## 4.2. Role of Synaptopodin in *de novo* formation of spine apparatuses

The spine apparatus is missing in synaptopodin-KO mice [Deller *et al.* , 2003]. This observation led to the hypothesis that restoration of synaptopodin expression might be sufficient to rescue spine apparatus formation in synaptopodin-KO mice. Using the single-cell electroporation approach, it was indeed possible to induce *de novo* formation of the spine apparatus in CA3 pyramidal neurons.

This result demonstrates that (I) synaptopodin-deficient neurons are potentially able to form a spine apparatus after genetic complementation, (II) the spine apparatus is formed in a cell autonomous manner and (III) that the molecules involved in spine apparatus formation are at steady state when synaptopodin has been overexpressed.

Although the spine apparatus was already described decades ago [Gray, 1959], its function and morphogenesis is poorly understood. Therefore, the present results raised a number

of questions as to how the overexpression of a single molecule can induce formation of a complex organelle, as well as to the subcellular location of this process and the molecular mechanisms associated with spine apparatus formation.

Previous studies provided evidence that genetic manipulation of a single molecule may control morphogenic properties of a neuronal organelle. Mice lacking the presynaptic cytoskeletal matrix protein bassoon display deficits in the formation of synaptic ribbons, a neuronal organelle involved in the turnover of the releasable pool of presynaptic vesicles [Frank *et al.* , 2010], [Dick *et al.* , 2003], [Khimich *et al.* , 2005], [tom Dieck *et al.* , 2005]. Interestingly, synaptic ribbons are most abundant in photoreceptor cells and sensory hair cells, suggesting that neuronal organelles support functional aspects of highly active neurons. It is conceivable that the formation of neuronal organelles in defined neuronal sub-populations may reflect specific demands and function.

Although bassoon and synaptopodin belong to different classes of proteins, they share some characteristic features, as both proteins act in cytoskeletal scaffolding to maintain morphological integrity of pre- and postsynaptic compartments, respectively.

It is well established that synaptopodin and other members of the synaptopodin family promote F-actin bundling and stability [Kremerskothen *et al.* , 2005], [Asanuma *et al.* , 2006], [Asanuma *et al.* , 2005], [Schroeter *et al.* , 2008], [Mundel *et al.* , 1997]. In spines, synaptopodin is strategically positioned in the neck of telencephalic dendritic spines and couples actin filaments to individual tubules of smooth endoplasmic reticulum. It has been proposed that such a mechanism may lead to the formation of the spine apparatus [Deller *et al.* , 2000]. Thus, the *de novo* formation of the spine apparatus in synaptopodin-KO mice by rescue of synaptopodin expression may rely on the linkage of the actin cytoskeleton to individual tubules of the smooth endoplasmic reticulum.

In addition to synaptopodin, other proteins may orchestrate the formation of the spine apparatus and its linkage to the actin cytoskeleton. From studies in the kidney, KIBRA protein was identified as a direct interaction partner of synaptopodin [Duning *et al.* , 2008]. Herein, KIBRA was associated with polarization of actin cytoskeleton dynamics. Its influence on actin or $\alpha$-actinin is supposed to regulate key aspects of cell motility in podocytes after binding to synaptopodin [Duning *et al.* , 2008]. Indeed, both proteins share many similarities. They have the same sites of activity in podocytes of the kidney as well as in the brain, where KIBRA is a component of postsynaptic densities [Johannsen *et al.* , 2008]. Both have been associated with the modification of synaptic plasticity and with memory formation [Makuch *et al.* , 2011], [Büther *et al.* , 2004], [Vlachos, 2011], [Segal *et al.* , 2010] and might be down-regulated in patients with Alzheimer's

disease [Hayashi *et al.*, 2010], [Reddy *et al.*, 2005]. According to all these functional similarities, it has been tested whether overexpression of KIBRA might be able to serve as a substitute for synaptopodin and rescue spine apparatus formation in synaptopodin-deficient mice.

My results show that restoration of the spine apparatus is exclusively mediated by synaptopodin, as KIBRA is not able to rescue spine apparatus formation and is therefore unable to compensate for the inimitable role of synaptopodin in the *de novo* formation of this organelle in mushroom-shaped CA3 pyramidal cells.

However, the obtained results revealed some insights into the interaction of KIBRA and synaptopodin. In wild-type mice, overexpressed eGFP-KIBRA showed a clustered appearance in dendrites and in the perikaryon of CA3 pyramidal neurons. These clusters were relatively large (diameters range from 0.712 µm$^2$ in dendrites to 1.045 µm$^2$ in the perikaryon) but their identity is yet unclear. The virtual lack of surrounding membranes makes it unlikely that these structures represent large membranous compartments such as late endosomes. eGFP-KIBRA was further observed in spines in close vicinity to the spine apparatus. The clustered appearance of eGFP-KIBRA but not its subcellular localization was lost in synaptopodin-KO mice, suggesting interaction of KIBRA and synaptopodin is not required to target KIBRA to spines.

KIBRA and synaptopodin proteins interact and therefore exhibit a high degree of co-localization in podocytes of the kidney [Duning *et al.*, 2008]. Both proteins might co-localize in an analogous manner in the brain, which may explain the formation and accumulation of large clusters after overexpression of KIBRA in CA3 pyramidal neurons.

## 4.3. Consequences of elevated synaptopodin levels for the morphology of the spine apparatus

Spine apparatuses are, under normal conditions, predominantly present in spines. This localization was restored in CA3 pyramidal neurons after genetic rescue of synaptopodin-KO mice by single-cell electroporation.

Of note, synaptopodin-overexpression led to highly significant increased surface areas of spine apparatuses in spines of the transfected KO condition. This effect might be due to a possible overload of transfected neurons with synaptopodin. In addition, the chosen time point for the introduction of synaptopodin at 21 DIV may complicate morphological

integration of these newly established organelles and is a critical factor for the overall morphology and persistent enlargement of spine apparatuses. There is no clear evidence, when exactly spine apparatuses develop in wild-type neurons or what signals lead to morphological restructurings of sER present in mushroom-shaped spines converting single sER tubules into fully established multitubular spine apparatuses. Spine apparatuses were shown to be established in one out of 24 mushroom-shaped spines at P21 and were completely absent at P15 [Cooney *et al.* , 2002].

An increase in the total number and surface area of spine apparatuses was also observed in dendrites of synaptopodin-overexpressing CA3 pyramidal neurons. Taken together, restoration of the spine apparatus by synaptopodin overexpression critically changed the absolute numbers and dimensions in dendrites and spines, likely due to a surplus of synaptopodin.

The overall increase in absolute numbers of spine apparatuses, which is most obvious in parent dendrites, leads to the hypothesis that synaptopodin-overexpression might induce retention of these organelles herein. However, this hypothesis implies that spine apparatuses are either transported along dendrites into spines or emerge from recruited and bundled tubules of the smooth endoplasmic reticulum, which penetrate into a subset of mushroom-shaped spines. To date, there is no evidence for these hypotheses.

These results indicate that the total amount of synaptopodin protein present per cell does not automatically play a critical role in the strategic positioning of spine apparatuses in spines. Absolute numbers of these organelles in spines were diminished to a small extent by overexpression in the wild-type and in synaptopodin-deficient mice. Nevertheless, we cannot exclude that these variations might have occurred due to methodological limitations of analyzed random electron microscopic sections, the low sample size and the unknown total amount of synaptopodin present per cell.

The penetration of sER into individual spine heads and the establishment of fully elaborated spine apparatuses takes place only in a subset of mature mushroom-shaped spines. Interestingly, there is a high degree of ER turnover rate in spines penetrated with sER [Ng & Toresson, 2011]. Only a subset of spines housing sER keep their ER for prolonged time periods [Toresson & Grant, 2005]. This dynamic distribution and the linked heterogeneity in $Ca^{2+}$ signaling might reflect the difference between those spines housing a fully elaborated spine apparatus and those, which are penetrated by single sER tubuli. The first one might refer to the ones which have already achieved structural plasticity and the second ones, having the potential to achieve plasticity.

The establishment and formation of spine apparatuses in spines might contribute to

structural stability by providing an increased ability of active $Ca^{2+}$ conductance through the constricted necks of mushroom-shaped spines into the parent dendrite. Structural stability and spine plasticity might be orchestrated by an interplay between synaptopodin and the spine apparatus' intrinsic pools of ryanodine receptors (RyRs), which are necessary for calcium release events from the spine apparatus and F-actin. F-actin is necessary for the accumulation of AMPA-type glutamate receptor subunit GluR1 in spine heads, which was shown to correlate with the presence of synaptopodin [Vlachos *et al.* , 2009]. Application of actin-depolymerizing Latrunculin A reduces the accumulation of GluR1 and synaptopodin staining. Blocking of RyR stores prevents GluR1 evoked spine plasticity [Vlachos *et al.* , 2009]. This interplay between synaptopodin and the spine apparatus provides the basis for a profound structural stability in spines, which is a morphological prerequisite for spine plasticity.

Overexpression of synaptopodin caused the ectopic formation of extraordinary large spine apparatus-like structures in the perikaryon near the nucleus. These spine apparatus-like structures might have formed to a lower quantity on-side of plasmid entry and were retained in the perikaryon. It remains unclear, if this retention is caused due to their extraordinary large size and/or the absence of interdigitating filaments.

Spine apparatus-like structures have not been observed after overexpression of eGFP-actin domain alone (data not shown). Interestingly, overexpression of eGFP-KIBRA caused similar spine apparatus like structures in the perikaryon, as observed after overexpression with eGFP-synaptopodin.

The formation of spine apparatus-like structures is reminiscent to malformations of the smooth endoplasmic reticulum observed in neuronal cultures [Teuling *et al.* , 2007]. A mutation in the vesicle-associated membrane protein-associated protein B (VAPB), which is involved in vesicle transport, causes the aggregation in immobile tubular ER clusters [Teuling *et al.* , 2007] and forms permanent inclusions in the smooth endoplasmic reticulum leading to dramatic restructurings, which may underlie the pathogenesis of amyotrophic lateral sclerosis (ALS) [Fasana *et al.* , 2010].

At present state, it remains an open question whether ectopic formation of spine apparatus-like structures in the perikaryon modifies cellular physiology. Since the spine apparatus has been proposed to act as an internal calcium store, $Ca^{2+}$ imaging after overexpression of synaptopodin in non-polarized cell lines may answer this question.

## 4.4. Consequences of elevated and restored synaptopodin levels for the spine compartment

Hippocampal spines are enlarged under physiological conditions by neuronal activity. The spine apparatus has the potential to perform versatile physiological functions inside the spine compartment, as these organelles provide an internal source of calcium and at the same time house a stable F-actin pool. Therefore, the spine apparatus along with synaptopodin's properties to link cytoskeletal elements to individual tubules of the spine apparatus might as well influence the spine compartment in hippocampal CA3 neurons. This question was investigated by direct measurements of surface areas from spines housing spine apparatuses and, more precisely, by dividing the surface areas of spine apparatuses by those of directly related spines.

All analyzed conditions with a persistent increase in median surface area of spine apparatuses showed additionally a significant increase for appropriate spines.

In the wild-type, surface areas of mushroom-shaped spines and their intrinsic spine apparatuses are counterbalanced and did not increase by increasing levels of synaptopodin. By dividing the surface areas of spine apparatuses by their spines, it becomes obvious that the principle of proportionality is upheld in the wild-type.

In heterozygote mice, spine apparatuses gained surface area to a moderate extent, whereas the increase in the wild-type was quite large. The converse is true for the transfected KO condition, where spine apparatuses exhibited an ample morphology by greatly increased surface areas. This imbalance in synaptopodin expression is also reflected in the disturbed principle of proportionality in those two conditions.

This leads to the assumption that synaptopodin might be indirectly involved in processes leading to structural modifications in spines by stabilizing or enlarging the rigid F-actin pool in the spine apparatus. Indeed, the regulation of actin-bundling activity was shown to be governed by synaptopodin's isoform-specific interaction with $\alpha$-actinin [Asanuma *et al.* , 2005] and synaptopodin colocalizes with $\alpha$-actinin 2 along actin filaments in pyramidal spines [Sánchez-Ponce *et al.* , 2012].

Synaptopodin controls the morphogenic properties of spine apparatus formation and the spine apparatus influences appropriate spine morphology and size.

The close interaction between spine apparatuses and spines is also in line with Spacek and Harris finding of proportional dimensions and a correlated size of the spine apparatus to the overall spine and synapse size in the hippocampal CA1 region [Spacek & Harris, 1997].

In fact, it has been suggested that synaptopodin may contribute to the maintenance of the spine structure, which is highly dependent on polymerized actin [Fischer *et al.* , 1998], [Fukazawa *et al.* , 2003].

Additionally, synaptopodin has been mechanistically linked to spine head plasticity due to the correlation of spine head motility via Rho-signaling [Fischer *et al.* , 2000], [Pilpel & Segal, 2004], [Korkotian & Segal, 2007]. The protein may provide a link between the actin cytoskeleton, growth of spine head volume and calcium signaling leading to the enlargement and structural plasticity of individual spine heads [Asanuma *et al.* , 2006]. Our results indicate that mushroom-shaped spines are still endowed with the capacity for a sustained enlargement, underlining a certain degree of morphological flexibility of these highly specialized compartments. Nevertheless, the detailed mechanism, how the principle of proportionality between spines and spine apparatuses is established, remains elusive. Synaptopodin might act as a key molecule to stabilize F-actin bundles in spine heads inside the spine apparatus. It has been shown that synaptopodin with its intrinsic actin bundling ability may play an important role for direct spine shaping by regulating dynamics of the actin cytoskeleton [Kremerskothen *et al.* , 2005], [Okubo-Suzuki *et al.* , 2008]. To correlate these results with structural plasticity, it would also be interesting to investigate, if this enlargement is accompanied with the recruitment and insertion of AMPAR, which has been shown to be associated with synaptic plasticity [Matsuzaki *et al.* , 2004].

## 4.5. Pharmacological disruption of actin de-polymerization affects wild-type spine apparatuses

Many molecular signals that control changes in dendritic spine morphology are activity-dependent and act through the regulation of F-actin [Ethell & Pasquale, 2005]. It has been shown that synaptopodin associates with bundling and stabilization of F-actin. This suggests that inhibitors of neuronal activity may interfere with the restoration of spine apparatuses in synaptopodin KO mice. Furthermore, rescue of spine apparatuses formation might be also sensitive to inhibition of small Rho GTPases, which are critical regulators of F-actin assembly and stabilization [Li *et al.* , 2002], [Hall & Lalli, 2010], [Chardin, 1999], [Witte & Bradke, 2008]. To test this hypothesis, organotypic slices

were cultured upon synaptopodin transfection in the presence of the sodium-channel blocker TTX, the small Rho-GTPase inhibitor *Clostridium difficile* toxin B, Y-27632, which inhibits the small Rho GTPase downstream effector ROCK and Latrunculin A.

In spines of the transfected KO condition, the morphology of spine apparatuses was unaffected after disruption of neuronal activity or by interfering with actin polymerization. No alterations in the compartmental appearance and no severe morphological defects on the organelle itself was observed after bath-application of sodium-blocker TTX. This applies also for treatments with GTPase inhibitors *Clostridium difficile* toxin B, ROCK inhibitor Y-27632 and Latrunculin A. Even though, a tendency towards higher median surface areas was visible in the transfected KO condition due to application of TTX, toxin B, Y-27632 and Latrunculin A, this gain in median surface area was not significant. This finding is in line with a recent study showing clear differences between spines housing synaptopodin and synaptopodin-negative ones after exposure to F-actin depolymerizing Latrunculin A in slice cultures. After 2.5 hours of exposure, spines without synaptopodin were modified or eliminated, whereas spines bearing synaptopodin were morphologically less affected [Vlachos *et al.* , 2009]. The authors conclude that synaptopodin may protect F-actin from destruction in spines.

In dendrites of the transfected KO condition a highly significant increase in the median surface area of rescued spine apparatuses was observable after prolonged application of *Clostridium difficile* toxin B. No such increase was observed by treatment with other Rho GTPase inhibitors or with sodium-channel blocker TTX. The reason for this sustained increase after application of *Clostridium difficile* toxin B is not easy to explain, as such an increase and high significance was obtained selectively in dendritic compartments. Furthermore increase in median surface areas of the untransfected wild-type conditions after application of toxin B remains small. The extreme ample morphology and heterogeneity in surface areas of spine apparatuses in dendrites (indicated by the broad Interquartile range) and the relatively low total number might have led to statistical significance. If this effect is caused by the actin-depolymerizing *Clostridium difficile* toxin B remains unclear. It might also result from synaptopodin-overexpression and the late time point of introduction, which led in combination with the actin-depolymerizing effects of toxin B to heterogeneity and ample morphology of spine apparatuses in dendrites. Nevertheless, synaptopodin overexpression in the KO condition alone did not lead to significant increased surface areas of spine apparatuses in parent dendrites compared to those in spines, even though, significance level of 0.05 was close to achieve.

In spines of the wild-type condition, morphology of spine apparatuses can be targeted
by inhibition of Rho GTPase signaling. Application of the small Rho-GTPase inhibitors
*Clostridium difficile* toxin B or ROCK inhibitor Y-27632 both led to a similar increase
in surface areas of spine apparatuses in mushroom-shaped spines. The increase was
restricted to the spine compartment and not observed for spine apparatuses present
in parent dendrites. Similar results were obtained after inhibiting neuronal activity by
the sodium-channel blocker TTX. Nevertheless, application of TTX did not lead to the
same increase in surface areas for spine apparatuses in spines compared to those without
application of TTX, as significance of 0.05 was narrowly missed.

Possible explanation: prolonged treatments with Rho GTPase inhibitors may disturb the
counterbalancing effect of synaptopodin on F-actin fibers in the wild-type, leading to a
loosened linkage between individual tubules of the spine apparatus and interdigitating
F-actin fibers. This might cause an increase in surface area rather than a decrease, as
cohesion between individual tubules is lost. Deconstruction of the F-actin dependent
fraction of spine apparatuses in the wild-type was indeed observed through the applica-
tion of *Clostridium difficile* toxin B, ROCK inhibitor Y-27632 and Latrunculin A, which
target selectively the equilibrium of F-actin polymers and G-actin monomers. No such di-
rect morphologically damaging effect was observed by the application of sodium-channel
inhibitor TTX. Elevated synaptopodin levels in the transfected KO condition might coun-
terbalance spine apparatus assembly herein. These observations indicate that the loss
of cohesion of individual tubules might depend critically on the total amount of synap-
topodin; as soon as the organelle's ability to drive structural stabilization is lost, the
organelle drifts apart and increases its surface area. Overexpression of synaptopodin
along with application of Rho GTPase inhibitors might stabilize the F-actin based pool
and cohesion between individual tubules of the spine apparatus after transfection. This
counterbalancing effect is probably due to synaptopodin's ability to interconnect the
spine apparatus organelle to the rigid F-actin pool. Normal expression level of synap-
topodin might not be able to prevent prolonged deleterious effects on F-actin, leading
to severe deleterious effects and depletion of the organelle, which was observed in sev-
eral cases. This observation is in agreement with previous studies showing that F-actin
staining with rhodamin-phalloidin is highly reduced in spines after exposure of F-actin
depolymerizing Latrunculin A in slice cultures [Vlachos *et al.* , 2009]. Furthermore,
exogenous synaptopodin in Ptk2 cells suppressed the disruption of F-actin stress fibers
caused by staurosporine [Okubo-Suzuki *et al.* , 2008].

The exact mechanism leading to increased surface areas of spine apparatuses might

be explained by investigations at different time points after toxin application and by transfection of a well-defined quantity of synaptopodin. Our experimental set up allowed us to check for a defined concentration of plasmid, but not for the exact quantity, that diffuses through membrane pores during SCEP. We conclude from these observations that the interdigitating filaments are indeed composed of a quite rigid F-actin pool, as bath-applied Rho GTPase inhibitors interfering with F-actin polymerization led to the complete loss of those filaments in several cases in the wild-type. This finding is in line with the strong F-actin staining between the lamellae of spine apparatus in mushroom-shaped spines [Capani *et al.*, 2001]. Secondly, the coupling of F-actin fibers to the spine apparatus is mediated by synaptopodin. Overexpression of synaptopodin leads to an increased rate of F-actin polymerization and spine apparatus formation. The coupling of F-actin fibers to sER tubules is strongly reduced after application of GTPase inhibitors, which leads to damaging effects on the organelle's morphology and an increase in G-actin monomers. Damaging effects therefore occurred selectively in the wild-type, as a surplus of synaptopodin counterbalances deleterious effects leading to de-polymerization of F-actin by stabilizing the rigid F-actin pool in the spine apparatus.

If other actin binding proteins are additionally involved in establishing structural integrity of the spine apparatus remains unclear. The application of F-actin destabilizing factors might influence binding affinities for other actin binding partners as well, if both use the same docking sites. This feedback mechanism with respect to allosteric constrictions has been proposed as an explanation for the influence of Latrunculin on binding affinities for actin and thymosin β4 [Yarmola *et al.*, 2000].

## 4.6. Consequences of pharmacological inhibition for mushroom-shaped spines

The cellular and molecular base for growth and morphing processes in neurons is provided by a rigid and at the same time dynamic filamentous scaffolding matrix, the cytoskeleton, which relies upon an equilibrium of F-actin polymerization and G-actin depolymerization. Homeostatic mechanisms may balance morphological restructuration to set boundaries.

Small Rho GTPases play a prominent role in the regulation of morphological modifications and motility in spines [Chen *et al.*, 2012], [Cerri *et al.*, 2011], [Tashiro & Yuste, 2008]. It has been suggested that Rho-signaling mediated spine motility is associated

with spine head plasticity [Fischer *et al.* , 2000], [Pilpel & Segal, 2004], [Korkotian & Segal, 2007]. Synaptopodin links the actin cytoskeleton to the spine's intrinsic calcium store [Deller *et al.* , 2000] and has been also associated with synaptic plasticity [Vlachos, 2011], [Segal *et al.* , 2010]. This intrinsic calcium store might be responsible for orchestrating cell motility via Rho signaling [Asanuma *et al.* , 2006]. We wanted to test, whether the observed increase in surface areas of spine apparatuses after application of Rho GTPase inhibitors in the wild-type has an impact on the respective spine compartment.

For this endeavor, we investigated spines housing spine apparatuses by direct measurements of surface areas and by dividing the surface areas of spine apparatuses by those of directly related spines. As discussed previously for the influence of synaptopodin overexpression on mushroom-shaped spines, all analyzed conditions with a persistent increase in median surface area of spine apparatuses showed additionally a significant increase in the same range for appropriate spines after treatment with GTPase inhibitors. Application of Rho-GTPase inhibitors Y-27632, *Clostridium difficile* toxin B and Latrunculin A did not disturb the ratios for spine apparatuses divided by appropriate spines. This also accounts for the sodium-channel blocker TTX. Neither in the wild-type nor in the transfected KO condition the principle of proportionality was affected, underlining the close interaction between spine apparatus morphology and appropriate mushroom-shaped spines.

Likewise, our results obtained by bath-application of Rho GTPase inhibitors demonstrate that the protective effect of synaptopodin against treatments with Latrunculin A [Vlachos *et al.* , 2009] does not only apply for synaptopodin positive spines, but also for mushroom-shaped spines housing spine apparatuses. ROCK phosphorylates and activates LIM kinase, which phosphorylates cofilin (cofilin-P). Cofilin-P leads to stabilization of actin filaments, by inhibiting its continuous depolymerizing activity. Application of ROCK inhibitor Y-27632 might therefore lead to elevated depolymerization and thus an increase in the total number of G-actin monomers. A reduced polymerization ability might cause degradation of rigid F-actin and in consequence the deflation of the spine apparatus. The increase in diffusive G-actin monomers might contribute to an increase in spine motility. Inhibition of the Rho GTPase pathway, either selectively via ROCK inhibitor Y-27632 or as a whole with *Clostridium difficile* toxin B, might have led indirectly to an imbalance in the actin equilibrium by the increased availability of G-actin monomers. This imbalance in the actin equilibrium explains why deleterious effects after application of GTPase inhibitors in the transfected KO condition were relatively mild and why application of toxins in the wild-type led to increased surface areas. As spine apparatuses with their

intrinsic F-actin pool were already established in the wild-type, a surplus of synaptopodin did not lead to severe disturbances of the actin equilibrium inside the spine. Synaptopodin transfection in the KO condition might decrease this availability, as G-actin monomers first have to be integrated to form a rigid F-actin pool in between each tubules of the spine apparatus. It has been shown that downregulation of RhoA with short-hairpin RNA in hippocampal spines decreased transient volume change but did not affect sustained volume change. The authors suggest that Rho-ROCK pathway might be involved in both, the transient and sustained enlargement of spines, whereas the NMDAR-CaMKII-Cdc42-Pak pathway is selectively involved in sustained volume changes leading to sustained structural and functional plasticity [Murakoshi *et al.* , 2011].

## 4.7. Multivesicular bodies and their function in mushroom-shaped spines

Endosomes comprise three different compartments: early endosomes, late endosomes and recycling endosmes [Mellman, 1996]. Late endosomes lack tubules and contain close-packed lumenal vesicles giving them a multivesicular appearance. Therefore late endosomes are also called multivesicular bodies (MVBs). The maturation of late endosomes is mediated by small G proteins, such as Rab 5 and Rab 7 [Rink *et al.* , 2005], [Stenmark, 2009], [Russell *et al.* , 2006]. The occurrence of multivesicular bodies (MVBs) in hippocampal dendritic spines was reported several years ago [Cooney *et al.* , 2002], [Spacek & Harris, 1997]. These endosomal compartments are well known to sort membrane proteins for local recycling or for somatic degradation. Serial sections of hipppocampal CA1 dendritic spines revealed the presence of endosomal compartments in mushroom-shaped spines to 58% and the presence of smooth endoplasmic reticulum in mushroom-shaped spines to 45%. The concomitant appearance of both micro-compartments within dendritic mushroom-shaped spines occurred with 18%. This suggests that only one sorting endosome per 20 spines in the adult hippocampus contains a complex formed by these two compartments [Cooney *et al.* , 2002]. We observed an increase in the occurrence of multivesicular bodies in close vicinity to the spine apparatus after bath-application of Rho GTPase inhibitors. The occurrence of multivesicular bodies might be therefore closely associated with actin bundling and sorting processes in spines. Sorting processes in adult mushroom-shape spines are associated with morphological restructurings of the spine or with local degradation processes [Sorra & Harris, 2000]. The elevated numbers

of MVBs, which occurred after treatment with Rho GTPase inhibitors, are either related to recycling and degradation of proteins or to morphological restructurings. The latter hypothesis is strengthened by recent investigations, which link recycling endosomes to LTP-induced plasticity. Recycling endosomes were shown to supply AMPA receptors [Park *et al.* , 2004] and translocate into spines after LPT induction where they mediate structural growth and expansion during LTP in dendritic spines and induce structural remodeling of spines leading to structural plasticity in glutamatergic synapses [Park *et al.* , 2006].

## 4.8. Regulation of spine size and spine apparatus function in homeostasis and synaptic plasticity

I will provide some additional hypothesis about potential physiological functions of the spine apparatus in dendritic mushroom-shaped spines based on prevailing literature, as it is not possible to study or monitor spine stability or plasticity with the applied technique.

The impaired LTP and accompanied disruption in memory tasks of synaptopodin KO mice [Jedlicka *et al.* , 2008], [Deller *et al.* , 2003], relates the presence of Synaptopodin and its functional spine apparatus to the field of synaptic plasticity. The presence of this organelle is restricted predominantly to mushroom-shaped spines, which are thought to play a key role in synaptic plasticity. The role of the spine apparatus in cortical and central neurons including the hippocampus, seems to be additionally related to memory and learning tasks. As spine plasticity is based on structural changes, the spine apparatus seems to rely on the same dynamic structural principles. Mushroom-shaped spines endowed with a spine apparatus organelle seem to be not only more resistant to any kind of toxic treatment in terms of morphological restructurings, they might have developed mechanisms to counteract deleterious or instability-inducing effects evoked by elevated synaptopodin levels and/ or prolonged toxin application. This idea is consistent with recent reviews on spine morphology and functional plasticity. Kasai and co-workers prompted that the smaller, stubby spines, which undergo rapid restructurings are 'learning' spines, which are still highly plastic and mushroom-shaped spines may be the ones, which have already undergone learning processes and are therefore called 'memory' spines. He further speculates that these spines store memory, which is protected from being erased on a structural basis by making them more robust against morphological intentions to restructure their shapes [Kasai *et al.* , 2010]. This mech-

anism may be based on the dynamics of the actin-cytoskeleton, which controls many fundamental cellular processes and functions. It has been shown that the actin turnover rate in mushroom-shaped spines is slower and these spines might be stable through a lifetime of 60 years. The larger mushroom-shaped spines seem to be "writing-protected" like folders on a computer containing important data and the smaller spines seem to be "writing enabled", waiting for new information to be stored, or for elimination, if not strengthened by input. On the one hand, the spine apparatus provides an intrinsic stable F-actin pool, the key modulator for morphological restructurings like volume changes in spine heads, and on the other hand spine apparatuses are the perfect sensors and modulators for the spine's activity dependent $[Ca^{2+}]$i kinetics and oscillations. Both of these two features are refined in the spine apparatus and lead to a high degree of morphological specialization. Taken together, this feature make the spine apparatus a perfect candidate for fulfilling its function as a microdomain inside the spine compartment.

On a functional basis, spine apparatuses might be potentially seen as a relay system, providing a key role between morphology and functionality of specialized mushroom-shaped spine compartments. If the spine compartment functions like a transistor [Holcman *et al.* , 2005], the spine apparatus might at least partially adopt this function by providing restrictive conductance from large mushroom-shaped spines to dendritic compartments. This might happen selectively in those cases where the spine has adapted a compartmentalized shape constricted by its neck and conductance out of the compartment is highly reduced. If the neuronal sER can be seen on a functional basis as 'a neuron within a neuron' [Berridge, 1998] or as a cable inside a cable [Shemer *et al.* , 2008], the spine apparatus might function as a spine inside a spine, as it provides all morphological and functional key aspects ($Ca^{2+}$ store and intrinsic F-actin pool), which are essential for maintaining the morphology of mushroom-shaped spines and conductance stability. Although there are many indicators that calcium influx and actin dynamics might influence each other, it is still difficult to link morphological restructurings to neuronal activity in individual spine compartments. Unfortunately, technical limitations make it quite difficult to combine motility experiments inside spine compartments with exact measurements of calcium transients. Therefore, till today it is quite difficult to link calcium transients to morphological changes induced by the actin cytoskeleton. Furthermore washout processes of dyes, which are commonly used in whole cell patch clamp experiments were shown to remove ATP from the cells interior [Matsuzaki *et al.* , 2004] and can lead to either reduced or suppressed morphological changes [Oertner & Matus, 2005] and unpredictable side effects. Modern biophysical methods, like two-photon excitation-

induced glutamate uncaging, may guide us to a better understanding for a profound structure-function relationship. Recent technological advances in two-photon excitation of glutamate uncaging and optogenetic fluorescent markers, may help in the nearer future to provide a basis for understanding the morphological properties of neuronal sER in general and the spine apparatus in particular. These techniques are already in use today in cultured cells or organotypic slice cultures to understand low-range calcium dynamics and induce local calcium release, but there is still lack of *in vivo* application. Additionally, advances in computational models provide tools necessary to access the complex geometry of neuronal ER and the spine apparatus and may help to investigate the structure/function relationship under physiological conditions.

# Bibliography

[Allen *et al.* , 2011] ALLEN, SHELLEY J., WATSON, JUDY J., & DAWBARN, DAVID. 2011. The neurotrophins and their role in alzheimer's disease. *Curr neuropharmacol.*, **9**(4), 559–573.

[Amaral *et al.* , 1990] AMARAL, DAVID G., ISHIZUKA, NORIO, & CLAIBORNE, BRENDA. 1990. Neurons, numbers and the hippocampal network. *Chap. 1, pages 1–11 of:* STORM-MATHISEN, J., ZIMMER, J., & OTTERSON, OLE P. (eds), *Progress in brain Research: understanding the brain through the hippocampus the hippocampal region as a model for studying brain structure and function*, vol. 83. Elsevier Science Ltd.

[Ango *et al.* , 2008] ANGO, FABRICE, WU, CAIZHI, VAN DER WANT, JOHANNES J., WU, PRISCILLA, SCHACHNER, MELITTA, & HUANG, Z. JOSH. 2008. Bergmann glia and the recognition molecule CHL1 organize GABAergic axons and direct innervation of purkinje cell dendrites. *PLoS biol. 6(4):e103.*, **6**(4), e103.

[Asanuma *et al.* , 2005] ASANUMA, KATSUHIKO, KIM, KWANGHEE, OH, JUN, GIARDINO, LAURA, CHABANIS, SOPHIE, FAUL, CHRISTIAN, REISER, JOCHEN, & MUNDEL, PETER. 2005. Synaptopodin regulates the actin-bundling activity of -actinin in an isoform-specific manner. *J clin invest.*, **115**(5), 1188–1198.

[Asanuma *et al.* , 2006] ASANUMA, KATSUHIKO, YANAGIDA-ASANUMA, ETSUKO, FAUL, CHRISTIAN, TOMINO, YASUHIKO, KIM, KWANGHEE, & MUNDEL, PETER. 2006. Synaptopodin orchestrates actin organization and cell motility via regulation of RhoA signalling. *Nat cell biol.*, **8**(5), 485–491.

[Ballmaier *et al.* , 2008] BALLMAIER, MARTINA, NARR, KATHERINE L., TOGA, ARTHUR W., ELDERKIN-THOMPSON, VIRGINIA, THOMPSON, PAUL M., HAMILTON, LIBERTY, HAROON, EBRAHIM, PHAM, DANIEL, HEINZ, ANDREAS, & KUMAR, ANAND. 2008. Hippocampal morphology and distinguishing late-onset from early-onset elderly depression. *Am j psychiatry*, **165**(2), 229–237.

[Barry *et al.* , 2010] BARRY, JSHUA, GU, YUANZHENG, & GU, CHEN. 2010. Polarized targeting of l1-CAM regulates axonal and dendritic bundling in vitro. *Eur j neurosci.*, **32**(10), 1618–1631.

[Bartsch *et al.* , 2011] BARTSCH, THORSTEN, DÖHRING, JULIANE, ROHR, AXEL, JANSEN, OLAV, & DEUSCHL, GÜNTHER. 2011. CA1 neurons in the human hippocampus are critical for autobiographical memory, mental time travel, and autonoetic consciousness. *Proc natl acad sci u s a*, **108**(42), 17562–17567.

[Bas Orth *et al.* , 2007] BAS ORTH, CARLOS, SCHULTZ, CHRISTIAN, MÜLLER, CHRISTIAN M., FROTSCHER, MICHAEL, & DELLER, THOMAS. 2007. Loss of the cisternal organelle in the axon initial segment of cortical neurons in synaptopodin-deficient mice. *J comp neurol.*, **504**(5), 441–449.

[Benedeczky *et al.* , 1994] BENEDECZKY, ISTVAN, MOLNÁR, ELEK, & SOMOGYI, PÉTER. 1994. The cisternal organelle as a $Ca^{2}+$-storing compartment associated with GABAergic synapses in the axon initial segment of hippocampal pyramidal neurones. *Exp brain res.*, **101**(2), 216–230.

[Benson *et al.* , 2000] BENSON, DEANNA L., SCHNAPP, LYNN M., SHAPIRO, LAWRENCE, & HUNTLEY, GEORGE W. 2000. Making memories stick: cell-adhesion molecules in synaptic plasticity. *Trends cell biol.*, **10**(11), 473–482.

[Berridge, 1998] BERRIDGE, MICHAEL J. 1998. Neuronal calcium signaling. *Neuron*, **21**(1), 13–26.

[Biederer *et al.* , 2002] BIEDERER, THOMAS, SARA, YILDIRIM, MOZHAYEVA, MARINA, ATASOY, DENIZ, LIU, XINRAN, KAVALALI, EGE T., & SÜDHOF, THOMAS C. 2002. SynCAM, a synaptic adhesion molecule that drives synapse assembly. *Science*, **297**(5586), 1525–1531.

[Blaustein & Golovina, 2001] BLAUSTEIN, MORDECAI P., & GOLOVINA, VERA A. 2001. Structural complexity and functional diversity of endoplasmic reticulum $Ca(^{2}+)$ stores. *Trends neurosci.*, **24**(10), 602–608.

[Büther *et al.* , 2004] BÜTHER, KATRIN, PLAAS, CHRISTIAN, BARNEKOW, ANGELIKA, & KREMERSKOTHEN, JOACHIM. 2004. KIBRA is a novel substrate for protein kinase C. *Biochem biophys res commun. 317(3):703-7.*, **317**(3), 703–707.

[Capani *et al.* , 2001] CAPANI, FRANCISCO, DEERINCK, THOMAS J., ELLISMAN, MARK H., BUSHONG, ERIC, BOBIK, MARKETTA, & MARTONE, MARYANN E. 2001. Phalloidin-eosin followed by photo-oxidation: a novel method for localizing

f-actin at the light and electron microscopic levels. *J histochem cytochem.*, **49**(11), 1351–1361.

[Cashman *et al.* , 1992] CASHMAN, NEIL R., DURHAM, HEATHER D., BLUSZTAJN, JAN KRZYSZTOF, ODA, KENICHIRO, TABIRA, TAKESHI, SHAW, IVAN T., DAHROUGE, SIMONE, & ANTEL, JACK P. 1992. Neuroblastoma x spinal cord (NSC) hybrid cell lines resemble developing motor neurons. *Developmental dynamics*, **194**(3), 209–221.

[Cerri *et al.* , 2011] CERRI, CHIARA, FABBRI, ALESSIA, VANNINI, ELEONORA, SPOLIDORO, MARIA, COSTA, MARIO, MAFFEI, LAMBERTO, FIORENTINI, CARLA, & CALEO, MATTEO. 2011. Activation of rho GTPases triggers structural remodeling and functional plasticity in the adult rat visual cortex. *J neurosci. 31(42):15163-72.*, **31**(42).

[Chalovich & Schroeter, 2010] CHALOVICH, JOSEPH M., & SCHROETER, MECHTHILD M. 2010. Synaptopodin family of natively unfolded, actin binding proteins: physical properties and potential biological functions. *Biophysical reviews*, **2**(4), 181–189.

[Chardin, 1999] CHARDIN, PIERRE. 1999. Rnd proteins: a new family of Rho-related proteins that interfere with the assembly of filamentous actin structures and cell adhesion. *Prog mol subcell biol.*, **22**(May), 39–50.

[Chen *et al.* , 2012] CHEN, CHEN, WIRTH, ALEXANDER, & PONIMASKIN, EVGENI. 2012. Cdc42: an important regulator of neuronal morphology. *Int j biochem cell biol.*, **44**(3), 447–451.

[Chen & Sudol, 1995] CHEN, HENRY I., & SUDOL, MARIUS. 1995. The WW domain of yes-associated protein binds a proline-rich ligand that differs from the consensus established for Src homology 3-binding modules. *Proc natl acad sci u s a.*, **92**(17), 7819–7823.

[Cheng & Lemmon, 2004] CHENG, LING, & LEMMON, VANCE. 2004. Pathological missense mutations of neural cell adhesion molecule l1 affect neurite outgrowth and branching on an l1 substrate. *Mol cell neurosci.*, **27**(4), 522–530.

[Cooney *et al.* , 2002] COONEY, JAMES R., HURLBURT, JAMIE L., SELIG, DAVID K., HARRIS, KRISTEN M., & FIALA, JOHN C. 2002. Endosomal compartments serve multiple hippocampal dendritic spines from a widespread rather than a local store of recycling membrane. *J neurosci.*, **22**(6), 2215–2224.

[Czarnecki, 2005] CZARNECKI, KATHRIN. 2005. *Charakterisierung der expression von synaptopodin in der postnatalen entwicklung des hippocampus.* Ph.D. thesis, Albert-Ludwigs-Universität Freiburg.

[Czarnecki *et al.* , 2005] CZARNECKI, KATHRIN, HAAS, CAROLA A., BAS ORTH, CARLOS, DELLER, THOMAS, & FROTSCHER, MICHAEL. 2005. Postnatal development of synaptopodin expression in the rodent hippocampus. *J comp neurol.*, **490**(2), 133–144.

[Deller *et al.* , 2000] DELLER, THOMAS, MUNDEL, PETER, & FROTSCHER, MICHAEL. 2000. Potential role of synaptopodin in spine motility by coupling actin to the spine apparatus. *Hippocampus*, **10**(5), 569–581.

[Deller *et al.* , 2003] DELLER, THOMAS, KORTE, MARTIN, CHABANIS, SOPHIE, DRAKEW, ALEXANDER, SCHWEGLER, HERBERT, STEFANI, GIULIA GOOD, ZUNIGA, AIMEE, SCHWARZ, KARIN, BONHOEFFER, TOBIAS, ZELLER, ROLF, FROTSCHER, MICHAEL, & MUNDEL, PETER. 2003. Synaptopodin-deficient mice lack a spine apparatus and show deficits in synaptic plasticity. *Proc natl acad sci u s a.*, Sept., 18.

[Deller *et al.* , 2007] DELLER, THOMAS, BAS ORTH, CARLOS, DEL TURCO, DOMENICO, VLACHOS, ANDREAS, BURBACH, GUIDO J., DRAKEW, ALEXANDER, CHABANIS, SOPHIE, KORTE, MARTIN, SCHWEGLER, HERBERT, HAAS, CAROLA A., & FROTSCHER, MICHAEL. 2007. A role for synaptopodin and the spine apparatus in hippocampal synaptic plasticity. *Ann anat.*, **189**(1), 5–16.

[Delmas & Brown, 2002] DELMAS, PATRICK, & BROWN, DAVID A. 2002. Junctional signaling microdomains: bridging the gap between the neuronal cell surface and Ca2+ stores. *Neuron*, **36**(5), 787–790.

[Dent *et al.* , 2011] DENT, ERIK W., MERRIAM, ELLIOTT B., & HU, XINDAO. 2011. The dynamic cytoskeleton: backbone of dendritic spine plasticity. *Curr opin neurobiol.*, **21**(1), 175–181.

[Dick *et al.* , 2003] DICK, OLIVER, TOM DIECK, SUSANNE, ALTROCK, WILKO DETLEF, AMMERMÜLLER, JOSEF, WEILER, RETO, GARNER, CRAIG CURTIS, GUNDELFINGER, ECKART DIETER, & BRANDSTÄTTER, JOHANN HELMUT. 2003. The presynaptic active zone protein bassoon is essential for photoreceptor ribbon synapse formation in the retina. *Neuron*, **37**(5), 775–786.

[Drakew *et al.* , 1999] DRAKEW, ALEXANDER, FROTSCHER, MICHAEL, & HEIMRICH, BERND. 1999. Blockade of neuronal activity alters spine maturation of dentate granule cells but not their dendritic arborization. *Neuroscience*, **94**(3), 767–774.

[Dudek & Bear, 1993] DUDEK, SERENA M., & BEAR, MARK F. 1993. Bidirectional long-term modification of synaptic effectiveness in the adult and immature hippocampus. *J neurosci.*, **13**(7), 2910–2918.

[Duning *et al.* , 2008] DUNING, KERSTIN, SCHUREK, EVA-MARIA, SCHLÜTER, MARC, BAYER, MICHAEL, REINHARDT, HANS-CHRISTIAN, SCHWAB, ALBRECHT, SCHAEFER, LILIANA, BENZING, THOMAS, SCHERMER, BERNHARD, SALEEM, MOIN A., HUBER, TOBIAS B., BACHMANN, SEBASTIAN, KREMERSKOTHEN, JOACHIM, WEIDE, THOMAS, & PAVENSTÄDT, HERMANN. 2008. KIBRA modulates directional migration of podocytes. *J am soc nephrol.*, **19**(10), 1891–1903.

[Eichenbaum, 1999] EICHENBAUM, HOWARD. 1999. Neurobiology: the topography of memory. *Nature*, **402**(6762), 597–599.

[Ethell & Pasquale, 2005] ETHELL, IRYNA M., & PASQUALE, ELENA B. 2005. Molecular mechanisms of dendritic spine development and remodeling. *Prog neurobiol.*, **75**(3), 161–205.

[Fasana *et al.* , 2010] FASANA, ELISA, FOSSATI, MATTEO, RUGGIANO, ANNAMARIA, BRAMBILLASCA, SILVIA, HOOGENRAAD, CASPER C., NAVONE, FRANCESCA, FRANCOLINI, MAURA, & BORGESE, NICA. 2010. A VAPB mutant linked to amyotrophic lateral sclerosis generates a novel form of organized smooth endoplasmic reticulum. *The faseb journal*, **24**(5), 1419–1430.

[Fiala *et al.* , 1998] FIALA, JOHN C., FEINBERG, MARCIA, POPOV, VIKTOR, & HARRIS, KRISTEN M. 1998. Synaptogenesis via dendritic filopodia in developing hippocampal area CA1. *J neurosci.*, **18**(21), 8900–8911.

[Fifková *et al.* , 1983] FIFKOVÁ, EVA, MARKHAM, JEFFREY A., & DELAY, RONA J. 1983. Calcium in the spine apparatus of dendritic spines in the dentate molecular layer. *Brain res.*, **266**(1), 163–168.

[Fischer *et al.* , 1998] FISCHER, MARIA, KAECH, STEFANIE, KNUTTI, DARKO, & MATUS, ANDREW. 1998. Rapid actin-based plasticity in dendritic spines. *Neuron*, **20**(5), 847–854.

[Fischer *et al.* , 2000] FISCHER, MARIA, KAECH, STEFANIE, WAGNER, UTA, BRINKHAUS, HEIKE, & MATUS, ANDREW. 2000. Glutamate receptors regulate actin-based plasticity in dendritic spines. *Nat neurosci.*, **3**(9), 887–894.

[Frank *et al.* , 2010] FRANK, T., RUTHERFORD, M.A., STRENZKE, N., NEEF, A., PANGRŠIČ, T., KHIMICH, D., FEJTOVA, A., GUNDELFINGER, E.D., LIBERMAN, M.C., HARKE, B., BRYAN, K.E., LEE, A., EGNER, A., RIEDEL, D., & MOSER, T. 2010. Bassoon and the synaptic ribbon organize ca$^2$+ channels and vesicles to add release sites and promote refilling. *Neuron*, **68**(4), 724–738.

[Frost *et al.* , 2010] FROST, NICHOLAS A., KERR, JUSTIN M., LU, HSIANG-MIN E., & BLANPIED, THOMAS A. 2010. A network of networks: cytoskeletal control of compartmentalized function within dendritic spines. *Curr opin neurobiol.*, **5**(Oct.), 578–587.

[Fujisawa *et al.* , 1996] FUJISAWA, KAZUKO, FUJITA, AKIKO, ISHIZAKI, TOSHIMASA, SAITO, YUJI, & NARUMIYA, SHUH. 1996. Identification of the rho-binding domain of p160ROCK, a rho-associated coiled-coil containing protein kinase. *J biol chem.*, **271**(38), 23022–23028.

[Fukazawa *et al.* , 2003] FUKAZAWA, YUGO, SAITOH, YOSHITO, OZAWA, FUMIKO, OHTA, YASUHIKO, MIZUNO, KENSAKU, & INOKUCHI, KAORU. 2003. Hippocampal LTP is accompanied by enhanced f-actin content within the dendritic spine that is essential for late LTP maintenance in vivo. *Neuron*, **38**(3), 447–460.

[Förster *et al.* , 2005] FÖRSTER, ECKART, BARTOS, MARLENE, & ZHAO, SHANTING. 2005. Hippocampal slice cultures. *Pages 1–11 of:* POINDRON, PHILIPPE, PIQUET, PASCALE, & FÖRSTER, ECKHART (eds), *New methods for culturing cells from nervous tissues*, vol. 1. BioValley Monographs, Karger AG, Basel.

[Förster *et al.* , 2006] FÖRSTER, ECKART, ZHAO, SHANTING, & FROTSCHER, MICHAEL. 2006. Laminating the hippocampus. *Nature reviews neuroscience*, **7**(4), 259–268.

[Gerrow & Triller, 2010] GERROW, KIMBERLY, & TRILLER, ANTOINE. 2010. Synaptic stability and plasticity in a floating world. *Curr opin neurobiol.*, **20**(5), 631–639.

[Gray, 1959] GRAY, E.G. 1959. Electron microscopy of synaptic contacts on dendrite spines of the cerebral cortex. *Nature*, **183**(4675), 1592–1593.

[Hall & Lalli, 2010] HALL, ALAN, & LALLI, GIOVANNA. 2010. Rho and ras GTPases in axon growth, guidance, and branching. *Cold spring harb perspect biol.*, **2**(2), a001818.

[Hayashi *et al.* , 2010] HAYASHI, NORIYUKI, KAZUI, HIROAKI, KAMINO, KOUZIN, TOKUNAGA, HIROMASA, TAKAYA, MASAHIKO, YOKOKOJI, MIKIKO, KIMURA, RYO, KITO, YUMIKO, WADA, TAMIKI, NOMURA, KEIKO, SUGIYAMA, HIROMICHI, YAMAMOTO, DAISUKE, YOSHIDA, TETSUHIKO, CURRAIS, ANTONIO, SORIANO, SALVADOR, HAMASAKI, TOSHIMITSU, YAMAMOTO, MITSUKO, YASUDA, YUKA, HASHIMOTO, RYOTA, TANIMUKAI, HITOSHI, TAGAMI, SHINJI, OKOCHI, MASAYASU, TANAKA, TOSHIHISA, KUDO, TAKASHI, MORIHARA, TAKASHI, & TAKEDA, MASATOSHI. 2010. KIBRA genetic polymorphism influences episodic memory in alzheimer's disease, but does not show association with disease in a japanese cohort. *Dement geriatr cogn disord.*, **30**(4), 302–308.

[Hering & Sheng, 2001] HERING, HEIKE, & SHENG, MORGAN. 2001. Dendritic spines: structure, dynamics and regulation. *Nat rev neurosci.*, **2**(12), 880–888.

[Hoffman *et al.* , 2008] HOFFMAN, ELLEN J., MINTZ, C. DAVID, WANG, SOPHIA, MCNICKLE, DANIEL G., SALTON, STEPHAN R. J., & BENSON, DEANNA L. 2008. Effects of ethanol on axon outgrowth and branching in developing rat cortical neurons. *Neuroscience*, **157**(3), 556–565.

[Holbro *et al.* , 2009] HOLBRO, NIKLAUS, GRUNDITZ, SA, & OERTNER, THOMAS G. 2009. Differential distribution of endoplasmic reticulum controls metabotropic signaling and plasticity at hippocampal synapses. *Proc natl acad sci u s a*, **106**(35), 15055–15060.

[Holcman *et al.* , 2005] HOLCMAN, D., KORKOTIAN, E., & SEGAL, MENAHEM. 2005. Calcium dynamics in dendritic spines, modeling and experiments. *Cell calcium*, **37**(5), 467–475.

[Honkura *et al.* , 2008] HONKURA, NAOKI, MATSUZAKI, MASANORI, NOGUCHI, JUN, ELLIS-DAVIES, GRAHAM C. R., & KASAI, HARUO. 2008. The subspine organization of actin fibers regulates the structure and plasticity of dendritic spines. *Neuron*, **57**(5), 719–729.

[Hotulainen *et al.* , 2009] HOTULAINEN, PIRTA, LLANO, OLAYA, SMIRNOV, SERGEI, TANHUANPÄÄ, KIMMO, FAIX, JAN, RIVERA, CLAUDIO, & LAPPALAINEN, PEKKA. 2009. Defining mechanisms of actin polymerization and depolymerization during dendritic spine morphogenesis. *J cell biol.*, **185**(2), 323–339.

[Jedlicka *et al.* , 2008] JEDLICKA, PETER, VLACHOS, ANDREAS, SCHWARZACHER, STEPHAN W., & DELLER, THOMAS. 2008. A role for the spine apparatus in LTP and spatial learning. *Behav brain res.*, **192**(1), 12–19.

[Johannsen *et al.* , 2008] JOHANNSEN, S., DUNING, K., PAVENSTÄDT, H., KREMERSKOTHEN, JOACHIM, & BOECKERS, T. M. 2008. Temporal-spatial expression and novel biochemical properties of the memory-related protein KIBRA. *Neuroscience*, **155**(4), 1165–1173.

[Johnston & Amaral, 2003] JOHNSTON, D., & AMARAL, D. G. 2003. Hippocampus. *Page 432 of:* SHEPHERD, GORDON M. (ed), *The synaptic organization of the brain*, fifth edn. Oxford University Press, New York.

[Jontes & Smith, 2000] JONTES, JAMES D., & SMITH, STEPHEN J. 2000. Filopodia, spines, and the generation of synaptic diversity. *Neuron*, **27**(1), 11–14.

[Kalinichenko *et al.* , 2011] KALINICHENKO, S.V., VIKHREVA, P.N., & KOROBKO, I.V. 2011. Interaction between MAK-V protein kinase and synaptopodin. *Biochemistry moscow*, **76**(2), 196–201.

[Kasai *et al.* , 2010] KASAI, HARUO, HAYAMA, TATSUYA, ISHIKAWA, MOTOKO, WATANABE, SATOSHI, YAGISHITA, SHO, & NOGUCHI, JUN. 2010. Learning rules and persistence of dendritic spines. *Eur j neurosci.*, **32**(2), 241–249.

[Kenwrick *et al.* , 2000] KENWRICK, SUE, WATKINS, ALEX, & DE ANGELIS, ELENA. 2000. Neural cell recognition molecule L1: relating biological complexity to human disease mutations. *Hum mol genet.*, **9**(6), 879–886.

[Khimich *et al.* , 2005] KHIMICH, DARINA, NOUVIAN, RÉGIS, PUJOL, RÉMY, TOM DIECK, SUSANNE, EGNER, ALEXANDER, GUNDELFINGER, ECKARD D., & MOSER, TOBIAS. 2005. Hair cell synaptic ribbons are essential for synchronous auditory signalling. *Nature*, **434**(7035), 889–894.

[Korkotian & Segal, 1998] KORKOTIAN, EDUARD, & SEGAL, MENAHEM. 1998. Fast confocal imaging of calcium released from stores in dendritic spines. *Eur j neurosci.*, **10**(6), 2076–2084.

[Korkotian & Segal, 2007] KORKOTIAN, EDUARD, & SEGAL, MENAHEM. 2007. Morphological constraints on calcium dependent glutamate receptor trafficking into individual dendritic spine. *Cell calcium*, **42**(1), 41–57.

[Kosaka, 1980] KOSAKA, TOSHIO. 1980. The axon initial segment as a synaptic site: ultrastructure and synaptology of the initial segment of the pyramidal cell in the rat hippocampus (CA3 region). *J neurocytol.*, **9**(6), 861–882.

[Kremerskothen *et al.* , 2005] KREMERSKOTHEN, JOACHIM, PLAAS, CHRISTIAN, KINDLER, STEFAN, FROTSCHER, MICHAEL, & BARNEKOW, ANGELIKA. 2005. Synaptopodin, a molecule involved in the formation of the dendritic spine apparatus, is a dual actin/-actinin binding protein. *J neurochem.*, **92**(3), 597–606.

[Li *et al.* , 2002] LI, ZHENG, AIZENMAN, CARLOS D., & CLINE, HOLLIS T. 2002. Regulation of rho GTPases by crosstalk and neuronal activity in vivo. *Neuron*, **33**(5), 741–750.

[Liao *et al.* , 2007] LIAO, JAMES K., SETO, MINORU, & NOMA, KENSUKE. 2007. Rho kinase (ROCK) inhibitors. *J cardiovasc pharmacol.*, **50**(1), 17–24.

[Lin & Koleske, 2010] LIN, YU-CHIH, & KOLESKE, ANTHONY J. 2010. Mechanisms of synapse and dendrite maintenance and their disruption in psychiatric and neurodegenerative disorders. *Annu rev neurosci.*, **33**, 349–378.

[Lisman, 1999] LISMAN, JOHN E. 1999. Relating hippocampal circuitry to function: recall of memory sequences by reciprocal dentate-CA3 interactions. *Neuron*, **22**(2), 233–242.

[Majewska *et al.* , 2000] MAJEWSKA, ANIA, TASHIRO, AYUMU, & YUSTE, RAFAEL. 2000. Regulation of spine calcium dynamics by rapid spine motility. *J neurosci.*, **20**(22), 8262–8268.

[Makuch *et al.* , 2011] MAKUCH, LAUREN, VOLK, LEONORA, ANGGONO, VICTOR, JOHNSON, RICHARD C., YU, YILIN, DUNING, KERSTIN, KREMERSKOTHEN, JOACHIM, XIA, JUN, TAKAMIYA, KOGO, & HUGANIR, RICHARD L. 2011. Regulation of AMPA receptor function by the human memory-associated gene KIBRA. *Neuron*, **71**(6), 1022–1029.

[Maness & Schachner, 2007] MANESS, PATRICIA F., & SCHACHNER, MELITTA. 2007. Neural recognition molecules of the immunoglobulin superfamily: signaling transducers of axon guidance and neuronal migration. *Nat neurosci.*, **10**(1), 19–26.

[Marx *et al.* , 2012] MARX, MARIOLA, DIESTEL, SIMONE, BOZON, MURIEL, KEGLOWICH, LAURA, DROUOT, NATHALIE, BOUCHÉ, ELISABETH, FREBOURG, THIERRY, MINZ, MARIE, SAUGIER-VEBER, PASCALE, CASTELLANI,

VALÉRIE, & SCHÄFER, MICHAEL K. E. 2012. Pathomechanistic characterization of two exonic L1CAM variants located in trans in an obligate carrier of x-linked hydrocephalus. *Neurogenetics*, **13**(1), 49–59.

[Matsuzaki *et al.* , 2001] MATSUZAKI, MASANORI, ELLIS-DAVIES, GRAHAM C. R., NEMOTO, TOMOMI, MIYASHITA, YASUSHI, IINO, MASAMITSU, & KASAI, HARUO. 2001. Dendritic spine geometry is critical for AMPA receptor expression in hippocampal CA1 pyramidal neurons. *Nat neurosci.*, **4**(11), 1086–1092.

[Matsuzaki *et al.* , 2004] MATSUZAKI, MASANORI, HONKURA, NAOKI, ELLIS-DAVIES, GRAHAM C. R., & KASAI, HARUO. 2004. Structural basis of long-term potentiation in single dendritic spines. *Nature*, **429**(6993), 761–766.

[Matus *et al.* , 2000] MATUS, ANDREW, BRINKHAUS, HEIKE, & WAGNER, UTA. 2000. Actin dynamics in dendritic spines: a form of regulated plasticity at excitatory synapses. *Hippocampus*, **10**(5), 555–560.

[McAllister, 2007] MCALLISTER, A. KIMBERLEY. 2007. Dynamic aspects of CNS synapse formation. *Annu rev neurosci. 30:425-50.*, **30**, 425–450.

[McKinney *et al.* , 1999] MCKINNEY, R. ANNE, CAPOGNA, MARCO, DÜRR, ROLAND GÄHWILER, BEAT H., & THOMPSON, SCOTT M. 1999. Miniature synaptic events maintain dendritic spines via AMPA receptor activation. *Nat neurosci.*, **2**(1), 44–49.

[Megías *et al.* , 2001] MEGÍAS, M., EMRI, Z., FREUND, T. F., & GULYÁS, A. I. 2001. Total number and distribution of inhibitory and excitatory synapses on hippocampal CA1 pyramidal cells. *Neuroscience*, **102**(3), 527–540.

[Mellman, 1996] MELLMAN, IRA. 1996. Endocytosis and molecular sorting. *Annu rev cell dev biol.*, **12**, 575–625.

[Miyata *et al.* , 2000] MIYATA, MARIKO, FINCH, ELIZABETH A., KHIROUG, LEONARD, HASHIMOTO, KOUICHI, HAYASAKA, SHIZU, ODA, SEN-ICHI, INOUYE, MINORU, TAKAGISHI, YOSHIKO, AUGUSTINE, GEORG J., & KANO, MASANOBU. 2000. Local calcium release in dendritic spines required for long-term synaptic depression. *Neuron*, **28**(1), 233–244.

[Moon & Gomez, 2010] MOON, MYUNG-SOON, & GOMEZ, TIMOTHY M. 2010. Balanced vav2 GEF activity regulates neurite outgrowth and branching in vitro and in vivo. *Mol cell neurosci.*, **44**(2), 118–128.

[Morton *et al.* , 2000] MORTON, WALTER M., AYSCOUGH, KATHRYN R., & J., MCLAUGHLIN PAUL. 2000. Latrunculin alters the actin-monomer subunit interface to prevent polymerization. *Nat cell biol.*, **2**(6), 376–378.

[Mu & Gage, 2011] MU, YANGLING, & GAGE, FRED H. 2011. Adult hippocampal neurogenesis and its role in alzheimer's disease. *Mol neurodegener.*, **6**(85).

[Mundel *et al.* , 1997] MUNDEL, PETER, HEID, HANS W., MUNDEL, THOMAS M., KRÜGER, MEIKE, REISER, JOCHEN, & KRIZ, WILHELM. 1997. Synaptopodin: an actin-associated protein in telencephalic dendrites and renal podocytes. *J cell biol.*, **139**(1), 193–204.

[Murakoshi *et al.* , 2011] MURAKOSHI, HIDEJI, WANG, HONG, & YASUDA, RYOHEI. 2011. Local, persistent activation of rho GTPases during plasticity of single dendritic spines. *Nature*, **472**(7341), 100–104.

[Müller & Connor, 1991] MÜLLER, WOLFGANG, & CONNOR, JOHN A. 1991. Dendritic spines as individual neuronal compartments for synaptic ca2+ responses. *Nature*, **354**(6348), 73–76.

[Naisbitt *et al.* , 2000] NAISBITT, SCOTT, VALTSCHANOFF, JULI, ALLISON, DANIEL W., SALA, CARLO, KIM, EUNJOON, CRAIG, ANN MARIE, WEINBERG, RICHARD J., & SHENG, MORGAN. 2000. Interaction of the postsynaptic density-95/guanylate kinase domain-associated protein complex with a light chain of myosin-v and dynein. *J neurosci.*, **20**(12), 4524–4534.

[Negishi & Katoh, 2005] NEGISHI, MANABU, & KATOH, HIRONORI. 2005. Rho family GTPases and dendrite plasticity. *Neuroscientist*, **11**(3), 187–191.

[Neves *et al.* , 2008] NEVES, GUILHERME, COOKE, SAM F., & BLISS, TIM V. P. 2008. Synaptic plasticity, memory and the hippocampus: a neural network approach to causality. *Nat rev neurosci.*, **9**(1), 65–75.

[Ng & Toresson, 2011] NG, AI NG, & TORESSON, HÅKAN. 2011. Endoplasmic reticulum dynamics in hippocampal dendritic spines induced by agonists of type i metabotropic glutamate but not by muscarinic acetylcholine receptors. *Synapse*, **65**(4), 351–355.

[Nicolaidis, 2006] NICOLAIDIS, STYLIANOS. 2006. Metabolic mechanism of wakefulness (and hunger) and sleep (and satiety): Role of adenosine triphosphate and hypocretin and other peptides. *Metabolism*, **55**(10, Supplement 2), S24–S29.

[Noguchi *et al.* , 2005] Noguchi, Jun, Matsuzaki, Masanori, Ellis-Davies, Graham C. R., & Kasai, Haruo. 2005. Spine-neck geometry determines NMDA receptor-dependent Ca$^2$+ signaling in dendrites. *Neuron*, **46**(4), 609–622.

[Oertner & Matus, 2005] Oertner, Thomas G., & Matus, Andrew. 2005. Calcium regulation of actin dynamics in dendritic spines. *Cell calcium*, **37**(5), 477–482.

[Okubo-Suzuki *et al.* , 2008] Okubo-Suzuki, Raiko, Okada, Daisuke, Sekiguchi, Mariko, & Inokuchi, Karou. 2008. Synaptopodin maintains the neural activity-dependent enlargement of dendritic spines in hippocampal neurons. *Mol cell neurosci.*, **38**(2), 266–276.

[Oray *et al.* , 2006] Oray, Serkan, Majewska, Ania, & Sur, Mriganka. 2006. Effects of synaptic activity on dendritic spine motility of developing cortical layer v pyramidal neurons. *Cereb cortex*, **16**(5), 730–741.

[Osterweil *et al.* , 2005] Osterweil, Emily, Wells, David G., & Mooseker, Mark S. 2005. A role for myosin VI in postsynaptic structure and glutamate receptor endocytosis. *J cell biol.*, **168**(2), 329–338.

[Ostroff *et al.* , 2010] Ostroff, Linnaea E., Cain, Christopher K., Bedont, Joseph, Monfils, Marie H., & LeDoux, Joseph E. 2010. Fear and safety learning differentially affect synapse size and dendritic translation in the lateral amygdala. *Proc natl acad sci u s a*, **107**(20), 9418–9423.

[Palay *et al.* , 1968] Palay, Sanford L., Sotelo, Constantino, Peters, Alan, & Orkand, Paula M. 1968. The axon hillock and the initial segment. *J cell biol.*, **38**(1), 193–201.

[Papa & Segal, 1996] Papa, M., & Segal, Menahem. 1996. Morphological plasticity in dendritic spines of cultured hippocampal neurons. *Neuroscience*, **71**(4), 1005–1011.

[Papez, 1937] Papez, James W. 1937. A proposed mechanism of emotion. *Arch neurpsych.*, **38**(4), 725–743.

[Park *et al.* , 2004] Park, Mikyoung, Penick, Esther C., Edwards, Jeffrey G., Kauer, Julie A., & Ehlers, Michael D. 2004. Recycling endosomes supply AMPA receptors for LTP. *Science*, **305**(5692), 1972–1975.

[Park *et al.* , 2006] Park, Mikyoung, Salgado, Jennifer M., Ostroff, Linnaea, Helton, Thomas D., Robinson, Camenzind G., Harris, Kris-

ten M., & Ehlers, Michael D. 2006. Plasticity-induced growth of dendritic spines by exocytic trafficking from recycling endosomes. *Neuron*, **52**(5), 817–830.

[Peters *et al.* , 1968] Peters, Alan, Proskauer, Charmian C., & Kaiserman-Abramof, Ita R. 1968. The small pyramidal neuron of the rat cerebral cortex. the axon hillock and initial segment. *J cell biol.*, **39**(3), 604–619.

[Pilpel & Segal, 2004] Pilpel, Yair, & Segal, Menhahem. 2004. Activation of PKC induces rapid morphological plasticity in dendrites of hippocampal neurons via rac and rho-dependent mechanisms. *Eur j neurosci.*, **19**(12).

[R Development Core Team, 2009] R Development Core Team. 2009. *R: A language and environment for statistical computing*. Vienna, Austria: R Foundation for Statistical Computing.

[Reddy *et al.* , 2005] Reddy, P. Hemachandra, Mani, Geethalakshmi, Park, Byung S., Jacques, Joline, Murdoch, Geoffrey, Whetsell, William Jr., Kaye, Jeffrey, & Manczak, Maria. 2005. Differential loss of synaptic proteins in alzheimer's disease: implications for synaptic dysfunction. *J alzheimers dis. 7(2):103-17; discussion 173-80.*, **7**(2), 103–117.

[Richards *et al.* , 2005] Richards, David A., Mateos, José M., Hugel, Sylvain, de Paola, Vincenzo, Caroni, Pico, Gähwiler, Beat H., & McKinney, R. Anne. 2005. Glutamate induces the rapid formation of spine head protrusions in hippocampal slice cultures. *Proc natl acad sci u s a*, **102**(17), 6166–6171.

[Rink *et al.* , 2005] Rink, Jochen, Ghigo, Eric, Kalaidzidis, Yannis, & Zerial, Marino. 2005. Rab conversion as a mechanism of progression from early to late endosomes. *Cell*, **122**(5), 735–749.

[Roth *et al.* , 2001] Roth, Stephanie U., Sommer, Clemens, Mundel, Peter, & Kiessling, Marika. 2001. Expression of synaptopodin, an actin-associated protein, in the rat hippocampus after limbic epilepsy. *Brain pathology*, **11**(2), 169–181.

[Russell *et al.* , 2006] Russell, Matthew Robert Geoffrey, Nickerson, Daniel Patrick, & Odorizzi, Greg. 2006. Molecular mechanisms of late endosome morphology, identity and sorting. *Curr opin cell biol.*, **18**(4), 422–428.

[Ryu *et al.* , 2006] Ryu, Jubin, Liu, Lidong, Wong, Tak Pan, Wu, Dong Chuan, Burette, Alain, Weinberg, Richard, Wang, Yu Tian, &

SHENG, MORGAN. 2006. A critical role for myosin IIb in dendritic spine morphology and synaptic function. *Neuron*, **49**(2), 175–182.

[Rünker *et al.* , 2003] RÜNKER, ANNETTE E., BARTSCH, UDO, NAVE, KLAUS-ARMIN, & SCHACHNER, MELITTA. 2003. The C264Y missense mutation in the extracellular domain of l1 impairs protein trafficking in vitro and in vivo. *J neurosci.*, **23**(1), 277–286.

[Sachs, 2003] SACHS, LOTHAR (ed). 2003. *Angewandte statistik*. 11 edn. Springer Berlin Heidelberg.

[Schikorski & Stevens, 1997] SCHIKORSKI, THOMAS, & STEVENS, CHARLES F. 1997. Quantitative ultrastructural analysis of hippocampal excitatory synapses. *J neurosci.*, **17**(15), 5858–5867.

[Schmid & Maness, 2008] SCHMID, RALF S., & MANESS, PATRICIA F. 2008. L1 and NCAM adhesion molecules as signaling coreceptors in neuronal migration and process outgrowth. *Curr opin neurobiol.*, **18**(3), 245–250.

[Schneider *et al.* , 2010] SCHNEIDER, ARMIN, HUENTELMAN, MATTHEW J., KREMERSKOTHEN, JOACHIM, DUNING, KERSTIN, SPOELGEN, ROBERT, & NIKOLICH, KAROLY. 2010. KIBRA: a new gateway to learning and memory? *Front aging neurosci. 2:4.*, **2**(4).

[Schroeter *et al.* , 2008] SCHROETER, MECHTHILD M., BEALL, BRENT, HEID, HANS W., & CHALOVICH, JOSEPH M. 2008. In vitro characterization of native mammalian smooth-muscle protein synaptopodin 2. *Biosci reports*, **28**(4), 195–203.

[Schäfer & Frotscher, 2012] SCHÄFER, MICHAEL K. E., & FROTSCHER, MICHAEL. 2012. Role of L1CAM for axon sprouting and branching. *Cell tissue res.*, **349**(1), 39–48.

[Schäfer *et al.* , 2010] SCHÄFER, MICHAEL K. E., NAM, YUN-CHUNG, MOUMEN, ANICE, KEGLOWICH, LAURA, BOUCHÉ, ELISABETH, KÜFFNER, MERCEDES, BOCK, HANS H., RATHJEN, FRITZ G., RAOUL, CEDRIC, & FROTSCHER, MICHAEL. 2010. L1 syndrome mutations impair neuronal l1 function at different levels by divergent mechanisms. *Neurobiol dis.*, **40**(1), 222–237.

[Schäfer & Altevogt, 2010] SCHÄFER, MICHAEL K.E., & ALTEVOGT, PETER. 2010. L1CAM malfunction in the nervous system and human carcinomas. *Cell mol life sci.*, **67**(14), 2425–2437.

[Segal *et al.* , 2010] SEGAL, MENAHEM, VLACHOS, ANDREAS, & KORKOTIAN, E. 2010. The spine apparatus, synaptopodin, and dendritic spine plasticity. *Neuroscientist*, **16**(2), 125–131.

[Sharp *et al.* , 1993] SHARP, ALAN H., MCPHERSON, PETER S., DAWSON, TED M., CHIYE, AOKI, CAMPBELL, KEVIN P., & SNYDER, SOLOMON H. 1993. Differential immunohistochemical localization of inositol 1,4,5-trisphosphate- and ryanodine-sensitive ca2+ release channels in rat brain. *J neurosci.*, **13**(7), 3051–3063.

[Shemer *et al.* , 2008] SHEMER, ISAAC, BRINNE, BJÖRN, TEGNÉR, JESPER, & GRILLNER, STEN. 2008. Electrotonic signals along intracellular membranes may interconnect dendritic spines and nucleus. *PLoS comput biol.*, **4**(3).

[Sholl, 1953] SHOLL, D.A. 1953. Dendritic organization in the neurons of the visual and motor cortices of the cat. *J anat.*, **87**(4), 387–406.

[Smith & Mizumori, 2006] SMITH, DAVID M., & MIZUMORI, SHERI J. Y. 2006. Hippocampal place cells, context, and episodic memory. *Hippocampus*, **16**(9), 716–729.

[Sobczyk *et al.* , 2005] SOBCZYK, ALEKSANDER, SCHEUSS, VOLKER, & SVOBODA, KAREL. 2005. NMDA receptor subunit-dependent [Ca$^2$+] signaling in individual hippocampal dendritic spines. *J neurosci.*, **725**(26), 6037–6046.

[Sommer & Budreck, 2009] SOMMER, JULIA E., & BUDRECK, ELAINE C. 2009. Kalirin-7: linking spine plasticity and behavior. *J neurosci.*, **29**(17), 5367–5369.

[Somogyi *et al.* , 1983] SOMOGYI, P., SMITH, A.D., NUNZI, M.G., GORIO, A., TAKAGI, H., & WU, J.Y. 1983. Glutamate decarboxylase immunoreactivity in the hippocampus of the cat: distribution of immunoreactive synaptic terminals with special reference to the axon initial segment of pyramidal neurons. *J neurosci.*, **3**(7), 1450–1468.

[Sorra & Harris, 2000] SORRA, KARIN E., & HARRIS, KRISTEN M. 2000. Overview on the structure, composition, function, development, and plasticity of hippocampal dendritic spines. *Hippocampus*, **10**(5), 501–511.

[Spacek & Harris, 1997] SPACEK, JOSEF, & HARRIS, KRISTEN M. 1997. Three-dimensional organization of smooth endoplasmic reticulum in hippocampal CA1 dendrites and dendritic spines of the immature and mature rat. *J neurosci.*, **17**(1), 190–203.

[Spector *et al.* , 1989] SPECTOR, ILAN, SHOCHET, NAVA R., BLASBERGER, DINA, & KASHMAN, YOEL. 1989. Latrunculins—novel marine macrolides that disrupt microfilament organization and affect cell growth: I. comparison with cytochalasin d. *Cell motil cytoskeleton*, **13**(3), 127–144.

[Star *et al.* , 2002] STAR, ERIN N., KWIATKOWSKI, DAVID J., & MURTHY, VENKATESH N. 2002. Rapid turnover of actin in dendritic spines and its regulation by activity. *Nat neurosci.*, **5**(3), 239–246.

[Stenmark, 2009] STENMARK, HARALD. 2009. Rab GTPases as coordinators of vesicle traffic. *Nat rev mol cell biol.*, **10**(8), 513–525.

[Svoboda *et al.* , 1996] SVOBODA, KAREL, TANK, DAVID W., & DENK, WINFRIED. 1996. Direct measurement of coupling between dendritic spines and shafts. *Science*, **272**(5262), 716–719.

[Sánchez-Ponce *et al.* , 2011] SÁNCHEZ-PONCE, DIANA, DEFELIPE, JAVIER, GARRIDO, JUAN JOSÉ, & MUÑOZ, ALBERTO. 2011. In vitro maturation of the cisternal organelle in the hippocampal neuron's axon initial segment. *Mol cell neurosci. 48(1):104-16. epub 2011 jun 25.*, **48**(1), 104–116.

[Sánchez-Ponce *et al.* , 2012] SÁNCHEZ-PONCE, DIANA, BLÁZQUEZ-LLORCA, LIDIA, DEFELIPE, JAVIER, GARRIDO, JUAN JOSÉ, & MUÑOZ, ALBERTO. 2012. Colocalization of -actinin and synaptopodin in the pyramidal cell axon initial segment. *Cereb cortex. 22(7):1648-61. epub 2011 sep 21.*, **22**(7), 1648–1661.

[Tarrant & Routtenberg, 1979] TARRANT, SALLY B., & ROUTTENBERG, ARYEH. 1979. Postsynaptic membrane and spine apparatus: proximity in dendritic spines. *Neuroscience letters*, **11**(3), 289–294.

[Tashiro & Yuste, 2008] TASHIRO, AYUMU, & YUSTE, RAFAEL. 2008. Role of rho GTPases in the morphogenesis and motility of dendritic spines. *Methods enzymol.*, **439**, 285–302.

[Tashiro *et al.* , 2003] TASHIRO, AYUMU, DUNAEVSKY, ANNA, BLAZESKI, RICHARD, MASON, CAROL A., & YUSTE, RAFAEL. 2003. Bidirectional regulation of hippocampal mossy fiber filopodial motility by kainate receptors: a two-step model of synaptogenesis. *Neuron*, **38**(5), 773–784.

[Teuling *et al.* , 2007] TEULING, EVA, AHMED, SUAAD, HAASDIJK, ELIZE, DEMMERS, JEROEN, STEINMETZ, MICHAEL O., AKHMANOVA, ANNA, JAARSMA,

Dick, & Hoogenraad, Casper C. 2007. Motor neuron disease-associated mutant vesicle-associated membrane protein-associated protein (VAP)B recruits wild-type VAPs into endoplasmic reticulum-derived tubular aggregates. *J neurosci.*, **27**(36), 9801–9815.

[tom Dieck *et al.* , 2005] tom Dieck, Susanne, Altrock, Wilko D., Kessels, Michael M., Qualmann, Britta, Regus, Hanna, Brauner, Dana, Fejtová, Anna, Bracko, Oliver, Gundelfinger, Eckart D., & Brandstätter, Johann H. 2005. Molecular dissection of the photoreceptor ribbon synapse: physical interaction of bassoon and RIBEYE is essential for the assembly of the ribbon complex. *J cell biol.*, **168**(5), 825–836.

[Toresson & Grant, 2005] Toresson, Håkan, & Grant, Seth G. N. 2005. Dynamic distribution of endoplasmic reticulum in hippocampal neuron dendritic spines. *Eur j neurosci.*, **22**(7), 1793–1798.

[Trommer *et al.* , 1995] Trommer, Barbara L., Kennelly, John J., Colley, Patricia A., Overstreet, Linda S., Slater, N.Traverse, & Pasternak, Joseph F. 1995. AP5 blocks LTP in developing rat dentate gyrus and unmasks LTD. *Experimental neurology*, **131**(1), 83–92.

[Tyler & Pozzo-Miller, 2003] Tyler, William J., & Pozzo-Miller, Lucas. 2003. Miniature synaptic transmission and BDNF modulate dendritic spine growth and form in rat CA1 neurones. *J physiol.*, **553**(Dec.), 497–509.

[Uehata *et al.* , 1997] Uehata, Masayoshi, Ishizaki, Toshimasa, Satoh, Hiroyuki, Ono, Takashi, Kawahara, Toshio, Morishita, Tamami, Tamakawa, Hiroyuki, Yamagami, Keiji, Inui, Jun, Maekawa, Midori, & Narumiya, Shuh. 1997. Calcium sensitization of smooth muscle mediated by a rho-associated protein kinase in hypertension. *Nature*, **389**(6654), 990–994.

[Vlachos, 2011] Vlachos, Andreas. 2011. Synaptopodin and the spine apparatus organelle-regulators of different forms of synaptic plasticity? *Annals of anatomy*, **194**(4), 317–320.

[Vlachos *et al.* , 2008] Vlachos, Andreas, Maggio, Nicola, & Jedlicka, Peter. 2008. Just in time for late-LTP: a mechanism for the role of PKM in long-term memory. *Commun integr biol.*, **1**(2), 190–191.

[Vlachos *et al.* , 2009] Vlachos, Andreas, Korkotian, Eduard, Schonfeld, Eldi, Copanaki, Ekaterini, Deller, Thomas, & Segal, Menahem. 2009.

Synaptopodin regulates plasticity of dendritic spines in hippocampal neurons. *J neurosci.*, **29**(4), 1017–1033.

[Vos & Hofstra, 2010] VOS, YVONNE J., & HOFSTRA, ROBERT M.W. 2010. An updated and upgraded L1CAM mutation database. *Hum mutat.*, **31**(1), E1102–E1109.

[Witte & Bradke, 2008] WITTE, HARALD, & BRADKE, FRANK. 2008. The role of the cytoskeleton during neuronal polarization. *Curr opin neurobiol.*, **18**(5), 479–487.

[Yamagata *et al.* , 2003] YAMAGATA, MASAHITO, SANES, JOSHUA R., & WEINER, JOSHUA A. 2003. Synaptic adhesion molecules. *Curr opin cell biol.*, **15**(5), 621–632.

[Yamamoto *et al.* , 2006] YAMAMOTO, MISATO, UEDA, RYU, TAKAHASHI, KUNIAKI, SAIGO, KAORU, & UEMURA, TADASHI. 2006. Control of axonal sprouting and dendrite branching by the nrg-ank complex at the neuron-glia interface. *Current biology*, **16**(16), 1678–1683.

[Yamazaki *et al.* , 2001] YAMAZAKI, MATSUMI, CHIBA, KENZO, MOHRI, TETSURO, & HATANAKA, HIROSHI. 2001. Activation of the mitogen-activated protein kinase cascade through nitric oxide synthesis as a mechanism of neuritogenic effect of genipin in PC12h cells. *J neurochem.*, **79**(1), 45–54.

[Yanagida-Asanuma *et al.* , 2007] YANAGIDA-ASANUMA, ETSUKO, ASANUMA, KATSUHIKO, KIM, KWANGHEE, DONNELLY, MARY, CHOI, HOON YOUNG, CHANG, JAE HYUNG, SUETSUGU, SHIRO, TOMINO, YASUHIKO, TAKENAWA, TADAOMI, FAUL, CHRISTIAN, & MUNDEL, PETER. 2007. Synaptopodin protects against proteinuria by disrupting Cdc42:IRSp53:Mena signaling complexes in kidney podocytes. *Am j pathol.*, **171**(2), 415–427.

[Yarmola *et al.* , 2000] YARMOLA, ELENA G., SOMASUNDARAM, T, BORING, TODD A., SPECTOR, ILAN, & BUBB, MICHAEL R. 2000. Actin-latrunculin a structure and function. differential modulation of actin-binding protein function by latrunculin a. *J biol chem.*, **275**(36).

[Yuste & Denk, 1995] YUSTE, RAFAEL, & DENK, WINFRIED. 1995. Dendritic spines as basic functional units of neuronal integration. *Nature*, **375**(6533), 682–684.

[Yuste *et al.* , 1999] YUSTE, RAFAEL, MAJEWSKA, ANIA, CASH, SYDNEY S., & DENK, WINFRIED. 1999. Mechanisms of calcium influx into hippocampal spines: heterogeneity among spines, coincidence detection by NMDA receptors, and optical quantal analysis. *J neurosci.*, **19**(6), 1976–1987.

[Ziv & Smith, 1996] Ziv, Noam E., & Smith, Stephan J. 1996. Evidence for a role of dendritic filopodia in synaptogenesis and spine formation. *Neuron*, **17**(1), 91–102.

[Zoefel, 2000] Zoefel, Peter. 2000. *Statistik verstehen: Ein begleitbuch zur computerunterstützten anwendung*. 1 edn. Addison-Wesley Verlag.

# A.  Relevant data for each condition

Parameters for all analyzed condition include the following: total numbers of spine apparatuses or spines (n), Q1, graphically calculated medians (median), Q3, IQR, the lower and upper borders for the confidence intervals (CI_1 and CI_2), p-values of each condition, confidence levels and the calculated medians for the exact Wilcoxon rank sum test (Wilcoxon median) (Table A.1). If confidence levels of 95% were not reached due to small sample sizes, conditions were only qualitatively evaluated.

**Abbreviations used for the following tables** (Table A.1, Table A.2):

**spines**      mushroom-shaped spines

**SA**          spine apparatus

**SA / spines** spine apparatuses divided by appropriate spines

**+mSynpo**    transfected with synaptopodin cDNA (1 µg/µl)

**+Lat.A**      bath-application of 2.5 µM Latrunculin A for three consecutive days after electroporation

**+toxin B**    bath-application of 2 pM *Clostridium difficile* toxin B for three days consecutive after electroporation

**+Y-27632**    bath-application of 10 nM ROCK inhibitor Y-27632 for three consecutive days after electroporation

**+TTX**        bath-application of 1 µM TTX for three consecutive days after electroporation

**Table A.1.:** Relevant parameters for spine apparatuses and spines

| Condition | n | Q1 | median | Q3 | IQR | CI_1 | CI_2 | W | p-value | Conf. Level | Wilcoxon median |
|---|---|---|---|---|---|---|---|---|---|---|---|
| Heterozygous, SA in dendrites | 3 | 0.0363 | 0.0393 | 0.0734 | 0.0371 | 0.0333 | 0.107 | 6 | 0.25 | <span style="color:red">0.75</span> | 0.0548 |
| Heterozygous, SA in spines | 17 | 0.0279 | 0.0346 | 0.0413 | 0.0134 | 0.0278 | 0.0502 | 153 | 1.53E-005 | 0.95 | 0.0354 |
| Heterozygous, spines | 17 | 0.21 | 0.323 | 0.545 | 0.335 | 0.251 | 0.522 | 153 | 1.53E-005 | 0.95 | 0.368 |
| KO+mSynpo, SA in dendrites | 43 | 0.0725 | 0.15 | 0.346 | 0.274 | 0.138 | 0.298 | 946 | 2.27E-013 | 0.95 | 0.203 |
| KO+mSynpo, SA in spines | 24 | 0.0566 | 0.0721 | 0.213 | 0.157 | 0.0646 | 0.174 | 300 | 1.19E-007 | 0.95 | 0.121 |
| KO+mSynpo, SA in somata | 9 | 0.63 | 1.41 | 2.7 | 2.07 | 0.455 | 4.46 | 45 | 0.00391 | 0.95 | 1.66 |
| KO+mSynpo, spines | 24 | 0.215 | 0.366 | 0.997 | 0.783 | 0.315 | 0.779 | 300 | 1.19E-007 | 0.95 | 0.571 |
| KO+mSynpo+Lat.A, SA in dendrites | 3 | 0.141 | 0.157 | 0.2 | 0.0584 | 0.125 | 0.242 | 6 | 0.25 | <span style="color:red">0.75</span> | 0.17 |
| KO+mSynpo+Lat.A, SA in spines | 5 | 0.0783 | 0.1 | 0.148 | 0.0693 | 0.0542 | 0.214 | 15 | 0.0625 | 0.95 | 0.113 |

Table A.1 – continued from previous page

| Condition | n | Q1 | median | Q3 | IQR | CI_1 | CI_2 | W | p-value | conf. level | Wilcoxon median |
|---|---|---|---|---|---|---|---|---|---|---|---|
| KO+mSynpo+Lat.A, spines | 5 | 0.382 | 0.404 | 0.469 | 0.0877 | 0.23 | 0.572 | 15 | 0.0625 | 0.95 | 0.404 |
| KO+mSynpo+Y-27632, SA in dendrites | 10 | 0.134 | 0.186 | 0.34 | 0.206 | 0.129 | 0.404 | 55 | 0.00195 | 0.95 | 0.239 |
| KO+mSynpo+Y-27632, SA in spines | 24 | 0.0463 | 0.0818 | 0.132 | 0.0861 | 0.0641 | 0.112 | 300 | 1.19E-007 | 0.95 | 0.0886 |
| KO+mSynpo+Y-27632, SA in somata | 3 | 0.406 | 0.466 | 1.21 | 0.803 | 0.346 | 1.95 | 6 | 0.25 | <span style="color:red">0.75</span> | 0.808 |
| KO+mSynpo+Y-27632, spines | 24 | 0.216 | 0.341 | 0.447 | 0.231 | 0.275 | 0.407 | 300 | 1.19E-007 | 0.95 | 0.339 |
| KO+mSynpo+toxin B, SA in dendrites | 18 | 0.423 | 0.674 | 1.31 | 0.892 | 0.537 | 1.46 | 171 | 7.63E-006 | 0.95 | 0.872 |
| KO+mSynpo+toxin B, SA in spines | 15 | 0.0751 | 0.103 | 0.137 | 0.0616 | 0.0816 | 0.137 | 120 | 6.10E-005 | 0.95 | 0.107 |
| KO+mSynpo+toxin B, SA in somata | 11 | 1.18 | 2.04 | 2.35 | 1.17 | 1.2 | 2.62 | 66 | 0.000977 | 0.95 | 1.84 |
| KO+mSynpo+toxin B, spines | 15 | 0.274 | 0.363 | 0.523 | 0.249 | 0.3 | 0.523 | 120 | 6.10E-005 | 0.95 | 0.401 |

Table A.1 – continued from previous page

| Condition | n | Q1 | median | Q3 | IQR | CI_1 | CI_2 | W | p-value | conf. level | Wilcoxon median |
|---|---|---|---|---|---|---|---|---|---|---|---|
| KO+mSynpo+TTX, SA in dendrites | 30 | 0.0868 | 0.21 | 0.361 | 0.274 | 0.165 | 0.373 | 465 | 1.86E-009 | 0.95 | 0.243 |
| KO+mSynpo+TTX, SA in spines | 15 | 0.0868 | 0.094 | 0.129 | 0.0417 | 0.0797 | 0.122 | 120 | 6.10E-005 | 0.95 | 0.101 |
| KO+mSynpo+TTX, SA in somata | 2 | 1.78 | 2.04 | 2.3 | 0.523 | 1.52 | 2.56 | 3 | 0.5 | 0.5 | 2.04 |
| KO+mSynpo+TTX, spines | 15 | 0.332 | 0.362 | 0.542 | 0.21 | 0.332 | 0.543 | 120 | 6.10E-005 | 0.95 | 0.428 |
| KO, spines | 7 | 0.0518 | 0.15 | 0.193 | 0.141 | 0.0417 | 0.214 | 28 | 0.0156 | 0.95 | 0.127 |
| WT+mSynpo, SA in dendrites | 23 | 0.047 | 0.0742 | 0.109 | 0.0621 | 0.0579 | 0.0978 | 276 | 2.38E-007 | 0.95 | 0.076 |
| WT+mSynpo, SA in spines | 12 | 0.0173 | 0.0276 | 0.0395 | 0.0221 | 0.0202 | 0.0493 | 78 | 0.000488 | 0.95 | 0.0286 |
| WT+mSynpo, spines | 12 | 0.134 | 0.162 | 0.234 | 0.1 | 0.131 | 0.249 | 78 | 0.000488 | 0.95 | 0.185 |
| WT, SA in dendrites | 13 | 0.0261 | 0.0282 | 0.0385 | 0.0123 | 0.0261 | 0.0595 | 91 | 0.000244 | 0.95 | 0.0301 |
| WT, SA in spines | 29 | 0.0182 | 0.0238 | 0.0367 | 0.0184 | 0.0217 | 0.0328 | 435 | 3.73E-009 | 0.95 | 0.0265 |
| WT, spines | 29 | 0.0969 | 0.15 | 0.231 | 0.134 | 0.13 | 0.197 | 435 | 3.73E-009 | 0.95 | 0.163 |

Table A.1 – continued from previous page

| Condition | n | Q1 | median | Q3 | IQR | CI_1 | CI_2 | W | p-value | conf. level | Wilcoxon median |
|---|---|---|---|---|---|---|---|---|---|---|---|
| WT+Lat.A, SA in spines | 3 | 0.0274 | 0.0286 | 0.044 | 0.0166 | 0.0262 | 0.0594 | 6 | 0.25 | <span style="color:red">0.75</span> | 0.0357 |
| WT+Lat.A, spines | 3 | 0.238 | 0.323 | 0.444 | 0.206 | 0.154 | 0.565 | 6 | 0.25 | <span style="color:red">0.75</span> | 0.341 |
| WT+Y-27632, SA in dendrites | 1 | 0.0302 | 0.0302 | 0.0302 | 0 | 0.0302 | 0.0302 | 1 | 1 | <span style="color:red">0</span> | 0.0302 |
| WT+Y-27632, SA in spines | 10 | 0.0317 | 0.0407 | 0.071 | 0.0393 | 0.0274 | 0.0763 | 55 | 0.00195 | 0.95 | 0.0482 |
| WT+Y-27632, spines | 10 | 0.174 | 0.266 | 0.473 | 0.299 | 0.18 | 0.43 | 55 | 0.00195 | 0.95 | 0.311 |
| WT+toxin B, SA in dendrites | 6 | 0.0344 | 0.0461 | 0.0584 | 0.024 | 0.0125 | 0.0674 | 21 | 0.0313 | 0.95 | 0.0461 |
| WT+toxin B, SA in spines | 5 | 0.0245 | 0.0459 | 0.0835 | 0.0589 | 0.0244 | 0.0928 | 15 | 0.0625 | 0.95 | 0.054 |
| WT+toxin B, spines | 5 | 0.171 | 0.338 | 0.431 | 0.259 | 0.136 | 0.472 | 15 | 0.0625 | 0.95 | 0.304 |
| WT+TTX, SA in dendrites | 7 | 0.026 | 0.0561 | 0.0635 | 0.0375 | 0.0232 | 0.0814 | 28 | 0.0156 | 0.95 | 0.0481 |
| WT+TTX, SA in spines | 16 | 0.0226 | 0.0367 | 0.0498 | 0.0272 | 0.0264 | 0.0559 | 136 | 3.05E-005 | 0.95 | 0.0368 |
| WT+TTX, spines | 16 | 0.138 | 0.262 | 0.346 | 0.207 | 0.176 | 0.356 | 136 | 3.05E-005 | 0.95 | 0.253 |

**Table A.2.:** Relevant parameters for spine apparatuses divided by spines

| SA \ spines | n | Q1 | median | Q3 | IQR | CI_1 | CI_2 | W | p-value | conf. level | Wilcoxon median |
|---|---|---|---|---|---|---|---|---|---|---|---|
| WT | 29 | 0.137 | 0.165 | 0.205 | 0.068 | 0.147 | 0.21 | 435 | 3.73E-009 | 0.95 | 0.171 |
| WT+mSynpo | 12 | 0.13 | 0.169 | 0.206 | 0.0755 | 0.121 | 0.268 | 78 | 0.000488 | 0.95 | 0.172 |
| KO+mSynpo | 24 | 0.176 | 0.242 | 0.319 | 0.144 | 0.208 | 0.299 | 300 | 1.19E-007 | 0.95 | 0.253 |
| Heterozygous | 17 | 0.0775 | 0.0989 | 0.173 | 0.0951 | 0.0854 | 0.157 | 153 | 1.53E-005 | 0.95 | 0.118 |
| KO+TTX | 15 | 0.213 | 0.249 | 0.288 | 0.0747 | 0.206 | 0.288 | 120 | 6.10E-005 | 0.95 | 0.249 |
| KO+toxin B | 15 | 0.207 | 0.284 | 0.319 | 0.112 | 0.221 | 0.339 | 120 | 6.10E-005 | 0.95 | 0.268 |
| KO+Y-27632 | 24 | 0.177 | 0.276 | 0.326 | 0.148 | 0.225 | 0.304 | 300 | 1.19E-007 | 0.95 | 0.258 |
| KO+Lat.A | 5 | 0.214 | 0.235 | 0.365 | 0.151 | 0.205 | 0.375 | 15 | 0.0625 | 0.95 | 0.29 |
| WT+TTX | 16 | 0.12 | 0.149 | 0.219 | 0.0983 | 0.122 | 0.19 | 136 | 3.05E-005 | 0.95 | 0.159 |
| WT+toxin B | 5 | 0.143 | 0.18 | 0.194 | 0.0511 | 0.136 | 0.197 | 15 | 0.0625 | 0.95 | 0.168 |
| WT+Y-27632 | 10 | 0.147 | 0.177 | 0.205 | 0.0581 | 0.141 | 0.202 | 55 | 0.00195 | 0.95 | 0.174 |
| WT+Lat.A | 3 | 0.0969 | 0.105 | 0.138 | 0.0409 | 0.0887 | 0.171 | 6 | 0.25 | 0.75 | 0.117 |

# B. Abbreviations

| | |
|---|---|
| +/- | heterozygous |
| +/+ | wild-type |
| °C | grad celsius |
| BSA | bovine serum albumine |
| $Ca^{2+}$ | calcium |
| CA | Cornu ammonis |
| $ddH_2O$ | double-distilled water |
| DIV | Days in Vitro |
| DAPI | 4',6-Diamidino-2-Phenylindol |
| DNA | deoxyribonucleic acid |
| CAM | cell adhesion molecule |
| cDNA | complementary deoxyribonucleic acid |
| et al. | *et alii* (and others) |
| eGFP | enhanced green fluorescent protein |
| ER | endoplasmic reticulum |
| Fig. | Figure |
| g | gram |
| h | hour(s) |
| IgSF | immunglobulin superfamily |
| kDa | kilo daltons |
| l | liter |
| Lat.A | Latrunculin A |
| LB | Luria Bertani |
| M | Molar concentration (molarity) |
| $M\Omega$ | megohm |
| m | milli ($10^{-3}$) |
| μ | micro ($10^{-6}$) |
| mM | Millimol |

| | |
|---|---|
| mSynpo | mouse [Synaptopodin] cDNA |
| n | number |
| nm | nanometer |
| No | absolute number |
| PB | phosphate buffer |
| PSD | postsynaptic density |
| q.s. | quantity sufficient |
| RyR | Ryanodine receptor |
| SA | spine apparatus |
| SCEP | single cell electroporation |
| sER | smooth endoplasmatic reticulum |
| Synpo | Synaptopodin |
| Tab. | table |
| TTX | Tetrodotoxin |
| toxin B | *Clostridium difficile* toxin B |
| V | volt |
| vol | volume |
| WT | wild-type |
| w/v | weigth per volume |
| Y-27632 | ROCK-Inhibitor Y-27632 |

# Acknowledgements

Completing this thesis has only been possible with the continuous support, advice and encouragement of many people. First and foremost I want to thank **Prof. Dr. Dr. h.c. Michael Frotscher** for his willingness being my doctoral thesis supervisor. He is undoubtedly an outstanding scientist and advisor in questions regarding Anatomy and Cell biology of the brain. I have to thank him for giving me the opportunity to perform my PhD thesis in his group and I highly appreciate the possibility to work in the field of electron microscopy and for all the valuable scientific advices.

In addition, I am most grateful to the following people for so many aspects of my work, without them these pages would not be the same:

**Prof. Dr. Michael Schäfer** for giving me the opportunity to work in his research group, which I could witness growing from the very beginning in Freiburg. His scientific enthusiasm in combination with uncomparable experimental advice and profound knowledge of the literature was a constant source of inspiration.

**Prof. Dr. Ad Aertsen** for being my supervisor from the faculty of biology. He accompanied my way in the field of neurobiology from the very beginning and encouraged me to take my first steps in computational neuroscience. He inspired me on my way as a scientist in a truly exceptional manner.

**Dr. Yun-Chung Nam-Apostolopoulos** for her patience in introducing me into the single cell electroporation technique and teaching me the dissection of mice and slice culturing. She layed the cornerstone with her preliminary findings which were pathbreaking for my start in this project.

The technical assistants **Barbara Joch** and **Sigrun Nestel** from the ELMI Lab. Sigrun and Barbara spent numerous hours to relieve me from complex technical re-slicing procedure and laborious work at the electron microscope.

All the members of the Frotscher Lab for the warm working atmosphere, which I was lucky to experience and participate in. **Daniel Althof** in particular for fruitful discussions

and for being a most valuable friend.

**PD Dr. Joachim Kremerskothen** for the smooth collaboration on the KIBRA project and **Prof. Dr. Meyer** for providing diverse pharmacological inhibitors.

**Dr. Gunnar Grah** from the BCF for his helpful comments and advice in all questions related statistics and **Simon Dold** for his qualified advice, ideas and thank you for assisting me in Latex programming.

**Jessica Klima** for her excellent work in the lab as a research assistant and for proof reading and commenting on this thesis in the context of american english language style and grammar.

**Klaus Günnel** for his patience, critical advice and technical support during all phases of my PhD thesis.

**My parents Christa and Tony Küffner** for their endless love and constant encouragement to achieve the goals I set in my life.